Università degli Studi di Udine

Polythecnic Department of Engineering and Architecture

Ph.D. course: Environmental and Energy Engineering Science

Ph.D. Thesis

Applications of Coupled Heat and Moisture Transfer Simulations in Buildings

Candidate

Michele Libralato

Supervisor

Prof. Onorio Saro

Co-Supervisor

Prof. Daniele Goi

Reviewers

Prof. Giulio Lorenzini
Prof. Marco Manzan

Cycle XXXII — Year 2020

Institute Contacts
Polythecnic Department of Engineering and Architecture
Università degli Studi di Udine
Via delle Scienze, 206
33100 Udine — Italia
https://www.dpia.uniud.it/

Acknowledgements

I gratefully acknowledge the funding received from the Provincia di Udine for this PhD. First of all, I would like to thank my supervisors Professor Onorio Saro, Professor Daniele Goi and my research group, Alessandra De Angelis. I am grateful to Ing. Lorenzo Saccomano for the surveys on the church buildings, Geom. Marco Milanese and Arch. Sergio Contardo, from the technical office of the UTI, for the surveys at the school buildings and Ing. Alice De Agostini and Simone Demontis, from the technical office of the University of Udine, for the surveys in the university buildings. Many thanks go out to Giovanni Murano, from the Polytechnic University of Turin, for the fruitful collaboration. Special thanks go to Giovanni Pernigotto, from the Free University of Bozen-Bolzano, for inviting me as a visiting student. I am extremely grateful to Professor Carsten Rode and Professor Menghao Qin for having me at the Technical University of Denmark in Kongens Lyngby as visiting scientist and, most of all for all their time. I would like to thank the reviewers, Professor Marco Manzan and Professor Giulio Lorenzini, for their comments and suggestions that contributed to the quality of this work. Thanks to ARPA Veneto, ARPA FVG (OSMER), ARPA Piemonte, Centro Funzionale della Valle d'Aosta and ARPA Lombardia, Fondazione Edmund Mach for providing the meteorological data used in this work. Thanks to Bauklimatik Dresden Software GmbH for providing the access to the software DELPHIN, to the Fraunhofer Institute for Building Physics for providing access to the software WUFI Pro, WUFI 2D and WUFI Plus.

This work would not have been possible without all the people I met during these three years. A big thank you goes to my family and to my colleagues and friends in Udine, Bolzano and Kongens Lyngby.

Abstract

The uncontrolled presence of moisture in building envelopes and structures could be the cause of several typologies of damages (for example freeze-thaw cycles damage or corrosion of metal reinforcements) and health and safety hazard for the occupants (mould and fungi growth). Several heat and moisture transfer models could be used to simulate the phenomenon and, using the damage criteria, to predict the failure of the building envelopes or structures. Some commercial software tools are available to the practitioners but, not all the material producers provide the advanced hygrothermal material parameters necessary to perform the simulations. Moreover, the proper weather files that should be used to calculate the boundary conditions for the simulations are rarely available. In this thesis, the models implemented in the commercial software tools are presented and some of the limits met in the simulation process, mostly regarding material parameters and the weather files, have been studied and analysed.

First, a practical comparison between the widespread Glaser method, a simplified stationary method for the evaluation of the interstitial condensation, and a transient coupled heat and moisture transfer model is presented, underlining the limitations of the simplified method. With respect to the hygrothermal material parameters limitations, two simple experimental procedures for the evaluation of the material properties are presented. The obtained values are found to be consistent with the experimental results by a comparison with the simulation. Then, the influence of hysteresis on the transient hygrothermal behaviour of a cross-laminated timber wall is presented, showing that by considering the hysteresis in the model, the quantity of moisture retained in the structures during a year changes.

Regarding the boundary conditions, the procedures for the statistical selection of representative weather files - used to model the typical weather of a location - and the reference weather files - designed to represent the critical weather conditions of a location - are presented. The study has been undertaken on the typical building envelopes for different locations of Northern Italy.

Contents

I

Introduction

Introduction

An excessive presence of moisture in buildings is a well known cause of structural damages and health and safety hazards. Humid building materials in the indoor environment are a favourable environment for growth of bacteria, moulds and toxins, which are a well known cause of several kinds of diseases. First attempts to solve the problems related to uncontrolled moisture presence could be found in early literature [1]. Even if all of these failures are characterised by the presence of high levels of moisture, the causes could be generally different and the solution of the problem has to be designed considering the cause. An extended discussion on the identification of the causes is presented in [2]. Moreover, the studies of the moisture related problems are currently relevant, as proven by the series of international collaborative projects funded on the topic which produced relevant guidelines for the design and the conservation of buildings with moisture related problems. Some examples are IEA Annex 24 (Heat, Air and Moisture Transfer Through New and Retrofitted Insulated Envelope Parts (Hamtie)), IEA Annex 41 (Whole building heat, air, moisture response), MEWS project (Moisture Management for Exterior Wall Systems), EMERISDA project (Effectiveness of Methods against Rising Damp in Buildings) and the RIBuild project (Robust Internal Thermal Insulation of Historic Buildings).

Health and safety of building occupants

In [3] a cluster of inflammatory rheumatic diseases were identified in an moisture-damage office. Among the office workers, a high incidence of chronic inflammatory rheumatic diseases was found in presence of moisture related damages. The working environment had moisture and mould damages on the external walls and the indoor air was reported to be of a poor quality. After an investigation a limited area of the walls was repaired, without success. A reinvestigation confirmed the poor quality of the air and the mould contamination of the insulation materials of the wall and the illnesses continued to be found in the occupants. Also [4] identified a health centre with moisture damages as a disease cluster. In the considered building, the workers, also within a year of permanence, showed symptoms typically found in mouldy houses and had rheumatic complaints (joint pains, arthritis, mucocutaneous symptoms, nausea and fatigue). The building had water infiltration problems and damp ingress through the foundations causing the mould growth in the wall insulations and high relative humidity values in the floors of the health centre rooms.

The review presented in [5] discusses the effects of fungi on human health concluding that “Indoor exposure and dampness, on the other hand, appears to be associated with an increased risk of developing asthma in young children, and with asthma morbidity in

individuals who have asthma. Reduced indoor exposure using a variety of interventions primarily aimed at reducing moisture, killing fungi and removing contaminated materials, has been shown to decrease this risk of morbidity." Living or working in presence of dampness and mould growth on walls are also associated with the dampness and mould hypersensitivity syndrome (DMHS). The respiratory symptoms are presented in [6]: "As a rule, dampness and mold hypersensitivity syndrome (DMHS), as we call this clinical condition here presents with signs of irritation of the respiratory tract and/or the eyes. Subsequently, the patient may experience recurrent sinusitis or bronchitis and neurological manifestations, such as headaches, nausea, and unexplained fatigue. Some may develop rheumatic symptoms resembling fibromyalgia or neurological symptoms may progress into pains and/or numbness in the legs and arms and the so-called brain fog [...]. Some patients develop newly onset asthma, or may present asthma-like conditions, such as dyspnea, burning sensation in the respiratory tract, and productive or non-productive cough." (excerpt from [6]). The study [7] concerning respiratory symptoms, asthma and rhinitis confirmed a correlation with dampness and mould at home and at work.

Besides these striking examples, the uncontrolled presence of moisture in building envelopes and structures could also be the cause of several typologies of structural damages that will be addressed later, in Chapter 1. Numerical simulations could be a powerful tool to control the moisture transfer in buildings, but their application could be limited by some restrictions, that will also be discussed in the thesis.

Thesis outline

This thesis has the objective to identify some of the sources of uncertainties in the simulation of moisture and heat transfer in building materials and to produce some tools and methods that could be used to reduce these uncertainties.

First, in Part II, the principles and the theoretical description of the transient coupled heat and moisture transfer will be presented, providing the reader with the descriptions of the models used by the most common simulation tools.

Then, in Part III, in order to reduce the limitations imposed by the lack knowledge of the hygrothermal material parameters, two simple experimental procedures for the evaluation of the material properties are presented. The hygrothermal properties of building materials have to be evaluated with expensive and time consuming test procedures that require proper test facilities, and, thus, they are often unknown. The possibility to evaluate the validity of the material properties attributed to a material or to estimate them by a calibration process could be an alternative to the expensive procedures. In addition, the influence of hysteresis on the transient hygrothermal behaviour of a cross-laminated timber wall is presented. The moisture hysteresis is generally neglected with the hypothesis that its influence on the calculation results is small. This aspect will be here discussed.

Finally, in Part IV, the procedures for the statistical selection of representative weather files - that are used to model the typical weather of a location - and the reference weather files - designed to represent the critical weather conditions of a location - are presented. The weather files are an important part of the simulation process and, in the risk assessment procedure, the choice of the proper weather data defines the sta-

tistical validity of the results. For this reason it is not sufficient to use a weather file measured in the location of the considered building, but it is also important to chose the proper weather event that the building will be able to resist, without reaching failure conditions.

Publications

The work presented in this thesis has also led to the production and publication of 5 conference contributions (3 already accepted [8, 9, 10] and 2 currently under review [11, 12]). During the three years of post-graduate research, other 2 journal papers, on other topics, were accepted for publication: [13, 14].

II

Coupled heat and moisture transfer in building materials

1

Moisture damages in public buildings

First, to evaluate the relevance of the moisture related damages in buildings and their perception to the contractors, a short and informal survey has been conducted among the public agencies and technical offices. The involved agencies were the Unione Territoriale Intercomunale (UTI) del Friuli Centrale (Territorial Union of Municipalities of Central Friuli) and the Univerisità degli Studi di Udine (University of Udine). Each institution provided informations about a public building that suffered of rising dump and how the problem was solved. The study cases, together with the case of the parish church in Raspano, will not be presented in detail, but the focus will be pointed on the lack of simulation tools and calculation methods to support the design choices related to moisture in buildings. Then, the case of a restoration of a church in Raspano (UD) is briefly introduced. This chapter is intended to identify the critical points of the moisture control in existing buildings, the common practices and how the simulations could be useful for the design process.

1.1 Educational buildings

The UTI is the institution in charge of the management of the public school buildings in the municipality of Udine. UTI's technical office reported that the only two cases of moisture related damage in their stock of buildings was the main building of the Istituto di Istruzione Superiore "B. Stringher" and in the main building of the Liceo Scientifico "N. Copernico", both in Udine.

On the other hand, the technical office of the Università degli Studi di Udine reported the case of the conservative restoration of the Istituto Renati building in Udine, where there was a serious case of rising damp in the perimeter walls. The building was recently restored and it was not possible to observe the damages. In both cases, the technical offices reported the absence of mould growth phenomena, due to the fact that relevant moisture productions are not expected in the use of the buildings. To their knowledge,

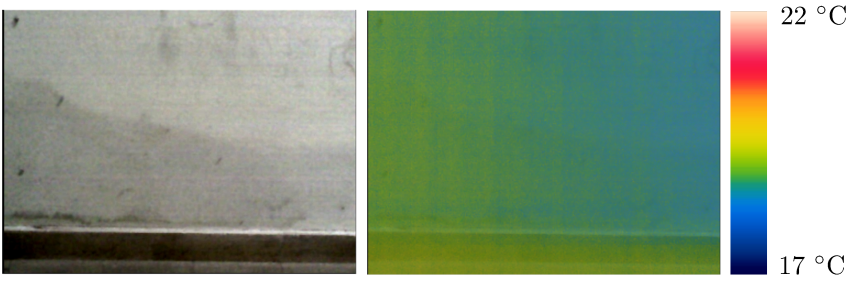

Figure 1.1: Picture (left) and infrared image (right) of the lower part of the wall of the underground level in Liceo Scientifico "N.Copernico". The part of the internal coating that was affected by rising damp has been substituted (darker area on the left picture).

the only moisture related damages were aesthetic damages caused by sporadic rising dump or water leaks.

1.1.1 UTI del Friuli Centrale

The first inspected building was the Liceo Scientifico "N. Copernico" main building, an high school in Udine. The school is a four floor building, realised in hollow bricks and concrete frame structure, with a underground floor under which the concrete foundations are in contact with ground. The underground floor internal walls are known to show effects of rising damp, like the detachment of the paint. The underground rooms with the condition are situated in the hallway and not in lecture rooms, so that the problem is not perceived as an health hazard and the use of temporary solutions is acceptable. At the moment of the inspection, the underground level of Liceo Scientifico "N. Copernico" was not showing any effects of rising damp because of a recent plaster renovation. The detail is shown in Fig. 1.1. The conditions of the ground are not known, as the presence of an infiltration or a water table.

The second study case, Istituto di Istruzione Superiore "B. Stringher", is a three level building with a frame structure in reinforced concrete, and envelopes in hollow bricks, with similar conditions in the underground level, in concrete over ground. In this case, the signs of the rising damp are still visible, also from the infrared photographs (Fig. 1.2. In this case the zone interested by the damage is rarely used by the occupants, so that the presence of the damage is acceptable.

In conclusion, the technical office did not have any tool or simulation approach to identify the cause of the problem or to evaluate quantitatively the effectiveness of a possible retrofit solution. When the damage of the rising damp is only aesthetic and the moisture content of the internal coating material is not high, the solutions are generally the periodic substitution of the superficial plaster, without acting on the cause of the problem. In similar situations, the moisture transfer simulation tools could help the designers to identify and evaluate possible solutions.

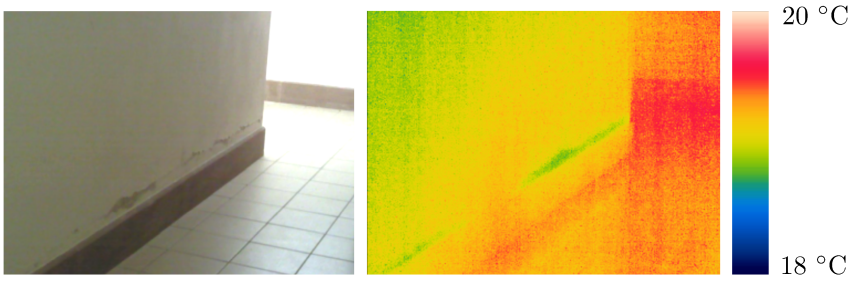

Figure 1.2: Picture (left) and infrared image (right) of the lower part of the wall of the underground level in Istituto di Istruzione Superiore "B. Stringher". The surface with lower temperatures is coloured in green (picture on the right), showing the evaporation zone.

1.1.2 Università degli Studi di Udine

The Istituto Renati was originally a school building in stone, first built in the second half of the 1700. The technical office of Università degli Studi di Udine indicated this building as recently undergone to a renovation process which was also performed to avoid a rising damp problem. The perimeter stone walls were known to have a relevant rising dump problem that should have been solved during this last retrofit design process. During the survey no visible signs of rising damp were found, as shown in the infrared picture shown in Fig. 1.3.

The will of providing a safe design solution for the restoration, brought the designers to use a further moisture control system, to use highly hygroscopic plaster on the internal surface of the wall, covering it with a naturally ventilated interspace created with a panel. The detail geometry is presented in Fig. 1.4. The highly hygroscopic plaster (in yellow) is applied only on a lower band of the wall, where the vapour and liquid migration, caused by rising damp, is more likely to happen and to cause aesthetic damage. This decision will ensure the drying process of the wall, but the definition of the height of the highly hygrothermal plaster was not supported by any calculation or numerical simulation involving moisture migration.

1.2 Churches

The churches of small communities could be subject to decay due to uncontrolled presence of moisture in the envelope. When the building is rarely occupied and the air ventilation is not performed, then it is possible to have damages on the internal coating (for example Fig. 1.5).

Rising damp is also a cause of serious damages in churches. The Example of the parish church of Raspano (UD), described by Ing. Lorenzo Saccomano, is an example of a restoration.

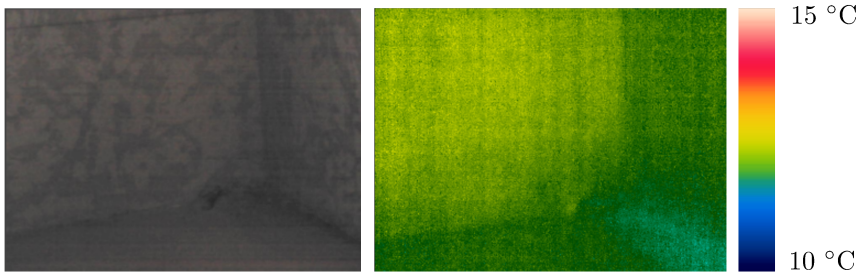

Figure 1.3: Picture (left) and infrared image (right) of the internal side of the perimeter stone wall of the building of Istituto "Renati" during the renovation. The wall has been structurally reinforced and the foundations have been protected from the ingress of water. The surface has a uniform colour (picture on the right) and thus, a uniform temperature and there are not signs of rising damp.

1.2.1 Parish church of Raspano (UD)

After the disruption of the marble floor of the church, caused by rising damp, an overall restoration of the envelope and the foundations at the perimeter was undertaken. First, a drain was realised around the church and a perched water table was found under the church. Then, the wall was covered with hygroscopic coating, to allow the moisture distribution in the structure. The drain allowed to advert most of the water from the foundation, avoiding the damage of the floor. The restored perimeter wall, next to the damaged floor, did not show externally any sign of the rising damp, but using the infrared camera it was possible to see an evaporation zone for most of the wall height (Fig. 1.6). Also in this case, it was not possible to evaluate quantitatively a priori, if the drain and the materials used would have been be sufficient to avoid the rising damp damages.

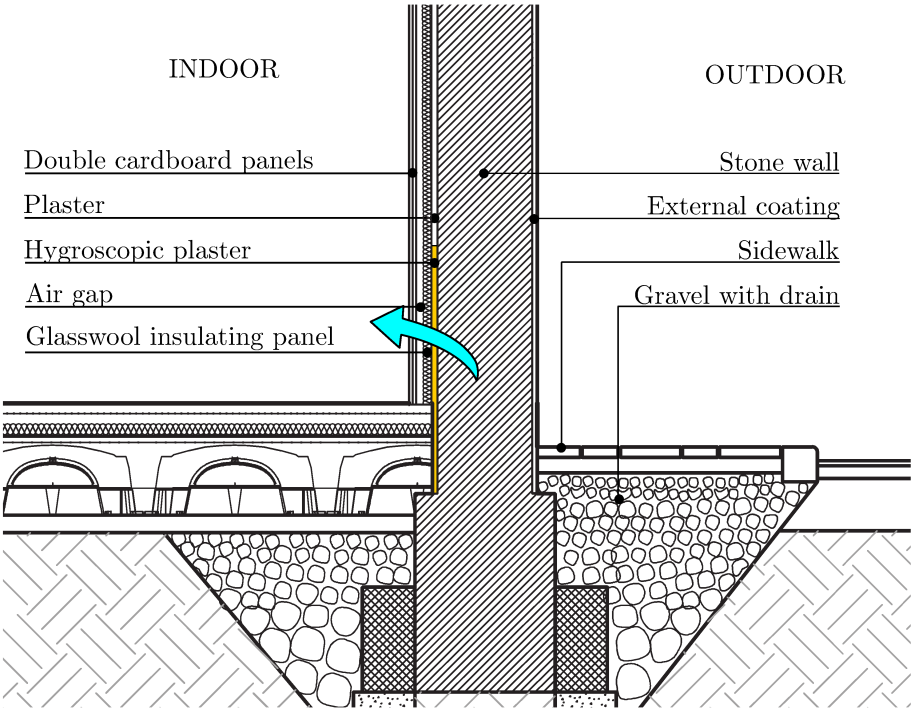

Figure 1.4: Qualitative description of the section of the foundation node of the Istituto Renati after the restoration. The gravel and the external coating should prevent from the moisture accumulation on the stone wall. The hygroscopic plaster allows the exit of the moisture (blue arrow) through the internal surface, reducing the potential aesthetic damage. The designers and the contractors are not using numerical simulations to predict the behaviour of the foundation.

Figure 1.5: Detail of an internal coating detachment of the parish church of Nogaredo di Prato (UD). The damage could be caused by a combined effect of rising damp, rain infiltration and superficial condensation also due to the heating system.

Figure 1.6: Detail of the internal side of the restored wall of the parish church of Raspano (UD). After the restoration the rising damp is not visible but the evaporative moisture transfer at the surface could be visualised with infrared photography. The hygroscopic coating allows the moisture migration without damage.

2

Principles

This chapter is intended as a quick introduction to the topics of humid air and coupled heat and moisture transfer, including nomenclature, definitions and explanations of ambiguities that often lead to misunderstandings. The main reference for this chapter is the lecture notes from the International Association of Building Physics (IABP) Graduate Course held form the 21st to the 23rd September 2018 at Syracuse University titled "Coupled Heat, Air, Moisture and Pollutant Simulations in Built Environment Systems (CHAMPS-BES): Modeling VOC Emissions and Sorption of Building Materials" by Professor Jense Zhang, Professor John Grunewald and Professor Carsten Rode. The theoretical aspects of humid air and coupled heat and moisture transfer are taken from the Professor Carsten Rode's lecture notes, while the following part on the models implemented in the software Delphin is taken from Professor John Grunewald's lecture notes. The reference book on humid air is [15] while the heat transfer book of reference is [16]. The theoretical introduction is limited to the heat and moisture diffusion in porous materials that will be used in this work. It is noted that in a complete discussion of the topic also air diffusion, convection and other transport mechanisms are relevant and should be studied. The reader is addressed to the aforementioned references for a presentation and discussion of these topics. Other references used in this brief presentation are specified in the text.

2.1 Humid air

Several parameters could be used to describe the thermodynamic state of air and its moisture content (humid air). In this section, the parameters useful for the description of the heat and moisture transfer models and its boundary conditions will be listed and briefly presented.

2.1.1 Ideal mixture of gases

Humid air could be considered as a mixture of two ideal gases, dry air and water vapour. The two differ for a crucial property: water vapour is condensable. To describe the state

of the two ideal gasses it is possible to use the ideal gas law on the gas mixture:

$$PV = nRT \tag{2.1}$$

$$p_a V = n_a RT \tag{2.2}$$

$$p_v V = n_v RT \tag{2.3}$$

Where:

P = Total pressure of the atmosphere, generally $P = 101\,325\,\text{Pa}$

p_i = Partial pressure of the ideal gas i (Pa)

V = Volume occupied by the ideal gases (m^3)

n = Total number of moles (mol)

n_i = Mole number of the ideal gas i (mol)

R = Universal gas constant R= 8.314 J/(mol· K)

T = Absolute temperature (K)

From the summation of the Eqs. 2.2, 2.3 and Eq. 2.1 the Dalton's Law is obtained

$$P = p_a + p_v = \frac{(n_a + n_v)RT}{V} \tag{2.4}$$

A useful variable in the quantification of moisture content in air is mass. Let m_i be the mass of the ideal gas i expressed in kg. It is possible to define the molar mass M_i of the ideal gas i as:

$$M_i = \frac{m_i}{n_i} \tag{2.5}$$

The molar mass (unit: $\frac{\text{kg}}{\text{mol}}$) allows to explicit the mass variable in Eqs. 2.2 and 2.3, removing the moles number as in Eq. 2.6.

$$p_i V = \frac{m_i RT}{M_i} \tag{2.6}$$

That could be also found in the form of Eq. 2.7, with R_i gas constant of the ideal gas i, defined as $\frac{R}{M_i}$ (unit: $\frac{\text{J}}{\text{kg·K}}$).

$$p_i V = m_i R_i T \tag{2.7}$$

relevant molar mass values for the humid air mixture are M_a for the dry air and M_v for the water vapour:

$$M_a = 28.97 \cdot 10^{-3} \frac{\text{kg}}{\text{mol}}$$

$$M_v = 18.02 \cdot 10^{-3} \frac{\text{kg}}{\text{mol}}$$

Then, the water vapour concentration ν_v (unit: $\frac{\text{kg}}{\text{m}^3}$) is defined as:

$$\nu_v = \frac{m_v}{V} \tag{2.8}$$

and the Eq. 2.6 becames:

$$p_v = \nu_v R_v T = \nu_v T \cdot 461.5 \frac{\text{J}}{\text{kg} \cdot \text{K}} \tag{2.9}$$

The water vapour concentration and the water vapour pressure are two parameters that describe the absolute amount of water vapour in an undefined volume of air. The specific humidity (or humidity ratio) x (unit: -)is a relative measure of the presence of water vapour in the air. It is defined as:

$$x = \frac{m_v}{m_a} = 0.622 \cdot \frac{R_v p_v}{R_a p_a} = 0.622 \cdot \frac{p_v}{P - p_v} \tag{2.10}$$

This relation could be, of course, also used to calculate vapour pressure from the specific humidity and the total pressure:

$$p_v = \frac{xP}{0.622 + x} \tag{2.11}$$

Another variable that could be used to describe the ideal gas properties, and it should not be confused with its reciprocal (the concentration ν), is the specific volume v, defined as follows:

$$v_i = \frac{V}{n_i M_i} = \frac{V}{m_i} \tag{2.12}$$

2.1.2 Vapour saturation

Water vapour has the tendency to change its state to liquid once the saturation conditions are reached. When the vapour pressure p_v reaches the saturation pressure p_s (unit: Pa), condensation happens. The value of saturation pressure for the problems studied in this dissertation depends on temperature and could be calculated with the Eq. 2.13 also used in [17].

$$p_s = \begin{cases} 610.5 \exp(\frac{17.269 \cdot (T - 273.15)}{T - 35.85}) & \text{if } T \geq 273.15\,\text{K} \\ 610.5 \exp(\frac{T - 251.275}{T - 18.65}) & \text{if } T < 273.15\,\text{K} \end{cases} \tag{2.13}$$

The saturation state could be also described by varying the temperature. With the decreasing of T, the vapour pressure p_s decreases according to 2.13 and reaches the p_v value. The T value that causes $p_v = p_s(T)$ is called dew point temperature, T_{dew}.

With the ratio between water vapour pressure and saturation pressure values it is possible to describe in a single variable the degree of saturation of the air. This variable is relative humidity φ (unit: - or %) and it could be the cause of different misunderstandings due to the dependence of p_s to the temperature of air and the definition of relative humidity to express the moisture content of a porous material.

$$\varphi = \frac{m_v}{m_s(T)} = \frac{\nu_v}{\nu_s(T)} = \frac{p_v}{p_s(T)} \tag{2.14}$$

The saturation pressure values are the upper limit for the vapour pressure values at a given temperature T. The value of the saturation pressure at 273.15 K (0 °C) calculated with the relation 2.13 is $p_s(273.15K) \approx 610$ Pa, while for $T = 293.15$ K (20 °C), $p_s(293.15K) \approx 2337$ Pa. At $T = 313.15$ K (40 °C), $p_s(313.15K) \approx 7371$ Pa.

2.1.3 Enthalpy of humid air

The calculation of the enthalpy of humid air is also performed considering separately dry air and water vapour. The total enthalpy of the humid air h is expressed as

$$h = h_a + xh_v \tag{2.15}$$

Where:

h_a is the specific enthalpy of dry air (J kg)

h_v is the specific enthalpy of water vapour (J kg)

The enthalpy values depend linearly to the temperature and they are calculated starting from a reference state. Conventionally, the reference state is at the temperature of 0°C.

$$h_a = c_{p,a}\Delta T + h_{a,0} = c_{p,a}\theta \tag{2.16}$$

$$h_v = c_{p,v}\Delta T + h_{v,0} = c_{p,v}\theta + r \tag{2.17}$$

Where:

$c_{p,i}$ = specific heat at constant pressure of the i ideal gas (J/kg K)

ΔT = temperature difference between the reference state difference and the actual temperature (K)

θ = temperature in Celsius degrees (°C)

$h_{i,0}$ = enthalpy of the reference state for the i ideal gas (J/kg K)

r = latent heat of evaporation of water at temperature of 0 °C, necessary to vaporize the unit of mass of water (J/kg K)

In conclusion, the total enthalpy of air could be calculated as:

$$h = c_{p,a}\theta + x(c_{p,v}\theta + r) \tag{2.18}$$

Where:

$c_{p,a}$ = Specific heat at constant pressure of dry air $c_{p,a} = 1006 \frac{\text{J}}{\text{kgK}}$

$c_{p,v}$ = Specific heat at constant pressure of water vapour $c_{p,v} = 1830 \frac{\text{J}}{\text{kgK}}$

r = latent heat of evaporation of water $r = 2501 \frac{\text{J}}{\text{kg}}$

2.2 Moisture retention in building materials

The aptitude of a porous material to absorb and store moisture in its pores is often referred to as moisture retention. The parameters used to describe this behaviour are presented in this section. Generic porous materials are considered, in absence of salts or other chemical reactions. Furthermore, porous materials have different pore structures, different pore dimensions or different pore surfaces, so that different behaviours have to be expected. It has been observed that the retention of moisture in a material depends on the moisture state, on the environmental conditions and on the previous retention states of the materials (its history). In order to describe the hygroscopic state of a material it is possible to express its moisture content with a set of variables. Similarly to the specific humidity x, the moisture content u is defined as:

$$u = \frac{m_{\mathrm{H_2O}}}{m_d} \tag{2.19}$$

Where:

u = moisture content ($\frac{\mathrm{kg}}{\mathrm{kg}}$ or %)

$m_{\mathrm{H_2O}}$ = mass of water in all its states (vapour, liquid or solid) (kg)

m_d = mass of the dry material, the dry state is considered at 105°C. (kg)

u is usually calculated from the weights of the samples before (m) and after the drying process (m_d):

$$u = \frac{m - m_d}{m_d} \tag{2.20}$$

The variable w is also known as moisture content, and, similarly to the vapour concentration in air ν, is defined as:

$$w = \frac{m_{\mathrm{H_2O}}}{V} \tag{2.21}$$

Where:

w = moisture content ($\frac{\mathrm{kg}}{\mathrm{m^3}}$)

V = volume of the material, pores included ($\mathrm{m^3}$)

Then the two values are in relation:

$$w = \rho_0 \cdot u \tag{2.22}$$

Where:

ρ_0 = density of the dry material ($\frac{\mathrm{kg}}{\mathrm{m^3}}$)

It is possible to define the quantity of moisture in the material using the occupied volume instead of the mass. Here, the notation of [18], [19] and [20] will be used. Starting from the definition of open porosity of the porous material 2.23 as the fraction between the volume of open voids and the total volume of the material:

$$\theta_{vac} = \frac{V_{vac}}{V} \tag{2.23}$$

Where:

θ_{vac} = open porosity $(\frac{\mathrm{m}^3}{\mathrm{m}^3})$

V_{vac} = volume of open pores (m^3)

Similarly, the volumetric moisture content θ_{H_2O} is defined as a volume fraction:

$$\theta_{H_2O} = \frac{V_{\mathrm{H_2O}}}{V} = \frac{\rho_0 \cdot u}{\rho_l} \tag{2.24}$$

Where:

ρ_l = density of liquid water $(\rho_l = 997 \frac{\mathrm{kg}}{\mathrm{m}^3})$

V_{H_2O} = volume occupied by moisture (m^3)

Another variable used for the determination of the water content is the relative humidity φ. In addition to the ambiguity of its physical meaning due to the temperature dependency, another ambiguity is added to the variable utilisation, when considering the porous materials instead of air. To explain the relative humidity meaning for porous media, the following conceptual experiment could be considered: a material in an environment filled with humid air, in constant stationary conditions, after an infinite time, reaches the equilibrium state with the air, absorbing some of the vapour phase in its pores. The value of the relative humidity of the environment could be use to identify the moisture content in the material. For example, a brick could reach equilibrium in a climatic chamber at 50 % of relative humidity and 20°C and contain the equilibrium moisture content w of 3.42 $\frac{\mathrm{kg}}{\mathrm{m}^3}$. In many contexts it would be assumed that the moisture content of the brick is 50 % of relative humidity, without distinguishing the state of the moisture in the porous, but only describing the equilibrium state of the brick. Moreover, due to material hygrothermal property known as hysteresis, the brick, depending on the previous moisture contents, could reach equilibrium with the same environment at 50 % but at different values of w, so that the relative humidity could not univocally identify the moisture content of the brick, but only its potential of exchanging moisture with an environment or a porous material in contact.

The relative humidity of a porous material could be confused with the water activity a_w commonly used in other disciplines. The water activity is defined as the ratio between the partial pressure of vapour available for a given reaction (for example mould growth) and the saturation pressure [21]. For the case of the porous materials, relative humidity and water activity coincide only in absence of chemical reactions or salts that could reduce the availability of moisture for the studied reaction.

The correlation between relative humidity and moisture content u is described by the moisture retention curve, also known as moisture storage function or sorption curve. The derivative of this curve is the moisture capacity ξ (unit: -):

$$\xi = \frac{\partial u}{\partial \varphi} = \frac{1}{p_s} \cdot \frac{\partial u}{\partial p_v} \tag{2.25}$$

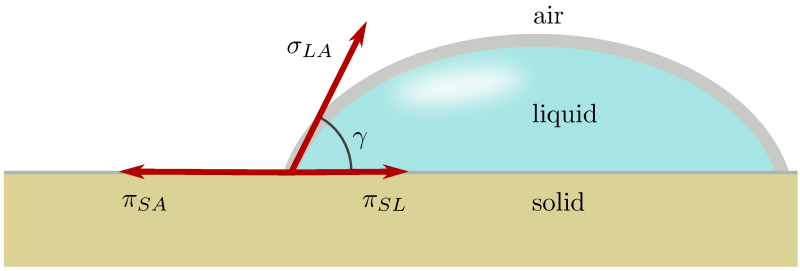

Figure 2.1: Surface pressure balance at the interface between the three phases, solid, liquid and air.

The relative humidity is used as a potential variable for low moisture contents and it quantifies the moisture that could be absorbed when the material is in contact with humid air at limited values of φ, for example $< 95\%$. The value of 95 % is a conventional value. After the 95 %, when the material is in contact with higher values of φ or with liquid water, small variations of φ could lead to high variations of moisture content w. For this range the capillary pressure also known as suction pressure P_c could be used as a potential.

To define the suction pressure, the boundary between the three phases (air, liquid and solid) is considered in Figure 2.1. The situation described in the figure is a simplified representation of what could happen on the internal surface of a porous inside a building material. The interface between the liquid phase and the air phase is in equilibrium due to the cohesion and adhesion forces and the surface tension. The difference between the pressure π_{SA} and the pressure π_{SL} defines the surface tension σ_{LA} which defines the contact angle γ according to Eq. 2.26 and the shape of the interface.

$$\pi_{SA} - \pi_{SL} = \sigma_{LA} \cdot \cos(\gamma) \tag{2.26}$$

π_{SA} = overpressure on the interface between the solid and the air phase $(\frac{\mathrm{N}}{\mathrm{m}})$

π_{SL} = overpressure on the interface between the solid and the liquid phase $(\frac{\mathrm{N}}{\mathrm{m}})$

σ_{LA} = surface tension between the liquid and the air phase $(\frac{\mathrm{N}}{\mathrm{m}})$

γ = contact angle (rad)

As an extreme simplification, the porous structure of a building material could be represented by a cylindrical capillary as shown in Fig. 2.2. The pressure balance on the liquid column is here presented. The capillary pressure is obtained integrating Eq. 2.26 along the interface between the three phases, on the perimeter of the capillary, as shown in Eq. 2.27.

$$P_c = P_l - P_g = \frac{2 \cdot \sigma \cdot \cos(\gamma)}{r} \tag{2.27}$$

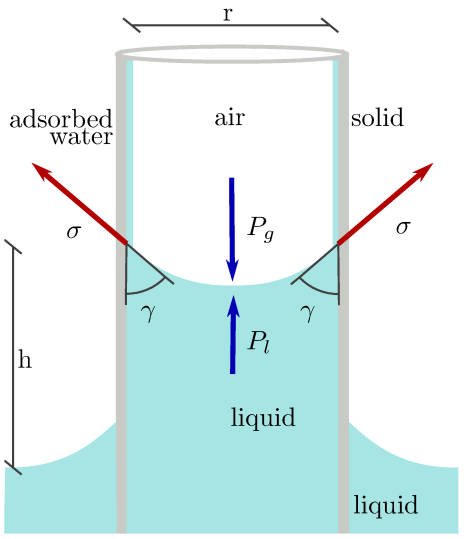

Figure 2.2: Surface pressure balance in a capillary at the interface between the three phases, solid, liquid and air. Image adapted from [20].

P_c = capillary pressure (Pa)

P_l = pressure of the liquid (Pa)

P_g = pressure of the air (Pa)

σ = surface tension (Pa)

r = radius of the capillary (m)

The suction pressure could be then defined as the absolute value of the hydraulic pressure P_h (unit: Pa), which has a negative value:

$$P_c = -P_h = -h\rho_l g_z \tag{2.28}$$

Where:

P_c = suction pressure or capillary pressure (Pa)

P_h = hydraulic pressure (Pa)

h = height of the column of water (m)

ρ_l = density of liquid water $(\frac{\text{kg}}{\text{m}^3})$

g_z = vertical component of the acceleration due to gravity $(\frac{\text{N}}{\text{kg}})$

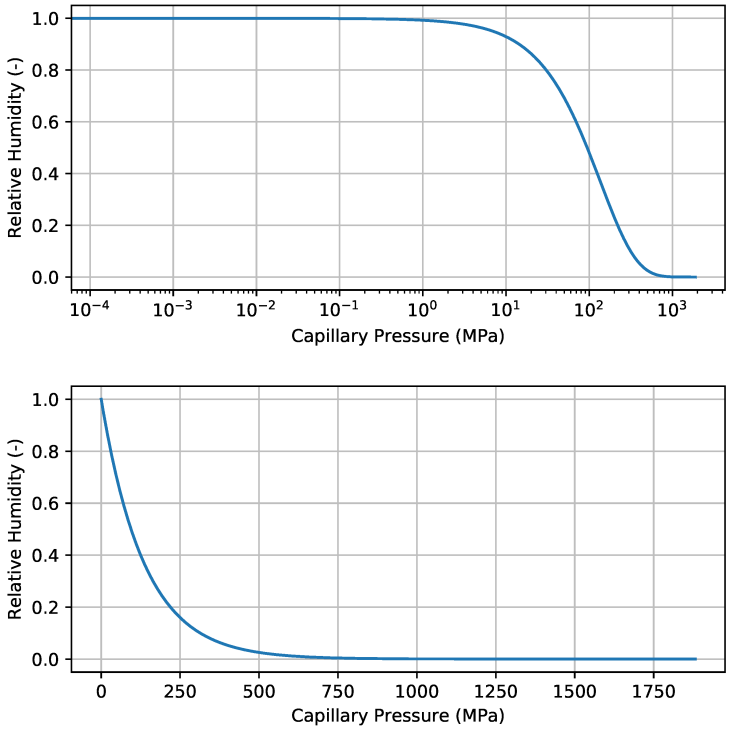

Figure 2.3: Plot of the Kelvin equation (Eq. 2.29) presented with the capillary pressure in linear scale and then with the logarithmic scale.

The suction pressure is then correlated to the relative humidity by the Kelvin equation:

$$\varphi = \exp(\frac{-P_c}{\rho_l R_v T}) \tag{2.29}$$

2.3 Moisture transport phenomena

The most simple transfer mechanism of an ideal gas is the diffusion. When two adjacent volumes have different water vapour concentration potentials, then a flux of vapour is established in between. The vapour transfer in still air could be considered a diffusive process. The diffusion, for the one-dimensional case, is described by Fick's law as follows:

$$g_v = -D \cdot \frac{\partial \nu_v}{\partial x} \tag{2.30}$$

Where:

g_v = water vapour flux $\frac{\text{kg}}{\text{m}^2\text{s}}$

D = water vapour permeability of air $\frac{\mathrm{m}^2}{\mathrm{s}}$

ν_v = water vapour concentration $\frac{\mathrm{kg}}{\mathrm{m}^3}$

x = position (m)

The value of D for P= 1 atm and T= 20 °C is $2.54{\cdot}10^{-5}\mathrm{m}^2/\mathrm{s}$ depends on the temperature T and on the total air pressure P:

$$D = \frac{2.26}{P} \cdot \frac{T}{273}^{1.81} \tag{2.31}$$

2.3.1 Vapour transport in porous media

Various transport mechanisms happen in porous media, depending on the porous dimensions and shapes. Similarly to ideal gas mixtures, the vapour flux through a porous media could be calculated with diffusion:

$$g_v = -\delta_\nu \cdot \frac{\partial \nu_v}{\partial x} \tag{2.32}$$

Where:

δ_ν = Water vapour permeability of the porous material for the vapour concentration potential $(\frac{\mathrm{m}^2}{\mathrm{s}})$

It is then possible to perform a change of variable, to express the diffusion potential as water vapour pressure p_v, using 2.9.

$$g_v = -\delta_\nu \cdot \frac{\partial \nu_v}{\partial x} = -\frac{\delta_\nu}{R_v T} \cdot \frac{\partial p_v}{\partial x} + \frac{\delta_\nu p_v}{R_v T^2} \cdot \frac{\partial T}{\partial x} \approx -\frac{\delta_\nu}{R_v T} \cdot \frac{\partial p_v}{\partial x} \tag{2.33}$$

This relation could be used neglecting the second term with the partial derivative of T. This simplification could cause an error of 5-6% and it is often made using the water vapour permeability δ_p for the water vapour pressure (unit: $\frac{\mathrm{m}^2 \cdot \mathrm{kg}}{\mathrm{m} \cdot \mathrm{s} \cdot \mathrm{Pa}}$).

$$\delta_p = \frac{\delta_\nu}{R_v T} \tag{2.34}$$

The well known parameter μ, the vapour diffusion resistance factor, is often used in standards and material catalogues and reports:

$$\mu = \frac{D}{\delta_\nu} \tag{2.35}$$

It is known that a porous material could contain some liquid water even if it is in equilibrium with a room with relatively low values of relative humidity (lower than 100 %). This phenomenon depends on the shape and dimensions of the porous inside the material and it could affect the water vapour transport properties of the material itself. Once a critical moisture content u_{cr} is reached, then the phase of water in the material is mainly liquid and its behaviour is less influenced by temperature. The Fick's diffusion and the water vapour permeability can be used to describe the water vapour transport

with a good approximation for al the range up to the critical moisture content if the permeability is expressed in function of moisture content.

A temperature change or gradient would influence the relative humidity values in the porous material, inducing, even for small T variations, a potential gradient causing a transport of vapour from the warm part of the material to the cold zone.

2.3.2 Liquid transport

Darcy's law, usually expressed in terms of hydraulic pressure P_h can be used to describe the transport of liquid in porous materials, using the suction pressure P_c as potential:

$$g_l = -K_l \cdot \frac{\partial P_c}{\partial x} \tag{2.36}$$

Where:

K_l = Hydraulic conductivity $(\frac{\text{kg}}{\text{Pa·m·s}})$

g_l = mass of liquid water flux $(\frac{\text{kg}}{\text{m}^2\text{s}})$

In this formulation the possible effects of overpressure and gravity are neglected with a small error due to the larger magnitude of the suction term (or matrix potential). This simplification is suitable for most of the applications in building physics.

The influence of temperature is of a small order and could be neglected. The temperature decrease reduces the capillary pressure values and the pressure gradients, while the viscosity of the liquid is also decreasing, allowing the fluid to flow more easily. The overall effect is the increase of liquid water conductivity for the higher temperatures.

2.3.3 Superficial moisture transfer coefficient

The moisture transfer between the porous media and the humid air, as it happens for the heat transfer equations, is mediated by a surface transfer coefficient. This coefficient β could be expressed in terms of vapour concentration β_ν or water vapour pressure β_{p_v}. Their value depends on the regime of the air flow of the environment.

$$g_v = \beta_{p_v} \cdot \Delta p_v = \beta_\nu \cdot \Delta\nu \tag{2.37}$$

Where:

β_{p_v} = Convective moisture transfer coefficient for vapour pressure potential $(\frac{\text{kg}}{\text{m}^2\text{s·Pa}})$

β_ν = Convective moisture transfer coefficient for vapour concentration potential $(\frac{\text{m}}{\text{s}})$

For laminar conditions the Lewis relation is a valid approximation:

$$\beta_\nu = \frac{h_k}{\rho_v \cdot c_p} \tag{2.38}$$

Where:

h_k = Convective heat transfer $(\frac{\text{W}}{\text{m}^2\text{K}})$

c_p = Specific heat capacity at constant pressure $(\frac{\mathrm{J}}{\mathrm{kg \cdot K}})$

ρ_v = Density of water vapour $(\frac{\mathrm{kg}}{\mathrm{m}^3})$

3

Coupled heat and moisture transfer models

The equations of the previous chapter are used to obtain transient continuity equations for enthalpy and moisture and then these are coupled in order to model the mutual influence of temperature on moisture content and vice versa. The effects of air transport and convection will be neglected for simplicity. For a complete discussion of these components see the references indicated in the previous chapter. The last sections of this chapter report the models implemented in the software used in this dissertation, MATCH, WUFI Pro and DELPHIN. These are commercial software tools available to the practitioners and distributed with a database of material properties and weather files. Other research programs have been presented in literature and are available for use, for example CalA (presented in [22], applications in [23], [24] and the manual in [25]), hamopy ([26] developed as a Python package and used in [27] and [28]) and many others (some of which are listed in [29] and [30])

3.0.1 Moisture balance equation

From Eq. 2.32, the vapour transfer could be expressed as:

$$\rho_0 \frac{\partial u}{\partial t} = -\frac{\partial g_v}{\partial x} = -\frac{\partial}{\partial x}\left(-\delta_p \cdot \frac{\partial p_v}{\partial x}\right) \tag{3.1}$$

It is possible to perform a change of variable to express the equation with a single potential variable, for instance the right hand term with p_v can be expressed in terms of moisture content u:

$$\rho_0 \frac{\partial u}{\partial t} = \frac{\partial}{\partial x}\left(\delta_p \cdot \frac{\delta p_v}{\delta u} \cdot \frac{\partial u}{\partial x}\right) \tag{3.2}$$

With the definition of the moisture diffusivity of the water vapour transfer D_v:

$$D_v = \frac{p_s \delta_p}{\rho_0 \xi} \tag{3.3}$$

Then, Eq. 3.1 could be written as:

$$\frac{\partial u}{\partial t} = \frac{\partial}{\partial x}\left(D_v \cdot \frac{\partial u}{\partial x}\right) \tag{3.4}$$

The same transformations could be made on Eq. 2.36, with the substitution of g_l:

$$\rho_0 \frac{\partial u}{\partial t} = -\frac{\partial}{\partial x}\left(-K_l \cdot \frac{\delta P_c}{\delta x}\right) = \frac{\delta}{\partial x}\left(K_l \frac{\partial P_c}{\partial x} \cdot \frac{\partial u}{\partial P_c}\right) \tag{3.5}$$

From Eq. 3.5, the moisture diffusivity of liquid water transfer D_l is defined as:

$$D_l = \frac{K_l}{\rho_0} \cdot \frac{\partial u}{\partial P_c} \tag{3.6}$$

Thus Eq.3.5 becames:

$$\frac{\partial u}{\partial t} = \frac{\partial}{\partial x}\left(D_l \cdot \frac{\partial u}{\partial x}\right) \tag{3.7}$$

In this manner it is possible to express the migration of water vapour and liquid water with the same potential. The distinction between the two states is performed at the level of the definitions of the diffusivity coefficients D_v and D_l as functions of the moisture contents (both have units $\frac{\mathrm{m}^2}{\mathrm{s}}$). For low moisture contents, under the u_{cr} critical content the state of the moisture is considered vapour and $D_v > 0$, while $D_l = 0$ and the other way around for the liquid water state. The equation governing liquid and vapour transfer is:

$$\frac{\partial u}{\partial t} = \frac{\partial}{\partial x}\left[(D_l + D_v) \cdot \frac{\partial u}{\partial x}\right] = \frac{\partial}{\partial x}\left(D_{uu} \cdot \frac{\partial u}{\partial x}\right) \tag{3.8}$$

The sum of the two diffusivities will be referred as D_{uu}, the moisture diffusivity (unit $\frac{\mathrm{m}^2}{\mathrm{s}}$) . The equation of the moisture balance should also include the moisture transport caused by temperature gradients. This could be obtained with a change of differentiation in the Eq.3.1 and substituting p_v with $\varphi \cdot p_s$:

$$\rho_0 \frac{\partial u}{\partial t} = \frac{\partial}{\partial x}\left(\delta_p \cdot \frac{\partial(\varphi \cdot p_s)}{\partial T} \cdot \frac{\partial T}{\partial x}\right) = \frac{\partial}{\partial x}\left(D_{vt} \cdot \frac{\partial T}{\partial x}\right) \tag{3.9}$$

Where:

D_{vt} = thermal moisture diffusivity of vapour transfer $\left(\frac{\mathrm{m}^2}{\mathrm{s}\cdot\mathrm{K}}\right)$

The same procedure is applied to the liquid transport equation Eq.3.5

$$\rho_0 \frac{\partial u}{\partial t} = \frac{\partial}{\partial x}\left(K_l \cdot \frac{\partial P_c}{\partial T} \cdot \frac{\partial T}{\partial x}\right) \tag{3.10}$$

The thermal moisture diffusivity of the liquid transfer D_{lt} is defined as:

$$D_{lt} = \frac{K_l}{\rho_0} \cdot \frac{\partial P_c}{\partial T} \tag{3.11}$$

$$D_{ut} = D_{vt} + D_{lt} \tag{3.12}$$

Where:

D_{ut} = thermal moisture diffusivity $\left(\frac{\mathrm{m}^2}{\mathrm{s \cdot K}}\right)$

Combining the Eq. 3.7,3.10 and 3.9 the equation of moisture balance is obtained:

$$\frac{\partial u}{\partial t} = \frac{\partial}{\partial x}\left(D_{uu}\frac{\partial u}{\partial x}\right) + \frac{\partial}{\partial x}\left(D_{ut}\frac{\partial T}{\partial x}\right) \tag{3.13}$$

3.0.2 Enthalpy transfer equation

In a similar fashion the enthalpy balance equation is obtained. In this case the dry mass specific enthalpy $\bar{h}$ (unit: J/kg) is considered instead of the moisture content.

$$h = \bar{h} \cdot \rho_0 \tag{3.14}$$

Its value depends on the temperature and on the specific heat at constant pressure:

$$\mathrm{d}\bar{h} = c_p \cdot \mathrm{d}T \tag{3.15}$$

The value of c_p depends on the moisture content and on the physical phase of the moisture. In the following formula the indexes i, l and v indicate respectively the solid, liquid and vapour state of water.

$$c_p = c_{p,0} + \sum_{i=s,l,v} u_i \cdot c_{p,i} \tag{3.16}$$

Where:

u_i = mass fraction of the phase i (-)

$c_{p,i}$ = specific heat of the phase i $\left(\frac{\mathrm{J}}{\mathrm{kg \cdot K}}\right)$

With these variables, the Fourier's law is expressed as follows:

$$\rho_0 \frac{\partial \bar{h}}{\partial t} = \frac{\partial}{\partial x}\left(\lambda \frac{\partial T}{\partial x}\right) \tag{3.17}$$

Where:

λ = thermal conductivity of the porous material, considering its moisture content $\left(\frac{\mathrm{W}}{\mathrm{Km}}\right)$

Dividing the terms of the equation by $\rho_0 \cdot c_p$, T is isolated in the partial derivative of time.

$$\frac{\partial T}{\partial t} = \frac{\partial}{\partial x}\left(\frac{\lambda}{\rho_0 c_p} \cdot \frac{\partial T}{\partial x}\right) \tag{3.18}$$

Then, for simplicity, the heat diffusivity α is defined and substituted in the equation:

$$\alpha = \frac{\lambda}{\rho_0 c_p} \quad \left(\frac{\mathrm{m}^2}{\mathrm{s}}\right) \tag{3.19}$$

Then the enthalpy flux due to the moisture diffusion is considered with the following term:

$$\frac{\partial T}{\partial t} = \frac{\Delta \bar{h}_{vw}}{\rho_0 c_p} \cdot \frac{\partial g_v}{\partial x} \tag{3.20}$$

Where:

$\Delta \bar{h}_{vl}$ = Latent enthalpy required to perform a change of physical state from vapour to liquid state (J)

Then, the term is added to Eq. 3.17 and the flux g_v is substituted with Eq. 3.4.

$$\begin{aligned} \frac{\partial T}{\partial t} &= \frac{\partial}{\partial x}\left(\alpha \frac{\partial T}{\partial x}\right) + \frac{\Delta \bar{h}_{vl}\delta_p}{\rho_0 c_p} \cdot \left(\left.\frac{\partial p}{\partial T}\right|_u \cdot \frac{\partial T}{\partial x} + \left.\frac{\partial p}{\partial u}\right|_t \cdot \frac{\partial u}{\partial x}\right) \\ &= \frac{\partial}{\partial x}\left(\left[\alpha + \frac{\Delta \bar{h}_{vl}}{c_p} \cdot D_{vt}\right]\frac{\partial T}{\partial x}\right) + \frac{\partial}{\partial x}\left(\frac{\Delta \bar{h}_{vl}}{c_p} \cdot D_v \cdot \frac{\partial u}{\partial x}\right) \end{aligned} \tag{3.21}$$

Further substitutions are performed with the parameters D_{tt} and D_{tu}, and a form similar to Eq. 3.13 is obtained.

$$\frac{\partial T}{\partial t} = \frac{\partial}{\partial x}\left(D_{tt}\frac{\partial T}{\partial x}\right) + \frac{\partial}{\partial x}\left(D_{tu}\frac{\partial u}{\partial x}\right) \tag{3.22}$$

The two parameters D_{tt} and D_{tu} are defined as follows:

$$D_{tt} = \alpha + \frac{\Delta \bar{h}_{vl}}{c_p} \cdot D_{vt} \quad \left(\frac{\mathrm{m}^2}{\mathrm{s}}\right) \tag{3.23}$$

$$D_{tu} = \frac{\Delta \bar{h}_{vl}}{c_p} \cdot D_v \quad \left(\frac{\mathrm{m}^2 \cdot \mathrm{K}}{\mathrm{s}}\right) \tag{3.24}$$

Finally, the phenomenon of the coupled migration of heat and moisture can be described with the system of the two equations 3.24 and 3.13

$$\begin{cases} \frac{\partial u}{\partial t} = \frac{\partial}{\partial x}\left(D_{uu}\frac{\partial u}{\partial x}\right) + \frac{\partial}{\partial x}\left(D_{ut}\frac{\partial T}{\partial x}\right) \\ \frac{\partial T}{\partial t} = \frac{\partial}{\partial x}\left(D_{tu}\frac{\partial u}{\partial x}\right) + \frac{\partial}{\partial x}\left(D_{tt}\frac{\partial T}{\partial x}\right) \end{cases} \tag{3.25}$$

3.1 Rode's model

A simplified version of the aforementioned system of equations (Eq. 3.25) has been implemented in the software MATCH, first presented in [31] and in [32]. The model considers the following equations:

$$\begin{cases} \rho_0 \frac{\partial u}{\partial t} = \frac{\partial}{\partial x}\left(\delta_p \frac{\partial p_v}{\partial x} + K_l \frac{\partial P_c}{\partial x}\right) \\ \rho_0 \frac{\partial h}{\partial t} = \frac{\partial}{\partial x}\left(\lambda \frac{\partial T}{\partial x}\right) + h_v \frac{\partial}{\partial x}\left(K_l \frac{\partial P_c}{\partial x}\right) \end{cases} \tag{3.26}$$

and to achieve better numerical stability the solution a change of variable is performed.

As presented in [33], considering the capillary pressure as a potential causes the gradients to be of a high order of magnitude, as the transport coefficients, that would require an higher degree of discretization and a larger number of iterations for a numerical solution. To reduce the magnitudes, it is possible to express the equations in terms of the logarithm to the base 10 of the negative value of the capillary pressure $\log_{10}(-P_c)$. The system of Eq. 3.26 becames:

$$\begin{cases} \rho_0 \frac{\partial u}{\partial t} = \frac{\partial}{\partial x}\left[\delta_p \frac{\partial p_v}{\partial x} + K_l \cdot P_c \frac{\partial \log_{10}(-P_c)}{\partial x}\right] \\ \rho_0 \frac{\partial h}{\partial t} = \frac{\partial}{\partial x}\left(\lambda \frac{\partial T}{\partial x}\right) + h_v \frac{\partial}{\partial x}\left[K_l \cdot P_c \frac{\partial \log_{10}(-P_c)}{\partial x}\right] \end{cases} \tag{3.27}$$

which is the system solved by the software MATCH. Moreover,the model implemented in the software also considers the hysteresis of the moisture retention curve (the curve that defines the moisture content u for every value of φ). The model, also known as "empirical hysteresis model", is also presented in [31] and defines the moisture capacity ξ of the material depending on the moisture content u and the direction of the moisture retention process, absorption or desorption. Once the moisture capacity is calculated, the value of u for the considered value of φ is obtained. The ξ value is calculated from the values of ξ of the absorption curve and the desorption curve, which are given as material properties. The absorption curve is the moisture retention curve obtained conditioning the material after a drying process at 105 °C in a ventilated oven, while the desorption curve is obtained conditioning the material starting from the saturation, after having reached 100 % of relative humidity φ. The ξ could be calculated with Eq.3.28, while u is obtained from the variation of relative humidity $d\varphi$ in the time step $t+1$ with Eq. 3.29.

$$\xi = \begin{cases} \frac{(u-u_a)^2 \cdot \xi_d + 0.1 \cdot (u-u_d)^2 \cdot \xi_a}{(u_d-u_a)^2} & \text{for desorption} \\ \frac{0.1 \cdot (u-u_a)^2 \cdot \xi_d + (u-u_d)^2 \cdot \xi_a}{(u_d-u_a)^2} & \text{for absorption} \end{cases} \tag{3.28}$$

$$u_{t+1} = u + \xi \cdot d\varphi \tag{3.29}$$

Where:

u_a = moisture content for the current relative humidity, according to the absorption moisture storage function (-)

u_d = moisture content for the current relative humidity, according to the desorption moisture storage function (-)

ξ_a = moisture capacity for the current relative humidity, according to the adsorption moisture storage function (-)

ξ_d = moisture capacity for the current relative humidity, according to the desorption moisture storage function (-)

u = moisture content at the actual time step (-)

ξ = moisture capacity at the actual time step (-)

u_{t+1} = moisture content at the next time step (-)

$d\varphi$ = variation of relative humidity (-)

3.2 Künzel's model

The Künzel's coupled heat and moisture transfer model presented in [34] is the model implemented in the WUFI software family. The main features of this model is that the relative humidity φ is chosen as the only moisture transfer potential instead of moisture content u or suction pressure P_c for both vapour and liquid transfer, using the Kelvin's law (Eq. 2.29) and the possibility to differentiate between the liquid transport of suction and redistribution, changing the value of the liquid conduction coefficient whether the liquid water source is present and the transport is driven by capillary suction (suction) or not (redistribution), when the water supply is interrupted. The system of equations used in the model is shown in Eq. 3.30 and the explication of the material properties' dependencies accepted in the software is presented in the variable description. The first of the two equations is the enthalpy balance, while the second equation is the moisture balance.

$$\begin{cases} \frac{\partial h}{\partial T} \cdot \frac{\partial T}{\partial t} = \nabla \cdot (\lambda \nabla T) + h_v \nabla \cdot [\rho_0 \delta_p \nabla (\varphi p_s)] \\ \frac{dw}{d\varphi} \cdot \frac{\partial \varphi}{\partial t} = \nabla \cdot [D_\varphi \nabla \varphi + \delta_p \nabla (\varphi p_s)] \end{cases} \tag{3.30}$$

Where:

w = Moisture content ($\frac{\text{kg}}{\text{m}^3}$)

φ = Relative humidity (-)

T = Absolute temperature (K)

t = Time (s)

ρ_0 = Density of the dry material ($\frac{\text{kg}}{\text{m}^3}$)

$\delta_p(\varphi)$ = Water vapour permeability for the water vapour pressure ($\frac{\text{kg}}{\text{m·sPa}}$)

c = Heat capacity of the dry material ($\frac{\text{J}}{\text{kg·K}}$)

$h(\varphi, T)$ = Total enthalpy of water in all of its phases and of the porous material ($\frac{\text{J}}{\text{m}^3}$)

$\lambda(\varphi, T)$ = Thermal conductivity ($\frac{\text{W}}{\text{m·K}}$)

$h_v(T)$ = latent enthalpy of evaporation of water vapour ($\frac{\text{J}}{\text{kg}}$)

$D_\varphi(\varphi)$ = Liquid conduction coefficient with φ as a potential for suction or redistribution ($\frac{\text{kg}}{\text{m·s}}$)

The liquid conduction coefficient could be obtained from the diffusivity of liquid transfer D_l defined in Eq. 3.5 with the following relation:

$$D_\varphi = D_l \cdot \frac{dw}{d\varphi} = D_l \cdot \rho_0 \cdot \xi \tag{3.31}$$

Where:

ξ = Moisture capacity (-)

ρ_0 = Density of the dry material $\frac{\text{kg}}{\text{m}^3}$

D_l = Diffusivity of liquid transfer $\frac{\text{m}^2}{\text{s}}$

3.3 Grunewald's model

Grunewald's model was first presented in [18], while its numerical implementation, considering also dry air transport and salt transport, was later presented in [19]. This model is implemented in the software Delphin 5 and in its later versions. According to [19], the relative humidity is not an appropriate variable to be chosen as a potential because the high slope of the moisture retention curve after the 99 %. A small variation of relative humidity would cause a large variation of moisture content and moisture contents would need 10 or more significant digits, to avoid this, the capillary pressure is chosen.

Hereby, in Eq. 3.32 only the terms of the equations describing the transport of heat, liquid and vapour. In Eq. 3.32 and 3.33 an attempt to conform the equations to the here used nomenclature is presented. In 3.33 the change of variable (using Kelvin's equation Eq. 2.29), made before the numerical solution of the equations, is performed.

$$\begin{cases} \frac{\partial h}{\partial t} = \nabla \left[\lambda \frac{\partial T}{\partial x} + c_{p,l} \left(K_l \nabla P_c \right) + h_v \left(\frac{\delta_\nu}{R_v T} \nabla p_v \right) \right] \\ \frac{\partial w}{\partial t} = \nabla \left(K_l \nabla P_c + \frac{\delta_\nu}{R_v T} \nabla p_v \right) \end{cases} \tag{3.32}$$

$$\begin{cases} \frac{\partial h}{\partial t} = \nabla \left[\lambda \nabla T + u_w \left(K_l \nabla P_c \right) + h_v \left(\frac{\delta_\nu p_s \exp(\frac{P_c}{\rho_l R_v T})}{R_v T} \nabla P_c \right) \right] \\ \frac{\partial w}{\partial t} = \nabla \left(K_l \nabla P_c + \frac{\delta_\nu p_s \exp(\frac{P_c}{\rho_l R_v T})}{R_v T} \nabla P_c \right) \end{cases} \tag{3.33}$$

Where:

w = Moisture content ($\frac{\text{kg}}{\text{m}^3}$)

T = Absolute temperature (K)

P_c = Suction pressure (Pa)

t = Time (s)

ρ_l = Density of liquid water ($\frac{\text{kg}}{\text{m}^3}$)

$h(P_c, T)$ = Total enthalpy of water in all of its phases and of the porous material($\frac{\mathrm{J}}{\mathrm{m}^3}$)

$\lambda(P_c, T)$ = Thermal conductivity ($\frac{\mathrm{W}}{\mathrm{m}\cdot\mathrm{K}}$)

$h_v(T)$ = latent enthalpy of evaporation of water vapour ($\frac{\mathrm{J}}{\mathrm{kg}}$)

$K_l(P_c)$ = Hydraulic conductivity ($\frac{\mathrm{kg}}{\mathrm{Pa}\cdot\mathrm{m}\cdot\mathrm{s}}$)

4

Damage models

With the possibility to perform more realistic simulations, the evaluation of damage risk with deterministic models became available. With this, it became possible to perform the performance-based design procedures that, depending on the boundary conditions probability, allowed to obtain risk assessments (or performance criteria) for each failure mode.

Even if several of the heat and moisture transfer mechanisms could be simulated with a single model, each material and each failure typology require a dedicated analysis. When the damage criteria are different and depend on different parameters (for example relative humidity, moisture content, temperature or duration in time) the calculated risk will be generally different.

The common approach used in the design practice for the risk calculation is to perform the heat and moisture transfer simulation of the building detail considered and then to apply the algorithm for the damage prediction on the results of the simulation. This approach assumes the hypothesis that the material conditions are similar to the ones obtained in the measurements used for the definition of the damage functions.

In this chapter, some of the most used decay models will be presented with the concern to identify the most relevant variable for their simulation from the available literature. Moisture content and relative humidity are the common outputs of the heat and mass transfer simulations and, given the simplifying hypotheses of neglecting the hysteresis of materials, the two variables are considered to be equivalent and connected by a one-to-one moisture retention curve. When this hypothesis is abandoned, then the two variables have different physical meanings and therefore should be distinguished in the decay modelling.

4.1 Mould growth

What is commonly indicated as mould growth is a visual, non-structural damage dangerous for inhabitants' health, caused by the growth of one or more fungi species due to a high humidity content in buildings materials. [35] identified in literature about 200 species of fungi likely to grow in built environment. It usually happens on the interior

surface of external walls of low insulated buildings or in rooms without a proper ventilation. It appears as dark coloured spots on cold and not ventilated surfaces of the walls, on thermal bridges or behind the furniture. The mould found on building materials is composed by different types of fungi, that could be harmful to inhabitants in different ways. The mould fungi's natural habitat are humid, decomposing plants in soil and, for this reason, they could be found in every season and in nearly every environment [35]. Among the factors affecting mould growth, six parameters have been identified by [35]:

- Temperature;
- Relative humidity;
- Nutrients and salt content;
- pH value of surface;
- duration of exposure;
- oxygen content.

Among these, relative humidity, temperature and duration of exposure are the ones used in risk assessment procedures. Despite the well established design codes and advanced procedures, the mould growth models are not able to predict the actual behaviour of the fungi on the building materials. Due to the high number of factors involved, many could be the reasons that invalidate the calculated predictions. Examples of this discrepancies between model and reality are presented in [36] that considered other substrates than wood, typical of interior surfaces of residential buildings (gypsum board, areated concrete, wallpaper, paint, non woven glass felt and plaster). On the other hand [37] using substrates of pine wood, confirmed the reliability of the models in real conditions for the materials considered in the studied that developed the mould growth models. The VTT model and the WUFI Bio model obtained results closer to the experiments.

4.1.1 EN ISO 13788:2012

In order to avoid the mould growth on the internal surfaces of the walls, the standard EN ISO 13788:2012 prescribes to keep the internal superficial relative humidity values under the 80 % . This approach could be used with simple stationary heat transfer simulations and it complies to the Italian legislation (D.M. 26/06/2015). The standard differentiates the procedure for some details. With different boundary conditions, changing the external temperatures and indoor conditions, the conditions are adapted to the studied phenomenon.

Depending on the studied detail a different set of boundary conditions is prescribed.

- The external temperatures should be those, representative of a location, likely to occur once in 10 years. With this choice the weather file is a critical year positioned close to the 10 % of the cumulative distribution of the air dry-bulb temperature. Alternatively, if only typical weather years are available, then the air dry-bulb temperature should be increased of 2 K during the cooling months and reduced of 2 K during the heating months;

- When the calculation is performed for the solid ground floor or walls that are not exposed to the outdoor air, but to the ground, the ground should be included in the model domain for 2 m, below the floor and the monthly mean temperature in the ground should be calculated as the mean between the annual mean temperature and the monthly temperature shifted by one month, or, for a more detailed calculation, the monthly mean temperature obtained from the ISO 13370;

- For suspended floors also the ISO 13370, Annex E, should be used;

- For the roof the temperatures should be calculated considering the solar gains and the cooling by the long wave radiation, using the methodology described in ISO 13790.

On the other hand the relative humidity values are set to the monthly mean vapour pressure of the chosen weather year and to 100% for the ground.

For lightweight components, such as window frames, the critic relative humidity limit is moved to the 100 % and the external temperature, that defines the acceptable return time of the failure, is average of the minimum daily temperatures of a period longer than a year and the external relative humidity is 85 %.

When hourly simulation results are available, more advanced mould growth model could be used. These models generally agree on the fact that fluctuating conditions of the considered surface can slow the growing process [38] and, starting from the temperature and moisture-related conditions, try to predict the grow rate of the mould.

An extended systematic literature review of these methods limited to wood could be found in [38]. In this review the authors conclude that the models in literature have substantial differences in the calculation processes and in the way the result are represented, increasing the difficulty for the comparison of the efficiency. Generally the governing factors identified are temperature, relative humidity and time of exposure, but there are discrepancies on the growth interval. These differences are also caused by the fact that the models are obtained from different experimental setups.

A comparison of the results from different mould models is presented in [39] and a comparison with experimental results is shown in [40, 41]. A general disagreement has been found in both cases, among the models and the experimental results.

In order to overcame some of these discrepancies [42] presented a correlation between the results obtained from VTT model , expressed in terms of Mould Index, to the bio-hygrothermal mould growth model results, expressed in mm of mycelia (the roots of the fungi that compose the mould) growth. The **VTT model (also Viitanen model)**, developed at the VTT Technical Research Centre of Finland, presented in [43] and improved in [44] is also implemented as a post processing tool for the calculations of Delphin (in PostProc) and Wufi Pro (in Wufi Bio). The model has been developed from large laboratory studies on pine sapwood, then extended to other materials with corrective coefficients. The calculation of the mould index (M) from temperature, relative humidity and time of exposure is obtained from the integration of the derivative of M considering the time series of temperature (T) and relative humidity (φ):

$$\frac{dM}{dt} = \frac{k_1 k_2}{7 \cdot \exp(-0.68 \ln T - 13.9 \ln \varphi + 0.14W - 0.33SQ + 66.02)} \tag{4.1}$$

with:

- SQ Surface quality: 0 for sawn and 1 for kiln dried (used only for timber materials);
- W Wood type: 0 for pine or 1 for spruce (used only for timber materials);
- For other materials $W = 0$ and $SQ = 0$ are used.

The resulting M should be interpreted according to the following scale:

0. No growth;
1. Small amounts of mould on surface (microscope), initial stages of local growth;
2. Several local mould growth colonies on surface (microscope);
3. Visual findings of mould on surface, <10 % coverage, or <50 % coverage of mould (microscope);
4. Visual findings of mould on surface, 10 - 50 % coverage, or >50 % coverage of mould (microscope);
5. Plenty of growth on surface, >50 % coverage (visual)
6. Heavy and tight growth, coverage about 100 %

The **biohygrothermal model**, developed at the Fraunhofer Institute for Building Physics IBP and presented in [35]. After the identification of an hazardous class of fungi a hygrothermal balance of a hypothetical spore is calculated on the surface of the considered walls. The spores are modelled with a moisture retention curve and moisture diffusion coefficient. During the time the spore reaches a sufficient moisture content the mycelia are considered to grow, when the moisture content is low, the growth is interrupted. This method is based on the isopleths curves, curves in the $T - \varphi$ plane used to identify the growth rate associated with every $T - \varphi$ coordinate. The growth is divided in two phases, the first is the spore germination, in which the hyphen is not growing in lenght, the second is the mycelia growth. For the germination and the mycelia growth two different isopleths systems are necessary. The curves are identified as Lowest Isotherm for Mould (LIM), "the temperature dependent lowest relative humidity under which no fungus activity (spore germination or mycelium growth) is expected" (from [35]). A different LIM is identified for the following substrates:

Optimal culture medium;

I biodegradable building materials;

II building materials containing some biodegradable compounds (Building materials with high open porosity like brick or stucco);

III non-biodegradable building materials without nutrients(it is assumed that formation of mould fungi is not possible).

4.2 Wood decay

Wood decay is one of the most relevant moisture related damages. Due to fungi attack, the wooden structural parts are reduced in mass and strength. The wood decay process involves fungi growth and the grow rate depends, among other factors, on the wood type and on the fungi typology. The main typologies of rot depend on the fungi species and they are divided in three categories [45]:

- White rot, in which the colour of the wood appears clearer;
- Soft rot, causing decay of a shallow depth;
- Brown rot, the most common type in buildings, of a dark colour, the wood presents a "cubical checking appearance".

In most of the cases the decay is a result of the coexistence of different species, communities, that could build different kinds of relationships [46]. As presented in [47], it is agreed that the decay process is critically activated after the reaching of the fibre saturation point. It is well known that the fibre saturation point for the majority of woods is found between the 20 % and the 30 % of moisture content in mass [48], so that 20% is used as limit value for wood decay safety, even if laboratory tests presented in [49] have shown minimum moisture threshold (at 2 % of mass loss) for Norway spruce even at 16.3 % of moisture content in mass. Differently to Mould growth, wood decay is considered to be driven by moisture content: when free water is present in the cell walls, the fungi will start the degradation of the wood cellular structure. For this reason, the common assumption of a one to one function for the moisture retention curve, not considering the hysteresis, could lead to a misinterpretation of the conditions of the wood. In the extensive literature review for the available models for fungal wood decay presented in [50] it is shown that the first approaches to the problem were the climate indeces, for example the Climate Index developed by Scheffer [51], that provides an evaluation of the decay of wood that can be used for the comparison between geographic locations. The index is calculated considering the temperature and the number of days of rainfall. In absence of heat and moisture transfer simulation tools able to calculate the temperature and moisture content of timber structures, the only variables that could be used in wood decay evaluations are the environmental values of rainfall intensity, dry-bulb air temperature and relative humidity. Also, the widely used [52, 53, 54] VTT wood decay model, presented in [55], that calculates the mass loss due to fungi growth from the hourly values of temperatures and relative humidity, could be used to associate mass loss values to the weather file of a given location. With the hypothesis that the wooden detail of the buildings is in equilibrium with the environment, the authors proposed a series of maps of wood decay risk. With the now available heat and moisture transfer simulation tools it is possible to abandon this hypothesis and extend the validity of the model to wooden elements not in contact with the external environment, for example, subject to interstitial water accumulation. These models are also subject to other hypotheses limiting the representativeness of the results:

- The geometry of the studied domain is constant;
- The properties of the materials depend only on moisture content and temperature, and are not influenced by the decay process;

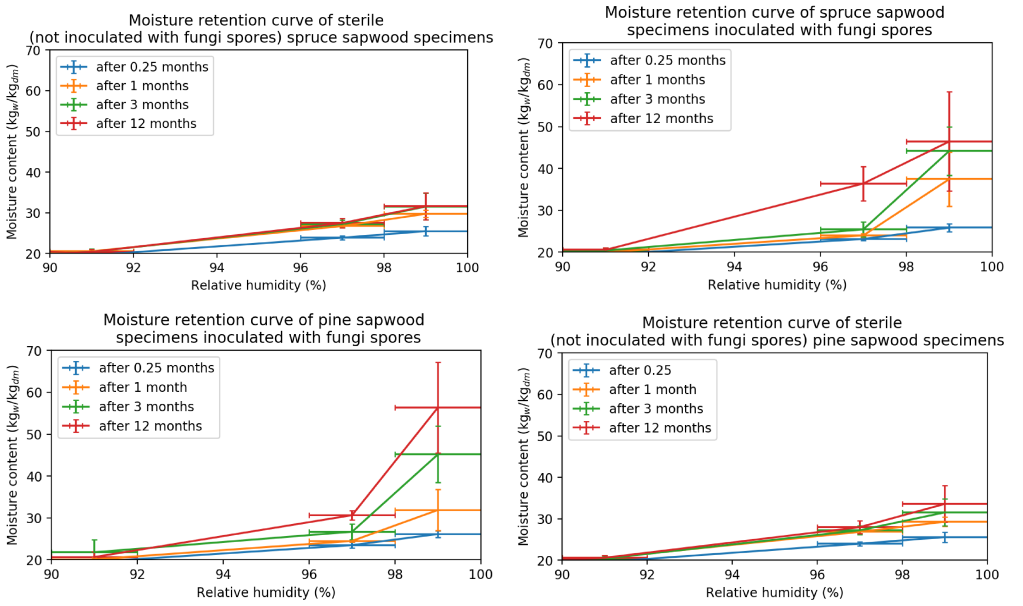

Figure 4.1: Moisture retention curves of wood specimens at 20°C presented in [57].

- The fungi do not produce water during the digestion process.

All of these hypothesis are not realistic but their effect is supposed to be negligible. In the presentation of the laboratory results of the VTT wood decay model [55], the water contents of the wooden samples are different between the samples inoculated with the fungi and the sterile control samples without the fungi. The results are presented in the plots in Fig. 4.1. It can be observed that the water contents of the inoculated with the fungi are higher, even if the test specimen is kept in hygrothermal equilibrium with salt solutions. The same behaviour is shown in [56], where the authors present a correlation between mass loss and temperature valid over critical values of relative humidity, together with a relation between the mass loss and the moisture production due to the decay for the Japanese red pine.

Following, the VTT wood decay model and the Logistic dose-response model are presented and discussed.

4.2.1 VTT wood decay model

The wood decay model presented in [55, 58] considers the relative humidity and the temperature in the wood element and allows to calculate the mass loss (ML) due to the fungi presence. The model is based on laboratory experiments on brown rot fungi on pine sapwood and spruce specimens. Using the relative humidity values instead of the moisture content the model allows also to draw hazard maps based on the weather measurements.

The correlation between mass loss (ML) and the stationary environmental conditions (relative humidity and temperature) has been first presented in, then in [57] a method

to calculate the ML in dynamic conditions is presented. The method consists in the calculation of the starting period, previous to the rot, and then, integrating the time derivative of the ML expression for the stationary conditions, with the dynamic values of temperature and relative humidity, it is possible to calculate the ML.

First, the authors present the ML calculation method for stationary conditions for pine:

$$\begin{aligned} ML_P(\varphi, T, t) = &- 42.945 \cdot t - 2.227 \cdot T - 0.0347 \cdot \varphi + \\ &0.1384T \cdot t + 0.0244 \cdot T \cdot \varphi + 0.437 \cdot \varphi \cdot t \end{aligned} \tag{4.2}$$

Where φ, T and t are respectively the relative humidity expressed in %, temperature in °C and time of exposure expressed in months and ML is the mass loss expressed as percentage of the original mass. The values φ and T are considered to be constant over the period t. This correlation is valid only above 95 % of relative humidity, corresponding to the fibre saturation point, and for Temperatures higher than 0°C. Then a model for sprice sapwood is presented:

$$\begin{aligned} ML_S(\varphi, T, t) = &- 41.224 \cdot t - 2.731 \cdot T - 0.0251 \cdot \varphi + \\ &0.1724 \cdot T \cdot t + 0.0291 \cdot T \cdot \varphi + 0.416 \cdot \varphi \cdot t \end{aligned} \tag{4.3}$$

The model for the variable conditions requires first the evaluation of the activation process. For each time-step considered the value of $\alpha(t)$, expressed as number between 0 (dry condition) and 1 (rot process activated), has to be calculated. The function α is defined in such way that when it reaches 1, after two years of dry conditions its value decreases linearly to 0:

$$\alpha(t) = \int_0^t d\alpha = \sum_0^t (\Delta\alpha) \text{with} \tag{4.4}$$

$$\Delta\alpha = \begin{cases} \frac{\Delta t}{t_{crit}(\varphi, T)} & \text{when } T > 0 \text{ and } \varphi > 95\%, \\ -\frac{\Delta t}{17520 \text{ h}} & \text{otherwise} \end{cases} \tag{4.5}$$

For pine sapwood:

$$t_{crit,P}(\varphi, T) = \frac{2.227 \cdot T + 0.0347\varphi - 0.0244 \cdot T \cdot \varphi}{-42.945 + 0.1384 \cdot T + 0.437\varphi} \cdot 30 \cdot 24 \text{ h} \tag{4.6}$$

while for the spruce sapwood:

$$t_{crit,S}(\varphi, T) = \frac{2.731 \cdot T + 0.0251\varphi - 0.0291 \cdot T \cdot \varphi}{-41.224 + 0.1724 \cdot T + 0.416\varphi} \cdot 30 \cdot 24 \text{ h} \tag{4.7}$$

For each time-step with $\alpha(t) = 1$ mass loss occurs and it could be calculated with the following equation:

$$ML(t') = \int_{t \text{ at } \alpha=1}^{t'} \frac{ML(\varphi, T)}{dt} = \sum_{t \text{ at } \alpha=1}^{t'} \frac{ML(\varphi, T) \cdot \Delta t}{dt} \tag{4.8}$$

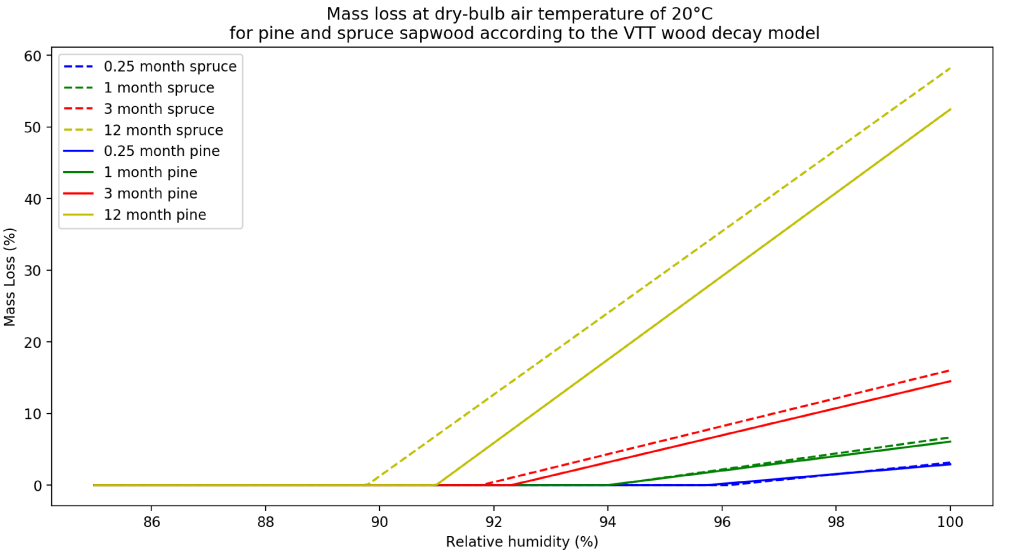

Figure 4.2: Mass loss of wood specimens at 20°C at different relative humidity values, according to VTT wood damage model.

with

$$\frac{ML(\varphi, T)}{dt} = -5.96 \cdot 10^{-2} + 1.96 \cdot 10^{-4} \cdot T + 6.25 \cdot 10^{-4} \cdot \varphi \tag{4.9}$$

In this case t is expressed in hours and the mass loss ML in percentage. In figure 4.2 the mass loss resulting from the VTT wood decay correlation is presented for different values of relative humidity. The correlations are different for the spruce and pine sap wood and for short periods of exposition the mass loss of the two wood types are similar.

In 4.3 the correlation between mass loss and the moisture content of wood is presented. The moisture content values are the lower bound values of the inoculated test samples presented in [57] for the spruce and pine sapwood at each considered time of exposure. The critical minimum moisture content that could activate the rot process for a year of exposure is above 20 % of mass content for the pine sap wood while for the spruce sap wood it is found to be lower than the 20 %. Anyway, as reported by the authors, a significant mass loss, above 5 %, is expected from moisture contents higher than the 20 %.

It is interesting to observe that the moisture retention curves change with the exposure time and between the inoculated and the sterile samples. The plots of the moisture retention curve are presented in 4.1

4.2.2 Logistic dose-response model

The logistic dose-response model, first presented in [59] is based on field test results on Scots pine sapwood and Doulgas fir heartwood test specimens in 23 different European test sites and it is intended for the implementation in performance based building codes

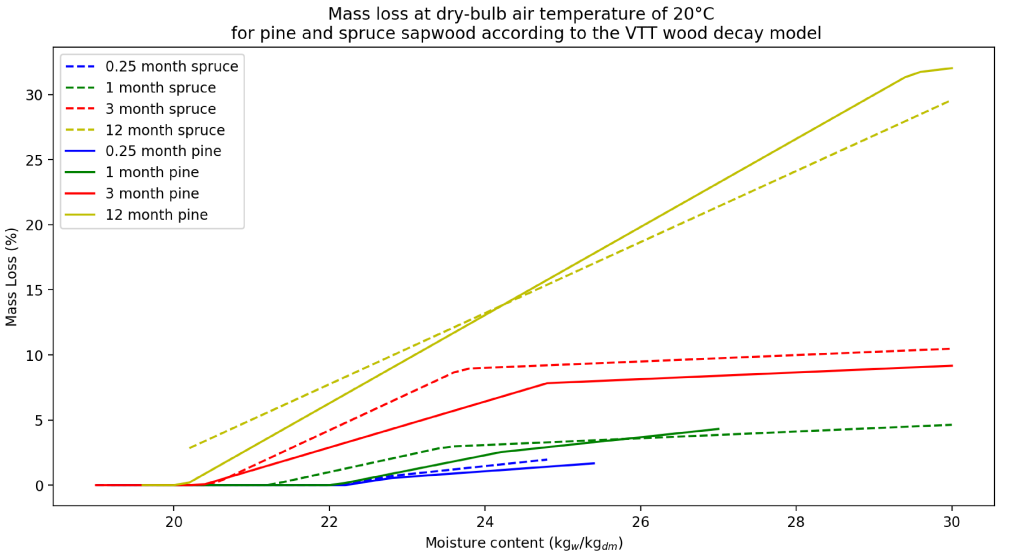

Figure 4.3: Mass loss of wood specimens at 20°C at different moisture contents, according to VTT wood damage model. The moisture contents are obtained from the test samples presented in [57].

and regulations.

The model is obtained as a correlation of the rot decay in terms of mean decay rating according to EN 252 (1990), a classification between 0 and 4:

0. **Sound**: No evidence of decay, discoloration, softening or weakening caused by microorganisms;

1. **Sight attack**: Limited evidence of decay, no significant softening or weakening up to 1 mm depth (corresponding to 4 % mass loss of the VTT wood decay model);

2. **Moderate attack**: Signification evidence of decay, with areas of decay (softened or weakened wood) from 2 to 3 mm depth (corresponding to 8 % mass loss of the VTT wood decay model);

3. **Severe attack** Strong evidence of decay, extensive softening an weakening, typical fungal decay at large areas from 3 to 5 mm depth or more (corresponding to 12 % mass loss of the VTT wood decay model);

4. **Failure**: Sample breaks after a bending test (corresponding to 16 % mass loss of the VTT wood decay model).

The model considers the daily mean values of moisture content in mass and temperature and not the relative humidity. In [60] it has been observed that using the moisture content allows the model to be independent to the wood type. On the other hand, the field tests used to obtain the correlation were exposed to high moisture contents (above 25 % in mass) and could be not representative of the conditions of timber elements in

buildings. Also, the activation process is not considered, also due to the field experimental conditions. The method is applied with the calculation of the dose value $D(n)$, with n number of days of the considered period:

$$D(n) = \sum_{1}^{n} D_i \tag{4.10}$$

with D_i, the daily dose, calculated as

$$D_i = (3.2 \cdot D_T(T) + D_u(u)) \cdot (3.2 + 1)^{-1} \tag{4.11}$$

with a temperature weighting factor, with D_u daily dose dependent on moisture content in mass u:

- if u≤25 %

$$\begin{aligned} D_u(u) =& 6.75 \cdot 10^{-10} \cdot u^5 - 3.50 \cdot 10^{-7} \cdot u^4 + 7.18 \cdot 10^{-7} \cdot u^3 + \\ & 7.22 \cdot 10^{-3} \cdot u^2 + 0.34 \cdot u - 4.96 \end{aligned} \tag{4.12}$$

- for the other values of u, $D_u(u) = 0$;

amd D_T daily dose dependent on daily average temperature value T:

- if T_{min} ≥0 °C or if $T_{max} \leq 40$ °C

$$\begin{aligned} D_T(T) =& 1.8 \cdot 10^{-6} \cdot T^4 + 9.57 \cdot 10^{-5} \cdot T^3 - 1.55 \cdot 10^{-3} \cdot T^2 + \\ & 4.17 \cdot T \end{aligned} \tag{4.13}$$

- And when T_{max} assumes other values, $D_T(T) = 0$.

The mean decay rating DR, according to EN 252(1990), is calculated from $D(n)$ with the dose-response function:

$$DR(D(n)) = 4 \cdot \exp(-\exp(1.7716 - (0.0032 \cdot D(n)))) \tag{4.14}$$

Another version of the model was presented in [61], with a simplified approach. The model, also referred as simplified logistic dose-response model, is designed to produce positive dose values also for moisture contents lower than the limit, which has been set to 30 % instead of 25 %. The only condition that sets the dose to 0 is for temperature lower than 0 °C.

$$D = D_u(u) \cdot D_T(T) \tag{4.15}$$

$$D_u(u) = \begin{cases} (u/30)^2 & \text{if } u \leq 30\% \\ 1 & \text{if } u > 30\% \end{cases} \tag{4.16}$$

$$D_T(T) = \begin{cases} 0 & \text{if } T < 0°\text{C} \\ t/30 & \text{if } 0°\text{C} \leq T \leq 30°\text{C} \\ 1 & \text{if } T > 30°\text{C} \end{cases} \tag{4.17}$$

The simplified logistic dose-response model has a lower degree of determination than the logistic dose-response model. The decay rating according to EN 252 is obtained with the relation 4.18.

$$DR(D(n)) = 4 \cdot \exp(-\exp(1.9612 - (0.0037 \cdot D(n)))) \tag{4.18}$$

The DR value will be a value up to 4 and, due to the model definition, the value is less likely to be equal to 0, like in the logistic dose-response model. In this way, it is possible to compare the performance of two solutions that present low decay levels.

In [61] it is observed that the logistic dose-response model is obtained from conditions with high moisture contents, above 25 % in mass, which are not common in timber dwellings, so a more general method is presented, based on linear relations: the two-step dose-response model. Also, it is observed that this model should be used to evaluate the initiation period and not for the subsequent growth process [61]. The model is based on Douglas fir heartwood data, with long periods with moisture content values below 25 % in mass. Similarly to the previously presented models, first the dose is calculated with the equations:

$$D(n) = \sum_{1}^{n} D_i \tag{4.19}$$

$$D_i = D_T(T) \cdot D_u(u) \tag{4.20}$$

$$D_u(u) = \begin{cases} 0 & \text{if } u < a \\ \frac{u-a}{b-a} & \text{if } a \leq u \leq b \\ 1 & \text{if } u > b \end{cases} \tag{4.21}$$

$$D_T(T) = \begin{cases} 0 & \text{if } T < c \\ \frac{T}{d-c} & \text{if } c \leq T \leq d \\ 1 & \text{if } T > d \end{cases} \tag{4.22}$$

where u is the percentage of moisture content in mass, T is the wood temperature expressed in °C. The coefficients are used to set the mould growth limits and set back points:

- a and b are the lower and upper boundaries of the critical moisture content interval in which the decay fungi are expected to grow, they could be set respectively to 25 and 30 %;
- c and d are the lower and upper boundaries of the critical temperature interval, set to 0°C and to 30 °C respectively;

The decay rating $DR(D(n))$ according to EN 252 is calculated according to Eq. 4.23. The value 130 is set as the lowest dose value before the decay and it is obtained as the average between the values of Douglas fir and Scots pine.

$$DR(D(n)) = \begin{cases} 0 & \text{if } D \leq 130 \\ 0.0051 \cdot D - 0.66 & \text{if } D > 130 \end{cases} \tag{4.23}$$

4.3 Metal corrosion

Another damage typology that could be caused by moisture is the corrosion of metal inclusions. When a porous building material is reinforced with metal inclusions and moisture transfer is allowed around them, then it is possible to calculate the temperature, relative humidity or the moisture content around the metal elements and, if a correlation is available, its corrosion rate at a given time. The corrosion by carbonation process is activated after the carbonation of the mortar (or concrete) around the inclusions. This phenomenon depends on the carbon dioxide diffusion in the material that could be modelled as well with the moisture and heat transfer. For the case of concrete, this model has been presented in [62]. In alternative it could be considered as a separate phenomenon, that will be interrupted during rainfall (water stops carbon dioxide diffusion), with simplified models, like [63, 64]. Also this kind of simulation relies on simplifying hypotheses, among the others:

- the geometry of the domain is not deformed by the expansion of the metal oxides;
- the metal inclusions are not in contact with noble materials that could increase the corrosion rate [65];
- the mortar carbonation has reached the surface of the inclusions; absence of sacrificial anodes or impressed currents that could provide cathodic protection;

In [66] and [67] a simple approach to the problem is presented for historical mortars. This method allows to calculate the time of corrosion of a bar, considering the initiation phase, characterized by the diffusion of carbon dioxide in mortar or concrete (modelled with one of the aforementioned models), and the corrosion phase, in which the reduction of the metal inclusion section is calculated from relative humidity and temperature.

First, the correlation between the corrosion rate and the relative humidity and temperature in the proximity of the metal inclusion is obtained from experimental results, then the model is used on the results of an heat and moisture transfer simulation. The experimental results are obtained in terms of moisture content and then converted with a moisture retention curve to relative humidity values. By hypothesis, corrosion is not considered to influence or to be influenced by the heat and moisture transfer. If the expansion of the oxides is considered to have developed a crack in the geometry a heat and moisture transfer in cracked media model should be preferred, for example [68, 69].

The corrosion rate i_{corr} is expressed as current density ($\mathrm{mA/m^2}$) and it is calculated according Eq. 4.24:

$$i_{corr} = \begin{cases} d_1 \cdot T \cdot \exp(a_1 \cdot T + b_1 \cdot \varphi + c_1) & \text{if } \varphi \leq 95\% \text{and } T > 0°\mathrm{C} \\ \frac{(k-100)\cdot\varphi}{100\cdot(k-\varphi)} \cdot a_{sat} \cdot T^{b_s at} & \text{if } \varphi > 95\% \text{and } T > 0°\mathrm{C} \\ 0 & \text{if } T \leq 0°\mathrm{C} \end{cases} \tag{4.24}$$

The parameter k, defined in Eq. 4.25 is used to smoothly connect the corrosion rate obtained in the hygroscopic region with the values of the over-hygroscopic region.

$$k = a_2 \cdot T^{b_2} + c_2 \tag{4.25}$$

Table 4.1: Thickness of corroded steel in the reinforcement bars in concrete walls or columns facing the external environment.

Concrete cover (cm)	Corrosion thickness (µm)
1	148
2	121
3	9
4	-

The parameters a_1, b_1, c_1,a_2, b_2 and c_2 are regression parameters. From the corrosion rate valure i_{corr} it is possible to calculate the thickness s of the metal inclusion lost over time by corrosion with the Faraday law:

$$\frac{ds}{dt} = 1.17 \cdot i_{corr} \tag{4.26}$$

With $\frac{ds}{dt}$ expressed in µm/year. This value is the reduction of the resisting area of the metal inclusions and, moreover, when a corrosion of 20 µm is reached, the oxides expansion causes the cracking and spalling of the concrete.

A similar approach was used in [70] to calculate the corrosion of metal fasteners embedded in wood. In this case, the corrosion rate calculation is performed with moisture content and temperature.

As an example of application, in [71] the correlations presented in [67] have been used to perform a series of simulation of the corrosion of a steel rebar in concrete in the city of Udine. The results are presented in Tab. 4.1. The corrosion thickness is calculated after a period of 50 years for 4 thicknesses of concrete cover (the layer of concrete that separates the bar from the exterior environment. The simulations were in compliance with the recommended value of the concrete cover in the Italian regulations: a concrete cover of at least 5cm should avoid the corrosion issues and following cracking.

4.4 Freeze-thaw damage

When the water fills the material's pores of the outer layer of a building and the temperature decreases under the freezing point, then the ice formations increase in volume, inside the pores, causing the cracking of the material. This damage concerns mainly cold climate zones and it can be triggered also in existing buildings when a change is made in the heating schedules or in the insulation of the envelope. For example, the envelopes of historical buildings, with low levels of insulation, have high energy consumptions and are crossed by a high heat flux and, as an effect, have high temperatures on the external surfaces. When, for the purpose or reducing the energy consumptions, the walls are retrofitted with large layers of insulation, the heat flow rate is reduced and the temperature on the external surface is lower, then it is possible that, during a cold winter, the water in the porous of the outer material, very likely to be stone, cracks for the excessive and repeated expansion of the ice. This could also happen if a building is

abandoned and the heating system is not contributing to increase the temperatures of the envelopes during winter.

A simple approach for the evaluation of the performance of a building envelope is the counting of the freeze-thaw cycles that the materials are expecting just computing the times that the temperature values cross the 0°C [72, 73].

Another, more advanced risk evaluation criterion is the determination of the critical degree of saturation using frost dilatometry. This method, first presented in [74] and used in [75],[76], [77] and [78] is based on the assumption that the damage due to freeze-thaw cycles happens only above a critical degree of saturation which could be determined by a laboratory procedure and not only at the saturation of the material. For example, if the saturation degree of a solid clay brick is at $u_{sat} = 0.22$, the critical saturation for the freeze-thaw cycle damage could be at $u_{[}crit = 0.19$. Once that the critical moisture content is identified it is possible to reduce the risk by designing the building envelope avoiding to reach the freezing point at 0 °C at the critical saturation content in the most exposed material of the wall.

In order to compare different design solutions it is possible to count the freeze-thaw cycles when the material reaches the critical saturation or to use other indicators such as the FTDR Index presented in [79].

5

Glaser method

This chapter is a summary of the results presented in [9]. The finality of the analysis is to assess the reliability the Glaser method (according to EN ISO 13788:2012) for the moisture accumulation risk assessments of building envelopes. The Italian legislation (Ministerial Decree of 26th June 2015) allows to perform the interstitial condensation risk analysis with both the Glaser method (monthly mean stationary method according to UNI EN ISO 13788:2013) and the advanced hourly transient simulations according to UNI EN 15026:2008. The choice between the methods is left on the designer, and thus it is not frequent that an advanced analysis is performed. Advanced risk analysis require an additional validated software tool (for example WUFI Pro, DELPHIN or MATCH), the availability of the advanced material properties (rarely provided by the material suppliers), the availability of the proper weather files, that should be selected to be representative of the critical weather events, in order to provide a conservative weather simulation.

The mentioned accurate simulation methods are based on coupled heat and moisture (HM) numerical models. The complexity of the HM models is clear starting from the seminar works on the models constructions, such as [80, 81], therefore a numerical implementation ([82, 83, 84]) is required, not without any complication due to the numerical representation of the driving potentials of the model equations (complications that are not found, for example in the conduction based heat transfer models) and user friendly software tools software simulation tools have been released. One of these, WUFI Pro [85], is used in this chapter following the UNI EN 15026:2008 standard. These models are utilised for many advanced applications, such as the ones presented in [67, 86, 87]. The considered HM model is quickly described in Subsection 3.2.

5.1 Assumptions

The Glaser method has been implemented using the integrated development environment Octave (Manual: [88]). The used script is available online at [89]. This method is based on many simplification assumptions listed in the describing standard, the ones that involve the model are:

- The moisture transfer phenomena in porous materials are slow, and thus, simulating the weather variables with the monthly mean values would cause negligible errors,
- Water vapour pressure distribution in a one-dimensional wall is influenced by the temperature distribution only when the dew point T_{dew} of saturation is reached inside the wall.
- The heat transfer caused by phase changes and thermal mass effects are ignored.
- liquid water transport is negligible.
- The material properties are independent of the temperature and the moisture content.
- The effects of driving rain and sun light are not considered.

5.1.1 Equations

With these hypotheses, the model is described by the stationary heat conduction law (Eq. 5.1) and by Fick's diffusion (Eq. 5.2).

$$\frac{\partial}{\partial x}\left(\lambda \frac{\partial T}{\partial x}\right) = 0 \tag{5.1}$$

$$\frac{\partial}{\partial x}\left(\delta_p \frac{\partial p_v}{\partial x}\right) = 0 \tag{5.2}$$

Then, the heat flux and the vapour flux could be calculated as:

$$q = -\lambda \frac{\partial T}{\partial x} \tag{5.3}$$

$$g_v = -\delta_p \frac{\partial p_v}{\partial x} \tag{5.4}$$

With these limitations, the Glaser method cannot be used for prediction purposes. For the ease of application and for the availability of the material properties, the Glaser method is often the only available procedure for technicians to perform moisture control in building envelopes and it could be used to evaluate the hygrothermal performance of a wall in a given weather.

5.2 Comparison

Few comparisons between HM models and the Glaser method are found in the literature. In [90] the Glaser method is compared to an early version of WUFI. A build-up of a cathedral roof is considered, and the amount of moisture stored in the build-up is evaluated varying the vapour permeability of a vapour retarder layer. According to [90] the moisture calculated by the Glaser method is comparable and conservative with respect to WUFI results since the considered structure has low thermal mass and because

the application the German standard that imposed conservative boundary conditions. Another comparison between an HM transient model and the Glaser method is presented in [91]. The considered structure is a cellular concrete roof and the Glaser method is compared to the results of a simulation performed with the model of Philip and De Vries [81]. The results of the Glaser method were less conservative. In both cases, the considered HM models are reported to be validated with experiments, and are expected to be more reliable than the Glaser method.

5.2.1 Method

The simulations are performed according the standards UNI EN 15026:2008 and UNI EN ISO 13788:2013 for four single-layer walls and for six wall types (depicted in Fig. 5.1). The single-layer walls are used as simple cases that allowed to identify general behaviours, while the six wall types were used as realistic cases.

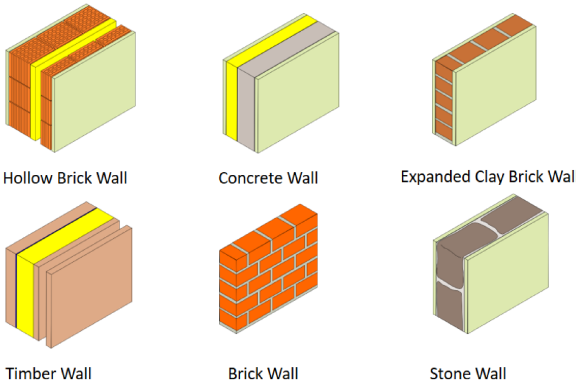

Figure 5.1: Wall types considered in this chapter and described in Table 5.1

The internal boundary conditions are obtained from the weather files according to the EN ISO 15026 standard for both the considered methods risk assessment methods.

The external boundary conditions for the HM transfer model are obtained from the weather files, and, in order to compare only the transport phenomena the driving rain and sun radiation are not used as boundary conditions. The Glaser method boundary conditions are obtained from the mean monthly temperatures and relative humidity of the weather files. The surface resistance values are R_{se} =0.04 $\frac{\mathrm{m^2 \cdot K}}{\mathrm{W}}$ and to R_{si} =0.13 $\frac{\mathrm{m^2 \cdot K}}{\mathrm{W}}$ according to the EN ISO 6946 standard.

The HM transfer simulation is a transient simulation, therefore the initial conditions influence the results of the simulation. In order to avoid the effects of the initial conditions, the simulations are performed for three years and only the last year of the simulation is considered, when the wall has reached the equilibrium with the environment.

The results of the HM transfer model are a hourly distributions in the wall of moisture content values, vapour pressures, saturation pressures, temperatures, moisture and

Table 5.1: Building envelope build-ups thermal properties

Wall Type	U $\left(\frac{\mathrm{W}}{\mathrm{K}\cdot\mathrm{m}^2}\right)$	c $\left(\frac{\mathrm{J}}{\mathrm{K}\cdot\mathrm{kg}}\right)$	S (m)	$w_{\vert_{\varphi=0.8}}$ $\left(\frac{\mathrm{kg}}{\mathrm{m}^3}\right)$
Solid brick wall	1.800	1530	4	1
timber wall	0.111	390	1537	20
Expanded clay block wall	0.452	760	3	6
Stone wall	1.824	1710	34	3
Hollow brick wall	0.251	550	8	6
Concrete brick wall	0.527	1440	35	13

heat fluxes. The result of Glaser method are the monthly mean distributions of temperatures and vapour pressures. In order to compare the two, the Glaser method vapour pressures are used to calculate the moisture content of the walls (indicated with w_G), using the moisture retention curves of the materials, and then these are compared with the monthly mean values of the HM transfer model results (indicated with w_{Wm} for the hourly values and w_W for the monthly mean values). The moisture content calculated with the Glaser method w_G is obtained from the vapour transport only, while the liquid water transfer is neglected.

The calculated variables for the comparison are:

w_W^{max} = the maximum moisture contents calculated with the HM transfer model

w_W^{min} = the minimum moisture contents calculated with the HM transfer model

w_{Wm}^{max} = the monthly mean maximum moisture contents calculated with the HM transfer model

w_{Wm}^{min} = the monthly mean minimum moisture contents calculated with the HM transfer model

w_G^{max} = the monthly mean maximum moisture contents calculated with the Glaser method

w_G^{min} = the monthly mean minimum moisture contents calculated with the Glaser method

The comparison is held with the parameter Δw (hourly values) and Δw_m (monthly values) defined respectively by Eq.5.5 and Eq. 5.6.

$$\Delta w = w_G - w_W \tag{5.5}$$

$$\Delta w_m = w_G - w_{Wm} \tag{5.6}$$

While the relative differences, expressed in % are calculated as follows:

$$\Delta w = \frac{w_G - w_W}{w_W} \tag{5.7}$$

$$\Delta w_m = \frac{w_G - w_{Wm}}{w_{Wm}} \tag{5.8}$$

Then the maximum and minimum values of the relative differences (calculated hourly) are expressed by $\Delta w_{\%}^{max}$ and $\Delta w_{\%}^{min}$. The maximum and minimum values of the absolute differences are indicated with $\Delta w_{\%}^{max}$ and $\Delta w_{\%}^{min}$, while the monthly mean values are Δw_m^{max} Δw_m^{min}.

5.3 Results

Four simulations of single-layer walls of fictitious materials with the same boundary conditions are performed in order to compare the behaviour of the considered methods in terms of mean monthly moisture contents. The weather file of Udine (from [92]) is used as outdoor climate. To evaluate the effect of the steady state simplifying hypothesis, four fictitious materials are created changing the properties that influence the thermal and hygroscopic transient behaviour. The property that influences the transient moisture transfer is the moisture retention curve which is taken alternatively from a Hygroscopic material (H) (20 kg/m^3 at $\varphi = 80\%$) and a Non-Hygroscopic material (NH) (2 kg/m^3 at $\varphi = 80\%$). The thermal mass is the property that influences the transient heat transfer and it is set to a high value (HTM), typical of a high thermal inertia material (c=1000 J/kg·K), and to a low value (LTM), from a low thermal inertia material (c=100 J/kg·K). The monthly mean results are presented in Fig. 5.2. The Glaser method solutions do not take in consideration the heat capacity or the moisture retention curves so that the simulations give out the same results in terms of vapour pressure. Nevertheless, the conversion in terms of moisture content gives different results between the hygroscopic and the non hygroscopic material, because a different moisture retention curve is considered for the two. The different heat capacity has a small influence on the moisture contents.

The Glaser method results are conservative during the year except for March and April, in which the moisture content is underestimated at most by 17 % for the hygroscopic materials and at most by 5 % for the non-hygroscopic materials. On the other hand, the maximum differences are of 14 % for a non-hygroscopic material and of 32 % for a hygroscopic material.

5.3.1 Building envelopes comparison

The build-ups illustrated in figure 5.1 are chosen in order to represent realistic envelopes with different hygrothermal properties. The quantitative description of the overall properties of the walls are listed in Table 5.1.

The weather files of Berlin, Vienna, Paris, Rome, Madrid (from [93]) and Udine (from [92]) are used in the simulations, while the material properties are taken from the material database of the HM transfer model. For the transient simulations, advanced

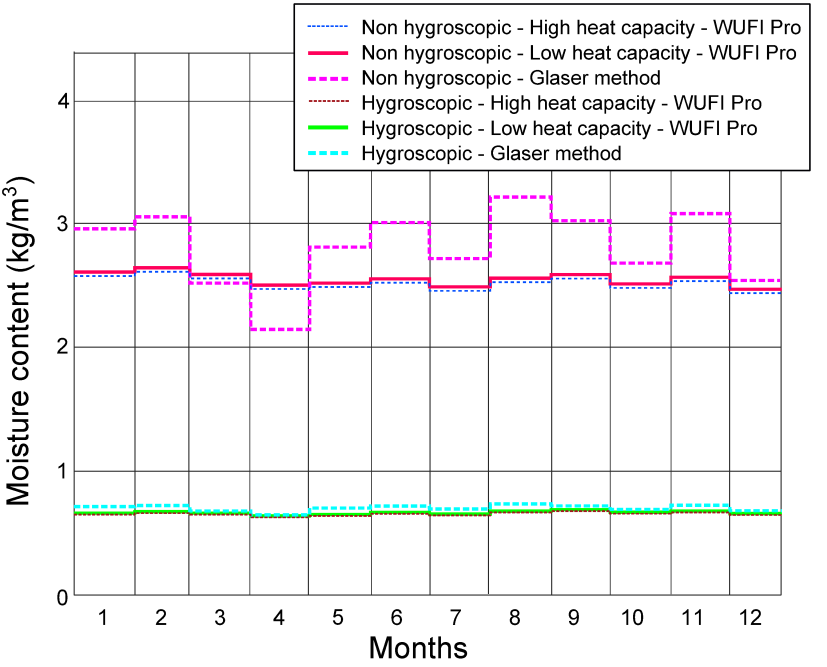

Figure 5.2: Moisture content calculated for a single layer wall of the four fictitious hygroscopic materials. Since the Glaser method is a stationary method, there is no difference between the results with different heat capacities.

material properties are considered (moisture content dependent thermal conductivity and vapour permeability), while the design material properties (measured in dried conditions) from WUFI Pro material database are used for the steady state simulations.

Monthly mean and hourly moisture content values are obtained from transient simulations (w_W and w_{Wm}). The Glaser method results w_G are compared with the maximum and minimum percentage differences with the hourly values (Δw^{max} and Δw^{min} annual maximum and minimum of the Δw values defined in Eq. 5.5) and with the mean monthly moisture content from the HM transfer model (Δw_m^{max} and Δw_m^{min} annual maximum and minimum of the Δw_m annual maximum and minimum of the Δw values defined in Eq. 5.6). From the former comparison, it is possible to evaluate the peaks calculated in the hourly simulations, while the latter comparison is relevant to common applications such as moisture accumulation assessment. The results are presented in the Tables form 5.3 to 5.8.

If $\Delta w > 0$, then results of the Glaser method are conservative, meaning that the higher moisture contents are higher than the ones of the HM transfer model. A positive Δw^{min} would indicate fully conservative Glaser method results, meaning that the Glaser method moisture content is always higher than the values obtained by the HM model. This never occurs in the obtained results, while mostly positive values of Δw^{max} are obtained, meaning that the maximum moisture content found by the HM simulation

Table 5.2: Results of the HM transfer model simulations for single layer walls of fictitious materials for the Udine weather file.

Fictional material	w_W^{max} $\left(\frac{kg}{m^2}\right)$	w_W^{min} $\left(\frac{kg}{m^2}\right)$	w_{Wm}^{max} $\left(\frac{kg}{m^2}\right)$	w_{Wm}^{min} $\left(\frac{kg}{m^2}\right)$	w_G^{max} $\left(\frac{kg}{m^2}\right)$	w_G^{min} $\left(\frac{kg}{m^2}\right)$	$\Delta w_{\%}^{max}$ (%)	$\Delta w_{\%}^{min}$ (%)
NH HTM	0.76	0.62	0.69	0.64	0.74	0.65	12	-5
NH LTM	0.70	0.61	0.69	0.64	0.74	0.65	14	-2
H HTM	2.71	2.41	2.64	2.47	3.21	2.14	30	-17
H LTM	2.68	2.37	2.62	2.44	3.21	2.14	32	-16

Table 5.3: Results of the HM transfer model simulations for the solid brick wall for six different weather files.

Climate	w_W^{max} $\left(\frac{kg}{m^2}\right)$	w_W^{min} $\left(\frac{kg}{m^2}\right)$	w_{Wm}^{max} $\left(\frac{kg}{m^2}\right)$	w_{Wm}^{min} $\left(\frac{kg}{m^2}\right)$	w_G^{max} $\left(\frac{kg}{m^2}\right)$	w_G^{min} $\left(\frac{kg}{m^2}\right)$	$\Delta w_{\%}^{max}$ (%)	$\Delta w_{\%}^{min}$ (%)	Δw_m^{max} (%)	Δw_m^{min} (%)
Berlin	0.964	0.759	0.936	0.821	0.929	0.817	10	-12	2	-6
Vienna	0.949	0.787	0.933	0.829	0.930	0.799	9	-9	3	-6
Paris	1.033	0.817	1.012	0.851	0.989	0.817	10	-18	3	-12
Udine	0.981	0.801	0.931	0.844	0.956	0.804	10	-11	4	-7
Rome	0.992	0.862	0.950	0.897	0.934	0.874	8	-9	1	-5
Madrid	0.955	0.647	0.912	0.706	0.918	0.715	12	-10	4	-7

Table 5.4: Results of the HM transfer model simulations for the timber wall for six different weather files.

Climate	w_W^{max} $\left(\frac{kg}{m^2}\right)$	w_W^{min} $\left(\frac{kg}{m^2}\right)$	w_{Wm}^{max} $\left(\frac{kg}{m^2}\right)$	w_{Wm}^{min} $\left(\frac{kg}{m^2}\right)$	w_G^{max} $\left(\frac{kg}{m^2}\right)$	w_G^{min} $\left(\frac{kg}{m^2}\right)$	$\Delta w_{\%}^{max}$ (%)	$\Delta w_{\%}^{min}$ (%)	Δw_m^{max} (%)	Δw_m^{min} (%)
Berlin	16.841	15.684	16.369	15.990	17.711	15.497	11	-6	8	-4
Vienna	16.526	15.462	16.235	15.729	17.796	14.541	13	-11	11	-9
Paris	17.870	16.465	17.567	16.806	20.429	14.127	20	-19	17	-17
Udine	17.330	15.990	16.974	16.338	20.188	14.040	23	-18	21	-15
Rome	17.996	16.842	17.575	17.290	18.335	16.641	9	-6	5	-5
Madrid	15.058	13.793	14.668	14.014	17.760	10.925	26	-25	23	-23

Table 5.5: Results of the HM transfer model simulations for the expanded clay block wall for six different weather files.

Climate	w_W^{max} $\left(\frac{kg}{m^2}\right)$	w_W^{min} $\left(\frac{kg}{m^2}\right)$	w_{Wm}^{max} $\left(\frac{kg}{m^2}\right)$	w_{Wm}^{min} $\left(\frac{kg}{m^2}\right)$	w_G^{max} $\left(\frac{kg}{m^2}\right)$	w_G^{min} $\left(\frac{kg}{m^2}\right)$	$\Delta w_{\%}^{max}$ (%)	$\Delta w_{\%}^{min}$ (%)	Δw_m^{max} (%)	Δw_m^{min} (%)
Berlin	4.022	2.932	3.867	3.038	5.733	2.708	67	-29	60	-26
Vienna	3.798	2.823	3.624	2.948	6.690	2.497	98	-32	92	-29
Paris	4.613	3.311	4.459	3.450	6.838	2.842	64	-31	53	-28
Udine	3.924	3.156	3.757	3.300	4.272	2.569	21	-31	17	-27
Rome	4.179	3.417	4.006	3.566	3.898	3.206	6	-15	2	-12
Madrid	3.219	1.787	3.074	1.877	4.459	1.689	71	-32	52	-22

Table 5.6: Results of the HM transfer model simulations for the stone wall for six different weather files.

Climate	w_W^{max} $\left(\frac{kg}{m^2}\right)$	w_W^{min} $\left(\frac{kg}{m^2}\right)$	w_{Wm}^{max} $\left(\frac{kg}{m^2}\right)$	w_{Wm}^{min} $\left(\frac{kg}{m^2}\right)$	w_G^{max} $\left(\frac{kg}{m^2}\right)$	w_G^{min} $\left(\frac{kg}{m^2}\right)$	$\Delta w_{\%}^{max}$ (%)	$\Delta w_{\%}^{min}$ (%)	Δw_m^{max} (%)	Δw_m^{min} (%)
Berlin	0.811	0.656	0.767	0.668	1.141	0.663	54	-15	49	-8
Vienna	0.772	0.646	0.741	0.664	1.278	0.647	77	-11	73	-8
Paris	1.056	0.769	1.001	0.787	1.276	0.674	37	-29	27	-25
Udine	0.886	0.676	0.795	0.698	0.860	0.653	16	-15	12	-11
Rome	0.934	0.795	0.877	0.817	0.783	0.680	-6	-23	-11	-18
Madrid	0.744	0.533	0.704	0.549	0.908	0.509	44	-17	33	-12

Table 5.7: Results of the HM transfer model simulations for the hollow brick wall for six different weather files.

Climate	w_W^{max} $\left(\frac{kg}{m^2}\right)$	w_W^{min} $\left(\frac{kg}{m^2}\right)$	w_{Wm}^{max} $\left(\frac{kg}{m^2}\right)$	w_{Wm}^{min} $\left(\frac{kg}{m^2}\right)$	w_G^{max} $\left(\frac{kg}{m^2}\right)$	w_G^{min} $\left(\frac{kg}{m^2}\right)$	$\Delta w_{\%}^{max}$ (%)	$\Delta w_{\%}^{min}$ (%)	Δw_m^{max} (%)	Δw_m^{min} (%)
Berlin	3.672	3.022	3.528	3.113	5.842	2.766	74	-20	67	-17
Vienna	3.521	2.940	3.401	3.056	6.521	2.510	98	-24	92	-21
Paris	4.704	3.616	4.527	3.718	7.185	2.937	70	-31	59	-27
Udine	3.831	3.241	3.663	3.367	4.437	2.598	29	-27	21	-23
Rome	4.270	3.778	4.058	3.920	4.369	3.557	14	-12	8	-10
Madrid	2.863	1.990	2.684	2.061	4.842	1.691	105	-30	83	-23

Table 5.8: Results of the HM transfer model simulations for the concrete brick wall for six different weather files.

Climate	w_W^{max} $\left(\frac{kg}{m^2}\right)$	w_W^{min} $\left(\frac{kg}{m^2}\right)$	w_{Wm}^{max} $\left(\frac{kg}{m^2}\right)$	w_{Wm}^{min} $\left(\frac{kg}{m^2}\right)$	w_G^{max} $\left(\frac{kg}{m^2}\right)$	w_G^{min} $\left(\frac{kg}{m^2}\right)$	$\Delta w_{\%}^{max}$ (%)	$\Delta w_{\%}^{min}$ (%)	Δw_m^{max} (%)	Δw_m^{min} (%)
Berlin	8.696	7.900	8.535	8.066	8.804	7.170	9	-16	8	-15
Vienna	8.609	7.893	8.548	8.011	9.050	6.876	12	-20	11	-18
Paris	9.411	8.321	9.278	8.414	9.368	7.153	12	-22	9	-20
Udine	9.203	8.387	9.038	8.521	10.258	7.049	17	-22	14	-20
Rome	9.821	9.240	9.687	9.419	10.727	8.022	14	-17	12	-16
Madrid	8.615	7.888	8.436	7.962	8.541	7.504	7	-12	5	-11

during the month is lower than the one obtained monthly by the Glaser method. Contained differences, $\pm 25\%$ in the cases of the Brick Wall, are found for the timber wall and for the concrete masonry wall. The small differences in the solid brick wall simulations (less than $\pm 12\%$ for all the climates) show that the behaviour is well predicted by the Glaser method during the whole year. The timber wall and the concrete masonry wall are composed by highly hygroscopic materials with higher moisture contents, higher absolute moisture variations, but lower percentage variations. In both cases the maximum differences are found generally during the cold season (November, December, January, February), in which the Glaser method underestimates the moisture contents, whereas during the warm months the moisture content is overestimated. A common trend is observed for the hollow brick wall, clay block wall and stone wall: for cold climates (Berlin, Vienna, Paris) during the cold months (November, December, January, February) the Glaser method predicts moisture contents that can reach twice the values predicted by the HM transfer model, while during the rest of the year they have differences smaller than 30%. For warmer climates (Rome, Udine, Madrid) the Glaser method estimations follow the HM transfer model results, except for the month of December of the Madrid simulations. For every case, the HM transfer model results have small daily and hourly variations, with respect to the mean monthly values. The plot of Fig. 5.3 represents the simulation results for a timber wall in the climate of Vienna. The daily variations of the HM simulation are small compared to the moisture content of the wall, confirming that for this case, a time step larger than 1 hour could be considered. On the other hand, the relatively large variations of the Glaser method show that the heat and moisture transfer is strongly influenced by the transient moisture storage properties of the materials and thus, a stationary method could be not representative of the phenomenon.This is confirmed by the lower moisture contents of the Glaser method from January to April and by the steep increase from April to June.

5.3.2 Relative humidity distributions

A further comparison is drawn on the timber wall and on the hollow brick wall for the Vienna weather file. The year results for the former wall are shown in Fig. 5.3. The HM

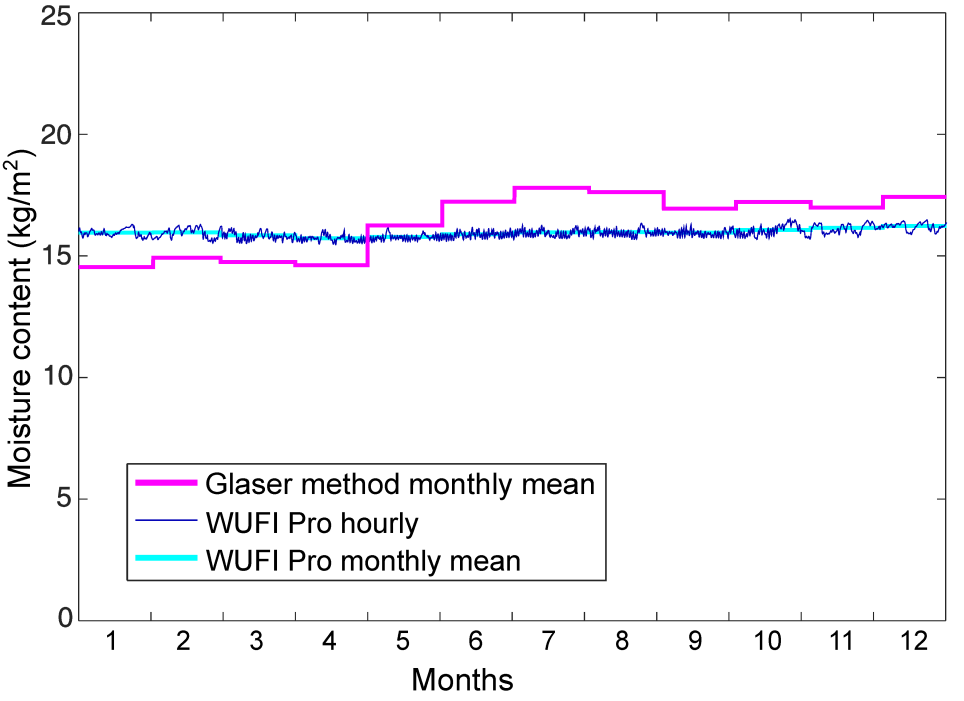

Figure 5.3: Moisture contents calculated for a timber wall with Vienna weather file using the HM transfer model and the Glaser method.

transfer model and the Glaser method are used to obtain the relative humidity profile through the building envelopes. The HM transfer model relative humidity monthly mean is obtained from the hourly relative humidity calculated on the control points, set on the layers interfaces.

The first comparison is used to understand the cause of the variation in moisture contents between the two methods. The relative humidity profiles for November is shown in Fig. 5.4. As expected a larger portion of the wall reaches higher relative humidity in the HM transfer model simulations due to the redistribution of moisture in the material. The moisture content difference between the two results is due to the hygroscopic behaviour of the timber and cellulose fibre layers. The moisture content increases in the higher relative humidity range ($\varphi = 95\%$), which is reached in a smaller region in the Glaser method results as can be seen in Fig. 5.4, between 10 and 20 cm.

The damage criteria for the HM transfer model results and the Glaser method are different. The HM transfer models allow to calculate with deterministic relations the growth of moulds or the wood decay, that correlate a risk even to relative humidity values lower than 100 % while the Glaser method is applied on the general concept of liquid water accumulation, which is a condition that is met when the relative humidity

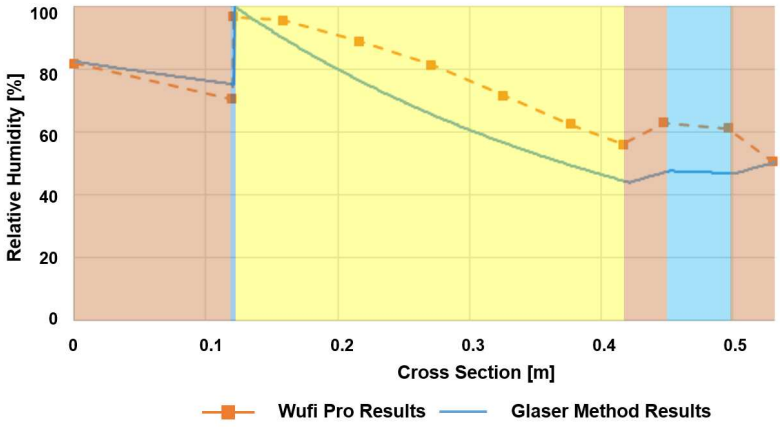

Figure 5.4: Comparison of relative humidity profiles obtained with different calculation methods for the timber wall in the climate of Vienna. The background of the plots is coloured to distinguish the wall layers.

is equal to 100 % in one of the layers of the wall. Even if the HM transfer methods calculates lower levels of relative humidity, depending on the damage criteria, it could be also related to a not acceptable risk level.

The second comparison is used to discuss the use of the mean monthly temperatures for the Glaser method. More conservative results could be obtained using lower temperatures or higher relative humidity values as external boundary conditions: in Fig. 5.5, the relative humidity calculated with the previously presented methods is compared to the distribution obtained considering the minimum 5-days mean design temperature, defined in the EN ISO 15927-5 standard (external temperature -10 °C and external relative humidity 80 %, which is met in the first days of February). With the extreme conditions, the condensation occurs in the layer between 10 and 25 cm, while the Glaser method monthly mean boundary conditions results do not show the presence of condensation and is in good agreement with the HM transfer model results. From this comparison, it is shown that considering 5-days mean design temperatures for this wall and climate could lead to over conservative designs of the building envelopes.

Finally, it is not possible to conclude that the Glaser method allows to obtain always more conservative results without the modification of the boundary conditions, while it has been shown, for the timber wall and the hollow brick wall, that the mean relative humidity distributions are similar. Nevertheless, it has to be considered that they have different meanings: the relative humidity of the HM transfer model could be considered as a predictive result to be used in deterministic risk assessment models, while the Glaser method should be considered as an indicative value, calculated with many simplifying hypothesis.

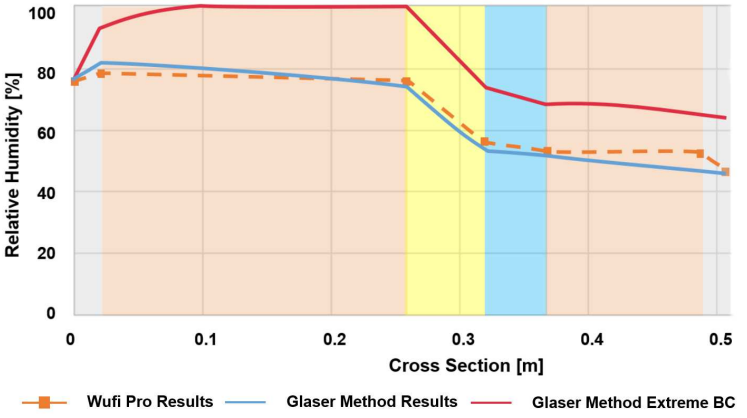

Figure 5.5: Comparison of relative humidity profiles obtained with different calculation methods for the hollow brick wall in the climate of Vienna. The background of the plots is coloured to distinguish the wall layers.

III

Material properties

6

Material Properties

One of the main obstacles for the utilization of the heat and moisture transfer tools is the material characterisation required by the model. As seen in the previous chapters, the material properties required for the solution of the equations depend on the model considered and on the chosen hypotheses.

The traditional approach to material modelling is to measure constant properties at design conditions, without considering the variation of moisture content. With these values it is possible to perform the majority of simulations regarding heat transfer and to use the Glaser method for the condensation risk assessment. For the calculations of heat transfer in building details with numerical methods or in building envelopes for the whole building simulations, it is commonly accepted to use constant material properties. Also for the Glaser method, the process of diffusion of water vapour is modelled with a constant vapour diffusion resistance factor. For this reason, most of the technical sheets provided by the producers contain the measurements of the thermal conductivity λ, the heat capacity of the dry material c, the dry density ρ_0 and the vapour diffusion resistance factor μ.

When a coupled heat and moisture transfer simulation has to be performed, then the material properties dependence to the moisture content and the temperature could be relevant. Using the software WUFI Pro, referring to Eq. 3.30, the required material properties for a complete simulation, are:

- ρ_0 = Density of the dry material $\left(\frac{\text{kg}}{\text{m}^3}\right)$
- c = Heat capacity of the dry material $\left(\frac{\text{J}}{\text{kg}\cdot\text{K}}\right)$
- $\lambda(\varphi, T)$ = Thermal conductivity $\left(\frac{\text{W}}{\text{m}\cdot\text{K}}\right)$
- $w(\varphi)$ = Moisture retention function $\left(\frac{\text{kg}}{\text{m}^3}\right)$
- $\delta_p(\varphi)$ = water vapour permeability for the water vapour pressure $\left(\frac{\text{kg}}{\text{m}\cdot\text{s}\cdot\text{Pa}}\right)$
- $D_\varphi(\varphi)$ = Liquid conduction coefficient with φ as a potential for the suction and the redistribution process $\left(\frac{\text{kg}}{\text{m}\cdot\text{s}}\right)$

Figure 6.1: Compostable insulation material MycoFoam®. The material is composed by wooden scraps, bounded by mycelium (fungi's roots).

These property functions are not commonly provided by the producers, thus, when an uncommon material should be modelled, a full characterisation is required. Different standardised direct measurement procedures could be used and, depending on the material consistency, they are more or less effective. When the direct methods are not effective, indirect methods could be considered. For example, performing the measurements of transient absorption of water vapour in a climate chamber, coupled with a material property calibration using numerical simulations, could be used to obtain an estimation of the water vapour permeability of the material. When experimental results are not available it could be also acceptable to use the material property functions of other materials that are known to be similar to the one studied. In this case it could be appropriate to perform the simulations considering more than one substitutive material in order to identify a set of possible results. In the next section, three examples of the comparison between the real and simulated behaviour of the construction material are presented in order to highlight the gap between experiments and simulations.

6.1 Vapour diffusion in insulating material

In a collaboration of Libera Università di Bolzano (Free University of Bozen-Bolzano) an experimental activity was conducted at the Building Physics Laboratory of the Free University of Bozen–Bolzano. The main objective of the activity was to identify the influence of the moisture content on the thermal behaviour of a new insulation material. The considered material, MycoFoam®, is a wood based insulation panel (Fig. 6.1), obtained bonding wood scraps together with fungi mycelia (mushroom roots).

6.1.1 Material description

After the growth of the mycelia, the wood scraps are kept together by the roots bonding and with a desiccation period, the growing process is stopped. This new material is designed to be compostable and it could be easily used in a design process with circular economy requirements. One of the limits of the usage of MycoFoam® is that the activation of the decomposing process occurs when the material is wet, which is a common temporary condition in building materials. For this reason, to use this material it is necessary to assess with heat and moisture transfer simulations the risk of water condensation and accumulation in its layer. Thus its hygrothermal properties should be known. The material, for its stiffness and low mechanical resistance, is not adapt for wet-cup or dry-cup measure water vapour permeability methods. Therefore an indirect method should be used, or the properties of similar materials could be considered.

6.1.2 Experimental method

These two approaches have been used to perform a preliminary evaluation of the influence of moisture on the thermal performance of building materials. This evaluation is presented in [12]. A hygrothermal characterization of the MycoFoam® insulation with a climatic chamber and with the heat flux meter was undertaken. The results were used to perform heat and vapour transfer simulations of a timber wall insulated with the MycoFoam®, to assess the influence of the heat transfer caused by the moisture transfer phenomena. The properties of the cross-laminated timber structural layer have been previously evaluated by the research group of the Free University of Bozen-Bolzano, and the results are reported in [94].

The dimension of the insulation panel are 0.3 x 0.3 x 0.05 m. The measurements of the conductivity were performed on the sealed specimens (sealed with a plastic foil and tape, as shown in Fig. 6.2) using a heat flow meter (Netzsch HFM 436/3 Lambda^{TM}) in compliance with ISO 8301:1991, EN 12664:2001 and EN 12667:2001. The measurements were performed at different temperatures from 10 to 50 °C with steps of 5 K, each at four moisture contents 0 %, 3.6 % (φ=10 %) , 8.0 % (φ=30 %) and 13.6 % (φ=80 %). The moisture content of 0 % was obtained after a conditioning in the ATT Angelantoni DM340 climatic chamber at 105 °C with ventilation. The obtained density was used to calculate the moisture contents.

The procedure is described in Fig. 6.3. First, the specimen is conditioned in the climatic chamber. The samples are weighted every 24 hours, until the equilibrium with the chamber's air is reached. The equilibrium is obtained when the difference between the new weight and the previous weight is lower than the 0.1 % of the new weight. At that point, the weight of the sample is used to calculate the moisture content and the measurement is inserted in the moisture retention curve. Afterwards the sample is sealed and it is inserted in the heat flow meter for the procedure of the thermal conductivity measurement at different temperatures (from 10 to 50 °C with steps of 5 K). The sample is sealed in order to maintain as much as possible the moisture content gained in the conditioning procedure. After this measurement, the sealing is removed from the sample and the conditioning is performed again, for the next value of relative humidity.

Figure 6.2: The samples are conditioned in the climatic chamber and then sealed with a plastic film and tape to avoid the loss of moisture content. The sealed samples are tested in the heat flow meter to measure their conductivity at different temperatures. The process is repeated changing the conditioning conditions of the climatic chamber.

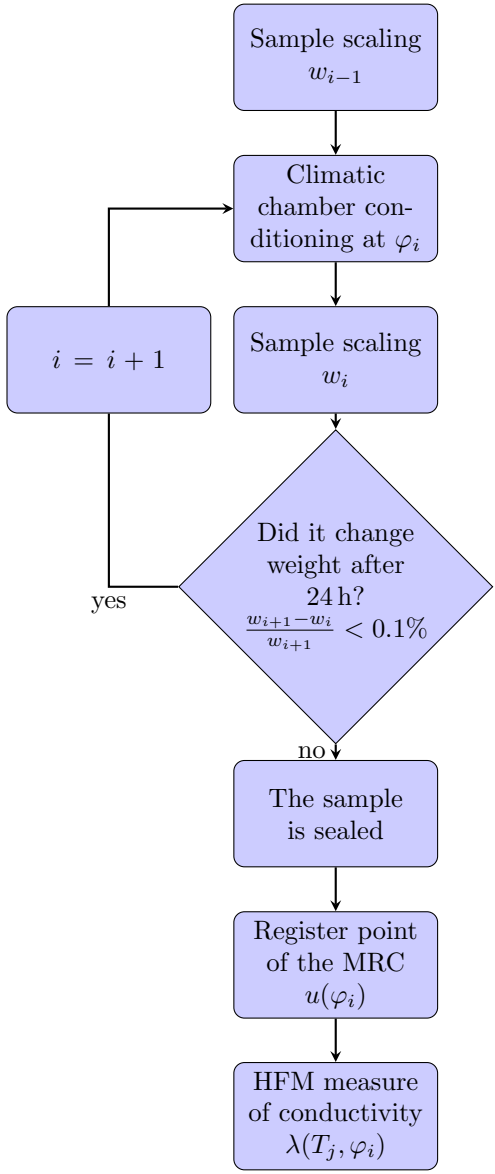

Figure 6.3: Description of the procedure used for the measurements of the thermal conductivity at different temperatures (with T_j= 10 to 50 °C with steps of 5 K) and of the moisture content for the construction of the moisture retention curve. The procedure is repeated for each relative humidity value (φ_i=0 %, 10 %, 30 % and 80 %). MRC stands for Moisture Retention Curve and HFM stands for Heat Flow Meter.

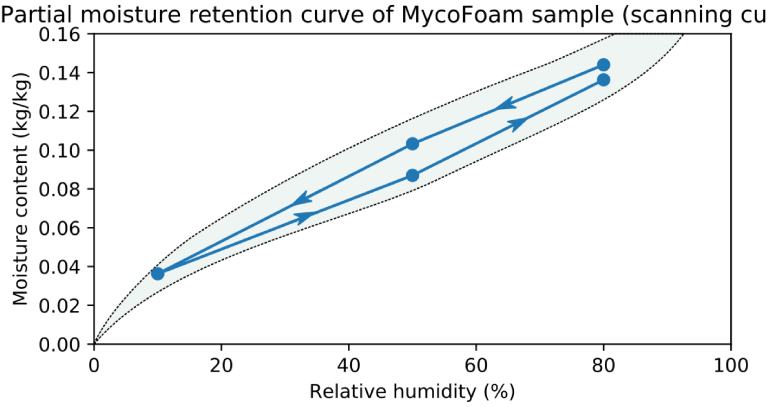

Figure 6.4: Scanning curves of the moisture retention function of the MycoFoam® insulation. The Moisture retention curve, complete with absorption and desorption curves will be the result of future work. The dashed line indicates the qualitative description of the possible absorption and desorption curves.

6.1.3 Results

With this procedure two scanning curves of the hysteretic moisture storage function were obtained. The results for a sample are shown in Fig. 7.1. These values could be used for a first estimation of the moisture retention function.

The heat flow meter conductivity measure allowed to measure also the temperatures of the two surfaces of the test specimen, along with the heat fluxes at the two sides. These values of the temperatures could be used as boundary conditions to perform a transient simulation of the heat transfer. The moisture distribution inside the specimen could lead to an internal variation of the moisture distribution that could vary the local values of thermal conductivity.

6.1.4 Comparison with simulation results

Using the overall thermal conductivities, the measured moisture retention curve, the simulation of the transient heat conduction in the heat flow meter could be used to estimate other material parameters. The estimation could be performed with a calibration method. Hereafter the results of a simple calibration are presented. The software tool used for the calibration is CHAMPS-BES, research software that shares the heat and moisture transfer model of DELPHIN. The performed simulation is simplified, only the heat transfer and the vapour diffusion are considered and the unknown material properties (specific heat and vapour resistance factor) are set to constant values. the moisture retention curve used is the absorption scanning curve obtained from the conditioning of the material in the climatic chamber. The thermal conductivity is defined as a function of moisture content only, not of temperature. First, the simulations are performed with the values used in [12], that means $c = 1281 \frac{\mathrm{J}}{\mathrm{K \cdot kg}}$ and $\mu = 2$, that were used for similar wooden based materials. The heat flux simulated and measured are compared in Fig.

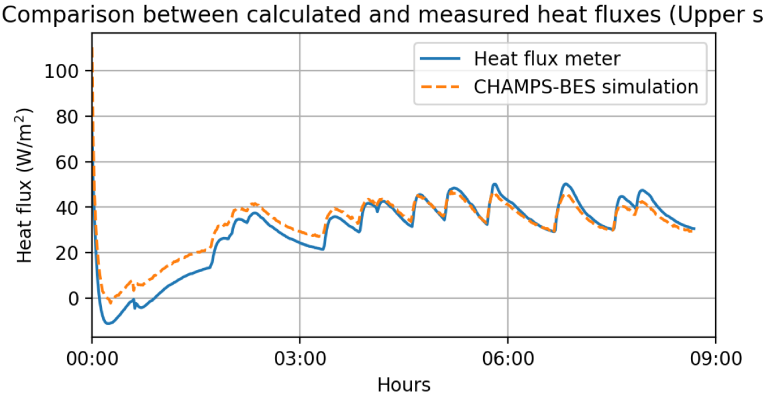

Figure 6.5: Comparison of the heat flux measured in the heat flow meter and simulated, using material properties from literature, of similar materials.

6.7 and 6.8 and the results are already similar.

Changing the values of c and μ in order to obtain heat fluxes values closer to the measured ones, other values are found that seem to better represent the material. The heat fluxes obtained with $c = 2500 \frac{\mathrm{J}}{\mathrm{K \cdot kg}}$ and for $\mu = 30$, values typical of spruce wood are presented in Fig. 6.7 and 6.8.

The composition of MycoFoam® is unknown due to the fact that it has been obtained from wood waste and the mycelium is not a common component of building materials. The calibrated values of the specific heat c could be attributable to the different wood composition, than the insulation panels in literature. On the other hand, the large value of the vapour diffusion resistance factor μ could be explained by the fact that different mechanisms of moisture transport might have been involved in the μ measurement test, like moisture transport due to air diffusion or air convection, that were reduced by the HFM test modality. For these reasons the use of the water vapour resistance from literature could be considered more reliable for a future simulation of the material in a building envelope.

In conclusion, the described test procedures coupled with the calibration of material properties could be used to evaluate the reliability of the assumed hygroscopic material property values with the use of instruments used for the heat transfer measurements.

6.2 Liquid transport in solid bricks

The experimental work for the thesis [95] allowed to evaluate the effectiveness of using the material properties provided by the software database to simulate the phenomenon of the capillary transport in the solid bricks that could be found in the market of the North East of Italy. This experiments do not consider the mortar between bricks, but the solid brick only, and that the results should not be extended to all the materials that are used to build a complete wall.

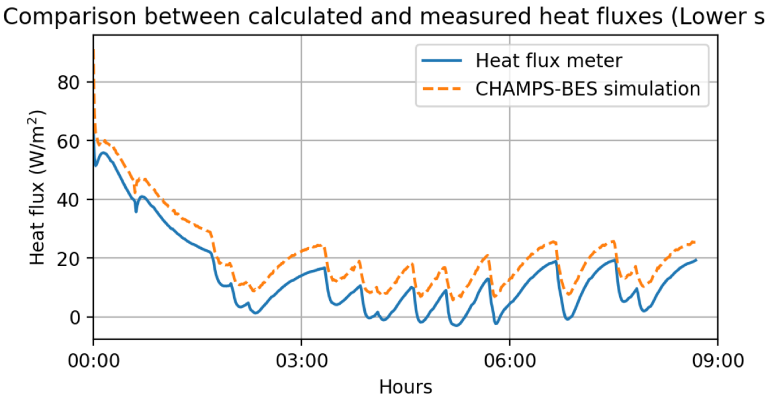

Figure 6.6: Comparison of the heat flux measured in the heat flow meter and simulated, using material properties from literature, of similar materials.

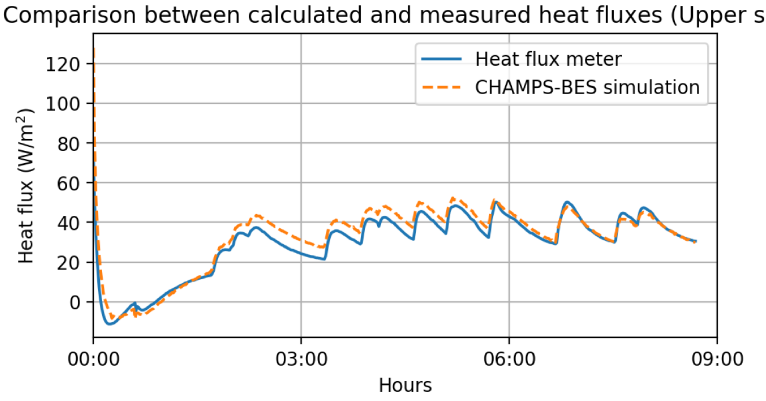

Figure 6.7: Comparison of the heat flux measured in the heat flow meter and simulated, using material properties obtained from a calibration process.

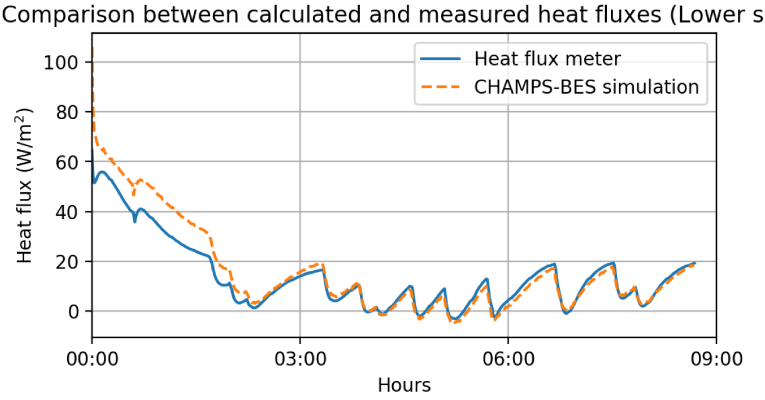

Figure 6.8: Comparison of the heat flux measured in the heat flow meter and simulated, using material properties obtained from a calibration process.

6.2.1 Experimental method

A solid brick produced in the Friuli-Venezia Giulia region has been divided in four samples of approximately 12 x 6 x 6 cm. The samples have been dried in the sun for a week, in order to reduce the their moisture content. The procedure is as similar as possible to EN ISO 15148:2014. The samples have been plunged in 5 mm of water, sustained on four points in order to expose the lower surface to water. The water is added periodically to maintain the 5 mm level. The samples are superficially dried with a wet towel and scaled every hour during the experiment, until the saturation is reached. The experiment has been filmed with the infrared camera and the apparent temperatures of the side of the sample have been registered. The sides of the brick are exposed to the ambient and the wet front is visible to the infrared camera because of the evaporation of the moisture on the sides. The experimental set up is shown in Fig. 6.9.

6.2.2 Experimental results and simulations

The moisture content of the samples is calculated and plotted over the time and then compared with the material properties of the material database of the software CHAMPS-BES. The results are similar so that it is possible to conclude that the solid brick material found in the database could be used to model the capillary sorption in the solid bricks used in the experiment. The results are shown in Fig. 6.10.

The simulation of the capillary sorption process is performed with the software CHAMPS-BES. The brick is modelled as a two-dimensional body and the lower surface is exposed to a pressure head of 5 mm of water, while the other surfaces are exposed to the interior environment, set to 20 °C and to 50 % of relative humidity.

The infrared pictures show the superficial temperature distribution of the samples. The superficial temperature field depends on the moisture flux inside the brick and on the surface. The liquid evaporation on the surface causes a heat flux from the

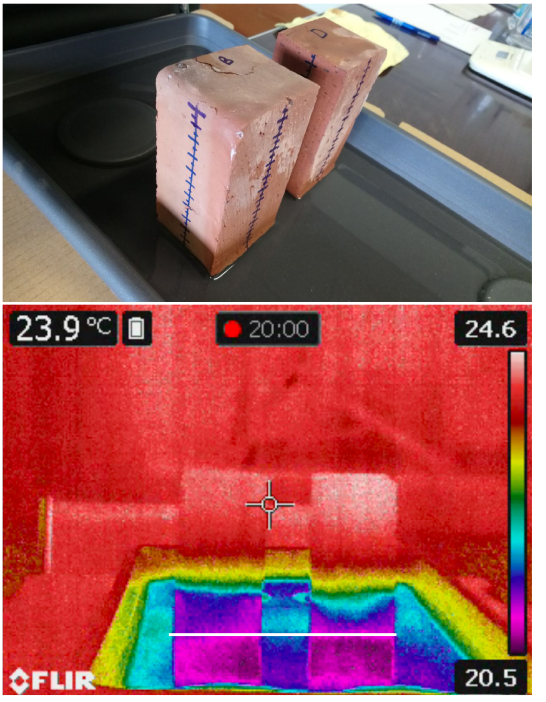

Figure 6.9: Experimental setup for the capillary sorption experiment on solid bricks. The samples are in contact with the water and the infrared camera is set to capture the temperature change on the sides caused by the evaporation flux. The white line in the lower picture denotes the line of the surface of the water on the side of the sample.

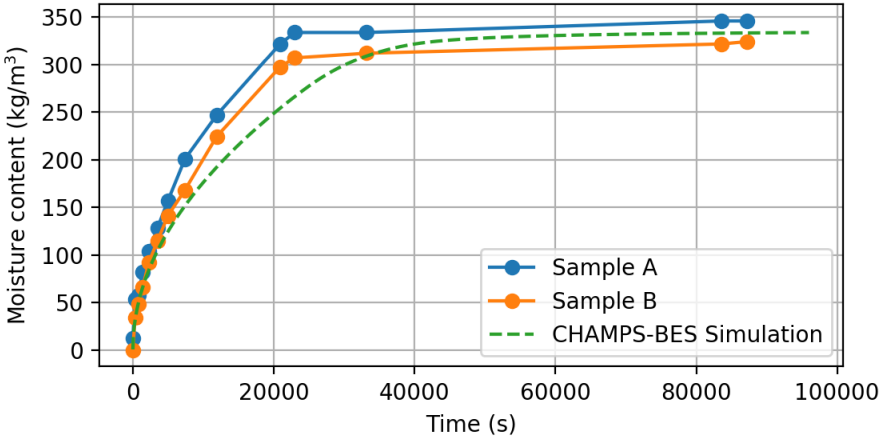

Figure 6.10: Comparison between the average moisture content of two test samples, A and B, and the simulation results.

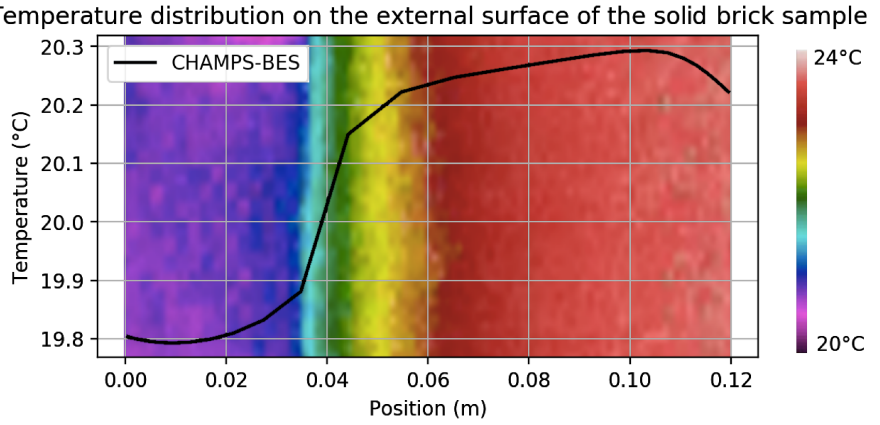

Figure 6.11: Comparison between the side surface temperatures of the brick sample (chromatic map) and the CHAMP-BES simulation results (black line) after 30 minutes of capillary suction. The temperature gradient denotes the presence of an evaporative heat transfer from the brick to the environment.

pores, that reduces the temperature up to the evaporation front. On one hand, the temperature difference between the dry surface and the wet surface, measured with a surface thermometer, is of about 1.5 K, while the difference obtained from the simulation is of about 0.5 K. On the other hand, from a qualitative point of view, the temperature distributions are similar between the two cases. As an example, Fig. 6.11 shows this accordance. This behaviour could be explained by an underestimation in the simulations of the latent heat exchange due to the vapour migration or by the influence of the difference in the boundary conditions.

In conclusion, the presented procedure, presented a validation procedure for the liquid transport material properties using a infrared camera and a scale, coupled with numerical simulations. The coupling between the moisture and heat transfer mechanisms allowed to evaluate the phenomena from a thermal point of view using the infrared camera and and to compare it with the numerical simulation, finding agreement between the experiment and the simulation.

7

Hysteresis

As seen in the previous sections, using a moisture storage function, defined as a one-to-one function between the driving potential of moisture transfer (φ, p_v, P_c or $\log_{10}(P_c)$), and the moisture content is a simplification of the moisture accumulation behaviour. Due to different reasons, depending also on the considered material, the moisture storage behaviour is often hysteretic. The main effect of hysteresis is that a material sample could reach equilibrium with the air of an environment set to a constant value of vapour pressure and temperature, with different moisture contents. This behaviour also affects the moisture balance equation parameter referred to as moisture capacity ξ, defined as the derivative of the moisture content with respect to relative humidity. The moisture capacity variation will define the next equilibrium positions in the moisture storage plane, depending on the previous positions. The curves formed by these positions are called scanning curves, which are generally between the absorption and desorption curves (Fig. 7.1). The absorption curve is defined as the curve followed by the equilibrium states of the material starting from a dry state, with no moisture content, and then conditioned at an environment with progressively higher values of relative humidity, starting from 0 %. The desorption curve is the curve of the equilibrium states obtained starting from the saturation state of the material and then conditioned to air with progressively lower relative humidity values, starting from the 100 %.

7.1 Modelling

In literature there are many examples of modelling approaches for the inclusion of hysteresis in the heat and moisture transfer simulations. One approach is the determination of the absorption and desorption curves to be used as lower or upper bound to the scanning curves. Different models are presented in literature, for example, the afore mentioned "empirical hysteresis model" (represented by Eq.3.28 and presented in [31] and in [32]), is simple to implement and, with other parametric adjustments, it could be tuned to better follow the scanning curves. For example, in Eq.7.1, a constant parameter

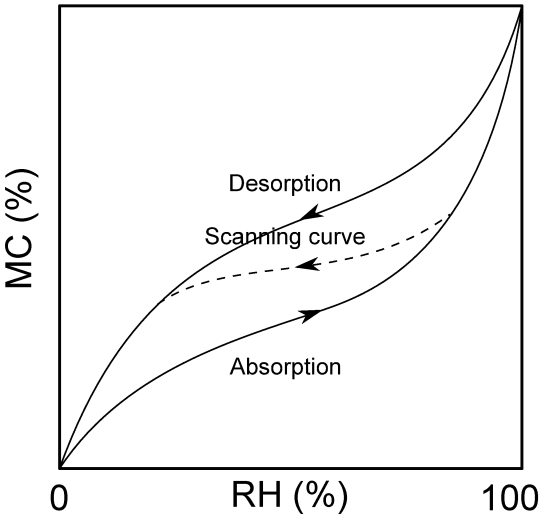

Figure 7.1: Qualitative description of absorption curve, desorption curve and a scanning curve in the moisture storage plane. The curves describe the succession of the possible equilibrium states of the material.

a is added instead of the value 0.1 first presented in Eq. 3.28.

$$\xi = \begin{cases} \frac{(u-u_a)^2 \cdot \xi_d + a \cdot (u-u_d)^2 \cdot \xi_a}{(u_d-u_a)^2} & \text{for desorption} \\ \frac{a \cdot (u-u_a)^2 \cdot \xi_d + (u-u_d)^2 \cdot \xi_a}{(u_d-u_a)^2} & \text{for absorption} \end{cases} \tag{7.1}$$

Other models are described in [96], [97], [98] and [99]. In [100] an extensive measurement of the equilibrium states, has shown that the hysteretic behaviour for Nordic spruce changes also with temperature.

7.2 Impact on simulations

One may ask if including the hysteresis in the simulation model could influence the results. This, of course, depends on the simulated phenomenon and on the finality of the simulation. Some evaluations are presented in literature, for example, the influence of hysteresis in building energy simulation is discussed in [101], in order to evaluate the performances of a new building material or in [102], where the hysteresis influence is discussed also for the moisture buffering effect on the indoors environment. In [103], the influence of hysteresis is evaluated for the risk assessment of degradation of the materials.

7.2.1 Simulations

Using the software MATCH it is possible to take in account the hysteresis of the moisture retention curve. In order to present the influence of the hysteresis in the simulations the heat and moisture transfer simulation is performed on a spruce cross-laminated timber wall, with the TRY weather file of Copenhagen (Denmark), without considering the rainfall, set as external boundary condition. The wall build-up is:

- outside
- CEMBRIT panel - 9 mm
- Rock Wool insulation - 380 mm
- Cross-laminated timber structural layer - 100 mm
- CEMBRIT panel -9 mm
- inside

The simulations have been performed considering the hysteresis, then, without the hysteresis, using as moisture retention curve the absorption curve only, the desorption curve only and finally the mean curve, calculated as the mean between the points of the desorption curve and the absorption curve.

7.2.2 Comparison

The comparison has been performed considering the eternal surface of the timber layer, between the external layer of insulation and the timber. The comparison is shown in terms of moisture content (Fig. 7.2), relative humidity (Fig. 7.3) and then, combining the two aspects, on the moisture retention plane, obtained plotting the moisture content against the relative humidity (Fig. 7.4).

In the Tables 7.1 and 7.2 the mean and the extreme values of the resulting moisture contents and relative humidity values are presented. It is shown that using the absorption curve or the desorption curve provide different extreme values than the hysteretic one, while it is observed that the mean curve provides similar results. From the moisture content plot (Fig. 7.2) it is easy to see that the extreme values for the hysteretic curve and the mean curve happen in different times of the year so that it is possible to conclude that it is not possible to generalise that the mean curve could replace the hysteretic behaviour of the material. While the moisture content of the mean curve seems to be a mean value between the absorption and the desorption curve's results, the resulting moisture content of the hysteretic curve has a different reaction to the weather solicitations, with smaller variations. In Fig. 7.4 the path on the moisture retention plane of the four solutions it is shown. The slope of the curves represent the moisture capacity, the term included in the moisture balance equation.

7.2.3 Moisture capacity

While for absorption, desorption and mean curves the moisture capacity coincides with the one of the moisture retention curves, the hysteretic moisture capacity is different

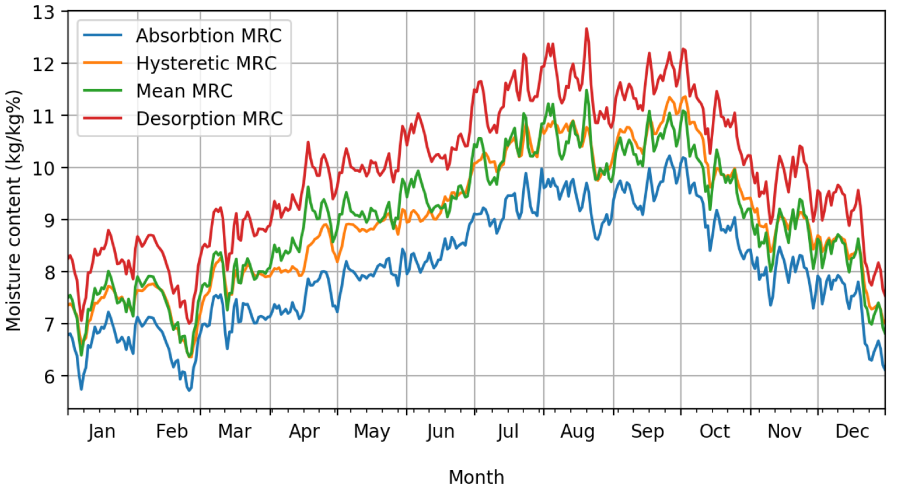

Figure 7.2: Daily mean moisture content (in terms of percentage of water mass over the dry mass of the timber) resulting from the heat and moisture transfer simulation of a spruce cross-laminated timber wall in the city of Copenhagen. The simulation does not consider driving rain.

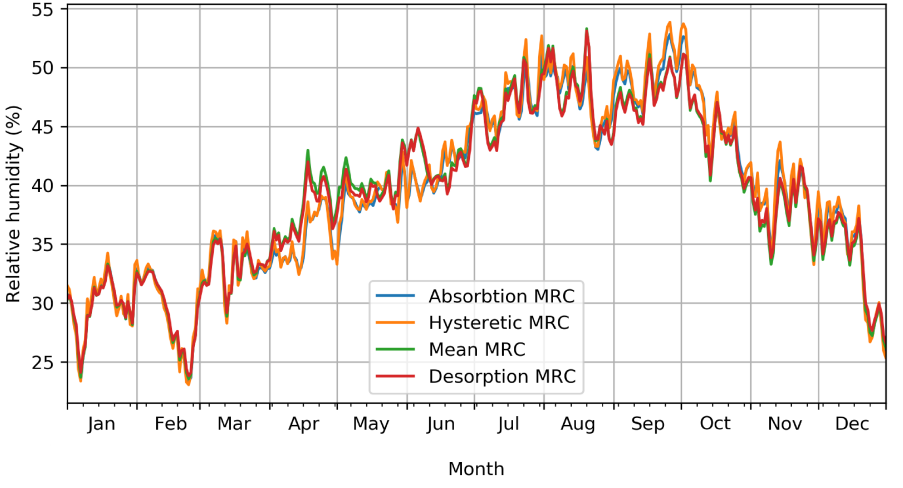

Figure 7.3: Daily mean relative humidity (unit: %) resulting from the heat and moisture transfer simulation of a spruce cross-laminated timber wall in the city of Copenhagen. The simulation does not consider driving rain.

Table 7.1: Relative humidity (unit: %) mean, maximum and minimum values obtained in the simulation with the use of the four moisture retention curves (MRC)

	Relative humidity (%)		
	mean	max	min
Absorption MRC	39.2	52.8	23.3
Desorption MRC	39.2	53.1	23.8
Hysteretic MRC	39.4	53.8	23.0
Mean MRC	39.2	53.2	23.6

Table 7.2: Moisture content (unit: kg/kg%) mean, maximum and minimum values obtained in the simulation with the use of the four moisture retention curves (MRC)

	Moisture content (kg/kg%)		
	mean	max	min
Absorption MRC	8.1	10.2	5.7
Desorption MRC	10.2	12.7	7.0
Hysteretic MRC	5.7	11.3	6.4
Mean MRC	10.0	11.5	6.4

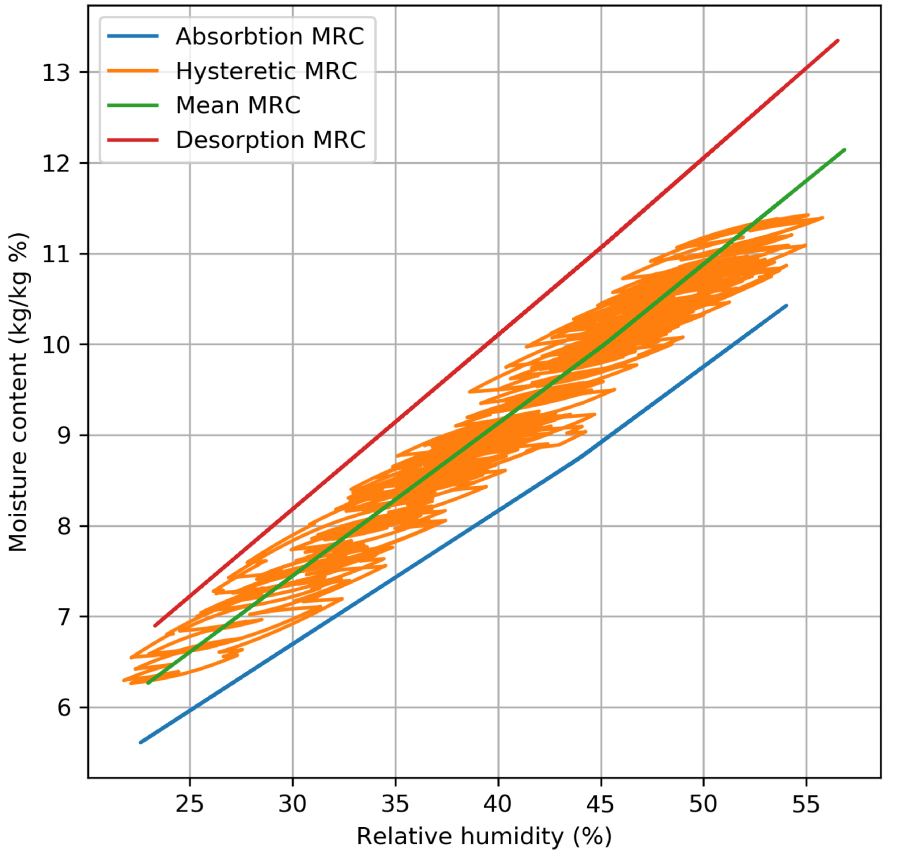

Figure 7.4: Description of the hourly hygroscopic state (in terms of percentage of water mass over the dry mass of the timber and relative humidity in percentage) of the timber resulting from the heat and moisture transfer simulation of a spruce cross-laminated timber wall in the city of Copenhagen. The simulation does not consider driving rain.

depending on the direction of the path. This could be seen in Fig. 7.5, where only the first four days of the simulation are represented. The hygrothermal state (meaning the equilibrium state, defined by the relative humidity and the moisture content) of the hysteretic material model draws four curves that correspond to the daily moisture variations on the outside environment. The curves change the slope every time they change from adsorption to desorption or vice-versa moving on these curves that eventually close passing on a previous state, in what they appear to be small cycles of few days. The other three curves are flattened on the moisture retention curve and thus cannot be visualised in the plot.

In conclusion, it has been shown that hysteresis in the moisture retention curve could be a relevant phenomenon to study. In particular when a simulation is meant to be part of a risk analysis based on moisture content threshold levels, the results obtained with

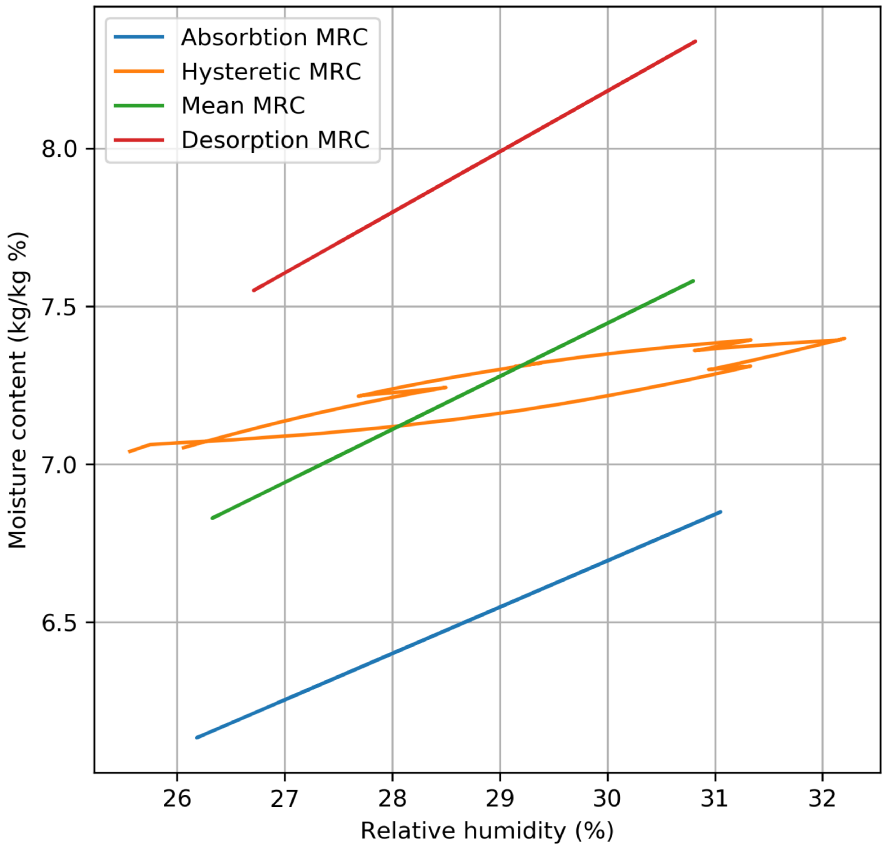

Figure 7.5: Cycle of equilibrium states of the obtained considering the hysteresis in the model (in orange) and the other results (obtained neglecting the hysteresis) of the first four days of the results shown in Fig. 7.4.

and without hysteresis could lead to different risk values.

IV

Weather files

8

Reference weather files

Depending on the finality of the analysis, besides the choice of the modelling equations and the choice of the level of detail used to model the material properties, the simulation of the heat and moisture transfer in building materials requires also the definition of the boundary conditions. Supposing that a transient coupled heat and moisture transfer problem is chosen, then, the time discretisation of the solution is commonly performed with time steps of one hour. The boundary conditions are defined to represent the heat and moisture fluxes and potentials of the indoor or outdoor environments to which the studied detail or building is exposed. These fluxes could be calculated from the following weather variables:

T = Dry bulb air temperature (K or °C)

p_v = Water vapour partial pressure (Pa)

E_d = Direct solar irradiance on the surface ($\frac{\mathrm{W}}{\mathrm{m^2}}$)

r_d = Driving rain intensity on the wall surface ($\frac{\mathrm{kg}}{\mathrm{m^2}}$)

These variables are described hourly in the weather files, measured by weather stations. The weather stations are often located in airports, or on towers and provide the weather variable measurements in that point, which could be different from the same variables on the surface of building envelopes. For each variable, many algorithms to extrapolate the variables for other locations, with other conditions are presented in literature. For example, for the calculation of the direct normal solar irradiance on the building envelope surface when the only global radiation data is given, a split algorithm is needed (an extensive comparison is presented in [104] and [105]) to obtain the diffuse horizontal irradiation component and the direct horizontal component and then, another algorithm for the calculation of the solar incidence angle, also considering the eventual presence of shadings (some models are presented in [106]). A similar transposition has to be performed for the driving rain on the considered wall. Some solutions for the calculation of driving rain from the rainfall intensity, wind speed and direction could be found in [107],[108],[109] and [110].

Once that the needed variables and the location are defined, the weather series for the simulations should be chosen. Using any weather series, without the characterisation of its probability, would not provide sufficient information for the risk analysis: it would be a simulation of the damage caused by the weather series, without any information on its probability of happening.

On the other hand, using a weather file intended to represent the average weather of a location would provide a risk analysis with not significant information: the calculated damage has the probability to happen on the 50 % of the time, meaning that the building envelope would not be designed to resist extreme weather conditions, but just the most common ones. This performance level would not be considered acceptable, given that one day out of two the wall would be in failure conditions. For these reasons a valid weather file should be selected, with a known and adequate probability.

8.1 Reference years for building energy simulations

The common approach used in the building energy simulations is to calculate the boundary conditions from a single year weather file, generated from the measured weather record file (here referenced as multi-year (MY) weather file) of a weather station near to the location and to run the simulations, repeating the year, for a longer period, until the stabilisation is achieved, which is to say that state when the moisture content and temperature at the first time step of the year are locally equal to the values at the last time step of the year and the influence of the initial conditions is not relevant to the solution.

This single year weather file is commonly referred to as reference year and it is designed to be used instead of the full weather record file. For the building energy simulations, the reference year is expected to be the most representative year for the weather of a considered location, thus, considering the aforementioned performance ranking of the weather series (ranking of weather years, in this case), the reference year will be the year that divides the critical years from the subcritical years, corresponding to the 50 % of the ranking. Similarly to the moisture transfer simulations, the weather series are not correlated with the building energy performance, and to achieve a reliable ranking of the weather series, the simulation of the whole weather record should be carried out. To avoid this time consuming procedure, an alternative ranking method is used.

8.1.1 Finkelstein-Schafer statistic

The standard EN ISO 15927-4:2005 [111] describes the ranking method to compose a year (from the months of the multi-year) that is the moist representative year of the multy-year. This representative year is designed to be used in building energy simulations. This method is in particular intended for the creation of Test Reference Years (TRY) and it is based on the Finkelstein-Schafer statistic method [112]. The standard will be considered as an example of the application of the statistic that will be used later for the design procedure of reference years for other applications.

First, a set of primary parameters (p indicates a general parameter) are selected as the most influential in the studied problem. The primary parameters used in [111] for the

generation of the TRY for building energy simulations are the dry-bulb air temperature (T), the global solar irradiance (E_g), the water vapour pressure (p_v) (also the relative humidity, the air absolute humidity and the dew point temperature could be used). This set of primary variables is used to generate a ranking of the MY months, ordered by representativeness using the Finkelstein-Schafer statistic. In addition, a secondary parameter is considered, the wind speed (v_w), to perform a secondary selection on the representativeness ranking and select the months that will compose the TRY.

For the generation of the TRY from the MY, the following procedure is used:

1. Calculation the daily means $\bar{p}$ of the primary variables p for the whole MY.

2. Calculation of the cumulative distribution function $\Phi(p, m(i), i)$ of the daily means $\bar{p}$ over the whole MY for each day i of a selected calendar month m, for each p. The variable i represents the ordered number of a day in the MY, from 1 to N (number of days in the MY), and it will be used as a timestamp. The function Φ is obtained from the ranking $K(\bar{p}, m, i)$ by numbering the values of the distributions of the considered p, separately for each m:

$$\Phi(p, m(i), i) = \frac{K(\bar{p}, m(i), i)}{N + 1} \tag{8.0}$$

3. Calculation of the cumulative distribution function of the daily means within each calendar month m of each year y, $F(p, y(i), m(i), i)$ from the rank order $J(\bar{p}, m(i), i)$, obtained by ordering the daily means $\bar{p}$ within the calendar month m and the year y:

$$F(p, m(i), i) = \frac{J(\bar{p}, y(i), m(i), i)}{n + 1} \tag{8.0}$$

where n is the number of days of the m calendar month considered.

4. The Finkelstein-Schafer statistic F_S is calculated for each p and each calendar month m in the MY as:

$$F_S(p, y, m) = \sum_{i=1}^{n} |F(p, y(i), m(i), i) - \Phi(p, m(i), i)| \tag{8.0}$$

5. For each p, the ranking R is assigned to each calendar month m, obtained from the ordering of the $F_S(p, y, m)$ of each y separately for each calendar month m:

$$R(p, y, m) = \frac{L(F_S)}{n_y + 1} \tag{8.0}$$

with n_y the number of years of the MY.

6. The ranking R of each calendar month is calculated for all the primary parameters and then summed, to obtain the total ranking R_{tot}:

$$R_{tot}(y,m) = R(T,y,m) + R(p_v,y,m) + R(E_g,y,m) + R(RI,y,m) \tag{8.0}$$

7. Each calendar month m of the TRY is chosen among the months m of the MY with a further secondary selection.

   - For each month ranking, the three months with the lowest R_{tot} are selected;
   - The deviation from the mean value of the secondary variables, in this case the wind speed v_w, is calculated;
   - The month m with the minimum deviation is selected.

8. The TRY is composed of the hourly series of the weather variables of the selected months and the continuity between months is set with a linear interpolation, in order to provide a smooth transition between months from different years.

8.2 Risk analysis

When the application is a risk assessment or a performance prediction, then, the definition of the weather series from which the boundary conditions are calculated is crucial. In both applications it is important to associate to the results a return period τ_R, an estimated average time between the happening of two weather series similar to the one used in the simulation. With this value, it is possible to identify $p = \frac{1}{\tau_R}$, the probability of happening of a weather series. At this point, if the intent is to carry out a performance based design of a building detail, the considered weather series can be correlated with a level of damage or a level of performance of the building detail, in the given weather series. With this correlation, the weather series could be ranked in terms of performance (or damage), from the one that causes the building detail to perform better to the one that corresponds to the worst performance. It could be convenient to define a performance level that is considered acceptable, below which all the performance values are considered failures. Then it could be also defined an acceptable probability of failure, for example $p_f = 10\%$, meaning that if a life period for the building of 10 years ($= \tau_R$ is considered it will be accepted to have a performance level under the failure threshold for less than the 10 % ($= p_f$) of the time (1 year). Using the weather series corresponding to the 10 % ($= p_f$) of the ranking to design the building detail, it will be designed to not fail for the other 90 % of weather series, thus it will have only the probability to fail $p_f = 10\%$, that corresponds to a return time $\tau_R = 10$ years. When a risk analysis is performed, a critical weather event could be identified and selected by its intensity or with respect to a performance indicator. In heat and moisture transfer phenomena, the intensity of a weather event, for example, of a rain event, could not be correlated with the performance indicator of a building detail without performing a full simulation and it could happen that a weather series causes the failure for a given building envelope, while another building envelope has a good performance.

8.3 Reference year for heat and moisture transfer simulations

When considering the moisture transfer risk assessment simulations, the expression "reference year" is used with another meaning. The typical applications of these kind of simulations are the risk analyses, therefore the weather files are chosen to represent extreme conditions: instead of the 50 % of the performance ranking, it should be chosen to represent the 10 % of the worst performing years. For the Glaser method procedure, the standard EN ISO 13788:2013 prescribes to use the mean monthly temperature values likely to occur once every 10 years and, if the only available weather file is a representative year (for example a weather file that could be used for building energy simulations), it recommends to subtract 2 K to the external air temperatures during heating period and to add 2 K during cooling period.

The procedure for the "Moisture Design Reference Year" suggested by the EN 15026:2007 is finalized to reach failure on an acceptable rate, for example once in ten years. Such a reference year should be selected among the years measured in the multi-year according to the studied problem. The standard provides three examples:

- For low temperature problems, it should be used the year with the mean temperature closest to the 10-percentile value of the distribution of the annual mean temperatures;
- For high temperature problems, the reference year should be the one with the mean temperature closest to the 90-percentile value of the distribution of the annual mean temperatures;
- For rain penetration problems, the year should have the annual rainfall value closest to the 90-percentile of annual rainfall values.

An application of the EN 15026:2007 criterion is presented in the book [113], where the example for the Belgium is provided. Three reference years are presented for the same location:

- a wet and windy year to be used for the rain leakage risk assessments,
- a year with sunny summers with regular rains fro the solar-driven vapour flow risk evaluation
- and then a cold, humid climate with a summer with small radiative fluxes for the interstitial condensation problems.

A moisture index approach is presented as an alternative, to perform a selection of the weather years without carrying out simulations of the walls. The use of moisture indexes, or other indexes used as derived weather variables, is at the base of other approaches, for example [114], or [115], which is based on the saturation deficit parameter which is not structure-dependent. In [116] the weather data is analysed using various methods to provide a ranking of the weather years with damage functions like the time of wetness, the mould growth index, and the maximum moisture content. More recently, [117] presented a preliminary selection of three weather years is performed using the Climate

Index. Then, the design year selection is completed using the risk assessment simulations with the three years. Then [118] for the selection of the months of the reference years for the hygrothermal assessment (HRY) have used median, mean, minimum, maximum value, the 25%, and the 75% quartile of air temperature and normal rain. The results of HRY was compared with the standard methodology of EN ISO 15927-4:2005 and with measured data on long-term.

9

Representative moisture weather files

The most recent extended set of reference weather files for the Italian climate was published by the Italian Thermotechnical Committee (CTI) in 2016, using the method reported in [119], [120] and [121] in accordance with [111]. Further research has been carried out on the topic, extending the TRY generation methodology using weighting coefficients, for example in [122], which provided a study on the representativeness of reference years obtained from sequentially reduced MY. A more recent study on the use weighting coefficients is reported in [123].

This chapter is a summary of the work presented in [8]. The method described by the standard EN ISO 15927-4:2005, typically used to design the TRY, has been extended with 34 variations of the procedure. The 34 generation criteria have been based on the assumption that the simulation results are influenced by rain deposition on the considered wall and that the weather selection procedure could be different for every considered wall exposure. For this reason, the procedure of the month selection presented in 9.1.1 has been followed considering the driving rain on five exposures as different weather variables, obtained combining the rainfall intensity, the wind velocity and the wind direction. The years of the climate of Turin (Italy) between 2002 and 2016 have been considered as multi-year for the generation of the reference years. The resulting years are intended to be representative of the weather climate, differently from the TRY, also considering the moisture related variables.

The main reason for the proposal of this procedure is the fact that it is easily applicable to all the hourly weather records in a structure independent procedure. The choice of the primary variables for the selection procedure should depend on the problem to be studied with the simulation. Given that every moisture related problem could be triggered by different weather conditions, it is useful to identify the representative year considering the critical variable that have major effect on the considered phenomenon. For example, when the rain is involved in the calculations of an interstitial condensation risk assessment, the standard TRY design procedure does not perform a statistical analysis of the rain distribution, while it could be the most important variable of the risk

assessment procedure. The selected months could be the most dry months and provide simulations with underestimations of the risk.

9.1 Method

The validation of the proposed representative years is carried out by comparing the hygrothermal behaviour of building components simulated with the new reference years, with the behaviour obtained with the weather conditions over the long term from the measured weather file. The 34 reference weather files have been generated changing the combination of the primary variables to be considered in the standard procedure of the TRY generation. The combinations used are presented in Table 9.1. The weather record data series, from 2002 to 2016, are provided by the Regional Agency for the Protection of the Environment (ARPA) of the Piedmont Region (Italy).

9.1.1 Month selection procedure

The procedure for the selection of the most representative months is a generalised version of the one presented in . In this case the set of primary variables p changes for every representative year. The considered sets are identified with I_{ID}, where ID is the number of the combination, listed in Table 9.1. In this procedure the secondary variable selection is not used.

1. Calculation the daily means $\bar{p}$ of the primary variables p from the selected set, for the whole MY.

2. Calculation of the cumulative distribution function $\Phi(p, m(i), i)$ of the daily means $\bar{p}$ over the whole MY for each day i of a selected calendar month m, for each p. The variable i represents the ordered number of a day in the MY, from 1 to N (number of days in the MY), and it will be used as a timestamp. The function Φ is obtained from the ranking $K(\bar{p}, m, i)$ by numbering the values of the distributions of the considered p, separately for each m:

$$\Phi(p, m(i), i) = \frac{K(\bar{p}, m(i), i)}{N + 1} \tag{9.0}$$

3. Calculation of the cumulative distribution function of the daily means within each calendar month m of each year y, $F(p, y(i), m(i), i)$ from the rank order $J(\bar{p}, m(i), i)$, obtained by ordering the daily means $\bar{p}$ within the calendar month m and the year y:

$$F(p, m(i), i) = \frac{J(\bar{p}, y(i), m(i), i)}{n + 1} \tag{9.0}$$

   where n is the number of days of the m calendar month considered.

4. The Finkelstein-Schafer statistic F_S is calculated for each p and each calendar month m in the MY as:

Table 9.1: Combinations of variables used for the generation of the 34 Moisture Reference Years. The MRYs generaon method is obtained changing the weather variables used in the EN ISO 15927-4:2005 method. The considered weather variables are dry-bulb air temperature (T), irradiation (E_g), relative humidity (φ), wind speed (v_w), rainfall intensity on a horizontal surface ($r_\perp$), rainfall intensity on a vertical wall (r_d) facing North, South, East or West (adapted from [8]).

ID	T	E_g	φ	v_w	$r_\perp$	$r_{d,S}$	$r_{d,E}$	$r_{d,N}$	$r_{d,W}$
ISO	x	x	x	x					
1	x	x	x			x			
2	x	x	x				x		
3	x	x	x					x	
4	x	x	x						x
5	x		x			x			
6	x		x				x		
7	x		x					x	
8	x		x						x
9			x			x			
10			x				x		
11			x					x	
12			x						x
13	x					x			
14	x						x		
15	x							x	
16	x								x
17		x				x			
18		x					x		
19		x						x	
20		x							x
21						x			
22							x		
23								x	
24									x
25			x						
26				x					
27	x								
28		x							
29	x	x	x		x				
30	x		x		x				
31			x		x				
32	x				x				
33		x			x				
34					x				

$$F_S(p,y,m) = \sum_{i=1}^{n} |F(p,y(i),m(i),i) - \Phi(p,m(i),i)| \tag{9.0}$$

5. For each p, the ranking R is assigned to each calendar month m, obtained from the ordering of the $F_S(p,y,m)$ of each y separately for each calendar month m:

$$R(p,y,m) = \frac{L(F_S)}{n_y + 1} \tag{9.0}$$

with n_y the number of years of the MY.

6. The ranking R of each calendar month is calculated for all the primary parameters of the chosen set and then summed, to obtain the total ranking R_{tot}:

$$R_{tot}(y,m) = \sum_{p \in I_{ID}} R(p,y,m) \tag{9.0}$$

7. The representative year is composed of the hourly series of the weather variables of the selected months and the continuity between months is set with a linear interpolation, in order to provide a smooth transition between months from different years.

9.1.2 Representative year description

It is possible to perform a first comparison of the obtained weather files comparing the annual average values of the main weather variables and to evaluate the effects of the statistical selection.

To highlight the differences among the considered years, a normalisation procedure is applied on the variables. For example, for a generic variable P, the normalised auxiliary variable I_P, the normalised index of the variable P, is calculated as:

$$I_P = \frac{P - P_{min}}{P_{max} - P} \tag{9.0}$$

Where:

P_{max} = maximum value of the variable P in the weather record

P_{min} = min value of the variable P in the weather record

To identify the years with the larger wetting loads, the normalised values of the rainfall on a horizontal plane are presented in Fig. 9.1.

The values of the years of the weather record are taken as reference then the normalised index for the weather record has a minimum of 0 (for the year 2010, indicating that it has the minimum average rainfall of the record) and a maximum of 1 (indicating that it has the maximum average rainfall of the record). The index for representative

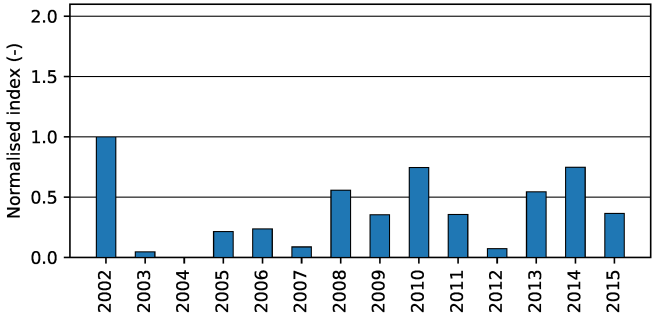

a) Index for the Turin weather record.

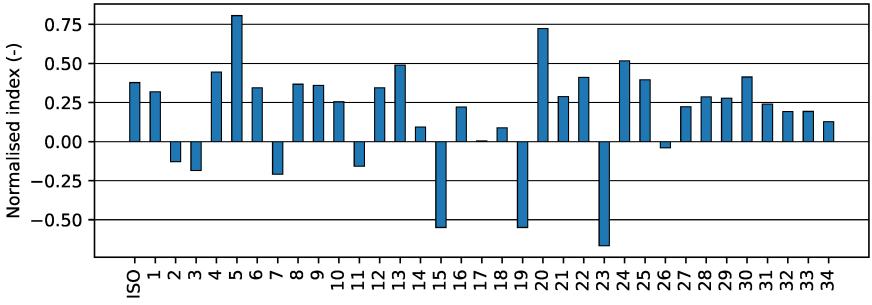

b) Index for the Turin moisture representative years.

Figure 9.1: Characterization of the designed moisture representative years with respect to the rainfall on a horizontal plane. The average of the weather record is 0.4

years are calculated with the maximum and minimum value of the weather record, for this reason the values could be larger than 1. Given that the average rainfall index for the whole weather record is 0.4, it could be observed that most of the year provide similar values, while the years obtained considering the driving rain on a wall facing North are the ones with the average rainfall lower than 0, meaning that the average of the reference year is lower than the minimum average rainfall of the weather record (ID 3,7,11,15,19,23), well representing the orientation with the lower levels of driving rain. The years ID 5 and 20 show high values of MI due to the selection of months with high values of rainfall intensity.

In [114], a generalised formulation of the concept of Moisture Index is presented as an index that could be used to compare different weathers depending on the moisture related weather variables. A Moisture Index (hereinafter referred to as MI), similar to the MEWS Moisture Index described in [114], is here used to evaluate the results of the representative year design process.

The MI is defined from two other indexes, the Drying Index (DI) and a Wetting Index (WI):

$$MI = \sqrt{WI^2 + (1 - DI^2)} \tag{9.0}$$

The value of the MI could be larger than 1 and, if the DI or the WI is negative it has been set to 0 before the calculation of MI. A low MI indicates that the year is less critical, from the point of view of the moisture loads and the drying potential. With this definition, the value of MI is defined with respect to the weather record (the MI is intended as a ranking system of different years). The Wetting Index WI is defined as the annual average rainfall $\bar{r_{\perp}}$ normalised with respect to the maximum and minimum annual average rainfall of the weather record, it corresponds to the previously defined rainfall normalised index (in Fig. 9.1):

$$WI = \frac{\bar{r_{\perp}} - \bar{r_{\perp min}}}{\bar{r_{\perp max}} - \bar{r_{\perp}}} \tag{9.0}$$

An higher WI indicates higher moisture loads, relatively to the values of the weather record. Similarly, the Drying Index DI is defined as the annual average saturation deficit $\bar{\delta}^{sat}$, also normalised with respect to the maximum and minimum annual average saturation deficit of the weather record:

$$DI = \frac{\bar{\delta}^{sat} - \bar{\delta}^{sat}_{min}}{\bar{\delta}^{sat}_{max} - \bar{\delta}^{sat}} \tag{9.0}$$

The saturation deficit is defined according to [115] as the difference between the humidity ratio and the humidity ratio of saturation calculated at the dry bulb air temperature:

$$\delta^{sat} = x_{sat} - x \tag{9.0}$$

A lower DI indicates a year with a lower drying potential with respect to the values of the weather record. The Drying Index values for the considered weather years are presented in Fig. 9.2, while the values of the Wetting Index are presented in Fig. 9.1. The Moisture Index is presented in Fig. 9.3. The Drying Index shows higher values

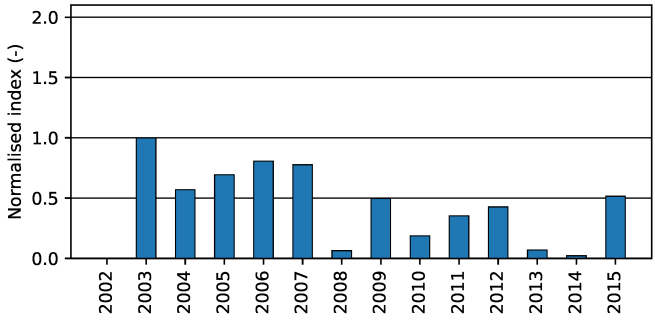

a) Index for the Turin weather record.

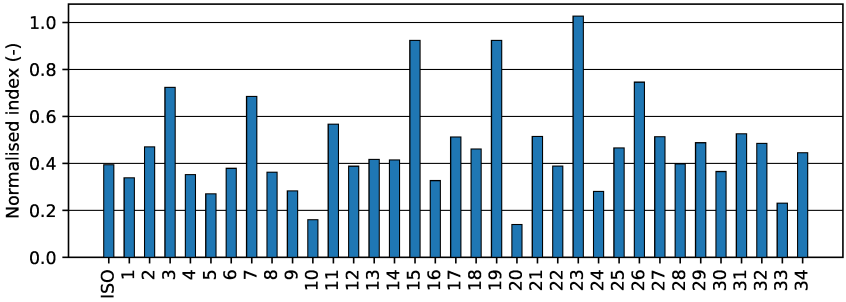

b) Index for the Turin moisture representative years.

Figure 9.2: Characterization of the designed representative years with the Drying Index. The weather record average Drying Index is 0.4.

also for the North wall exposure years (ID 3,7,11,15,19,23) demonstrating a correlation between the rainfall and the humidity ratio, while the years ID 10 and 20 obtained from the combination of φ, $r_{d,E}$ and E_g, $r_{d,W}$ respectively, obtained lower Drying Index values and consequently low Moisture Index values.

The North walls with low Wetting Index values (Fig. 9.1 also obtained low Moisture Index values accordingly, meaning that the designed representative years should be less critical respect to the others.

It is interesting to observe that the inclusion of ϕ as primary variable in the design process (ID 3,7,11) produced MI closer to the average value.

9.1.3 Representative year evaluation

The evaluation of the obtained representative years has been performed comparing the hygrothermal simulation results of two different building envelopes, a hollow brick wall and a timber wall. The simulations have been performed with the software WUFI Pro, based on the model presented in [34]. The comparison is held evaluating the monthly

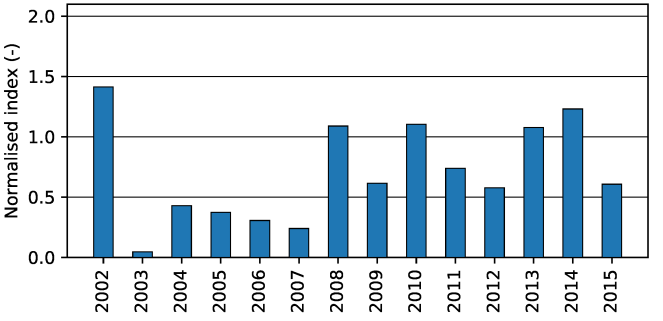

a) Index for the Turin weather record.

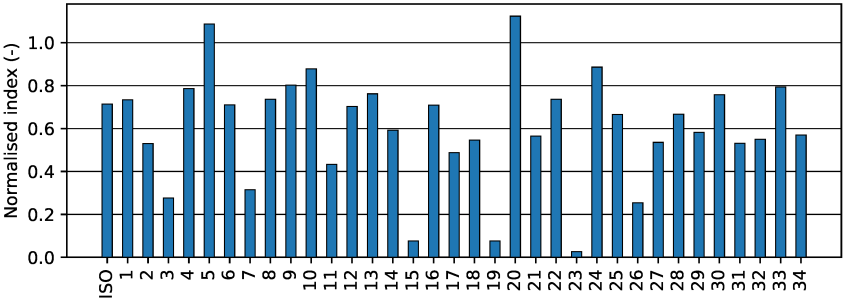

b) Index for the Turin moisture representative years.

Figure 9.3: Characterization of the designed representative years with respect to the moisture index. The weather record average Moisture Index is 0.7.

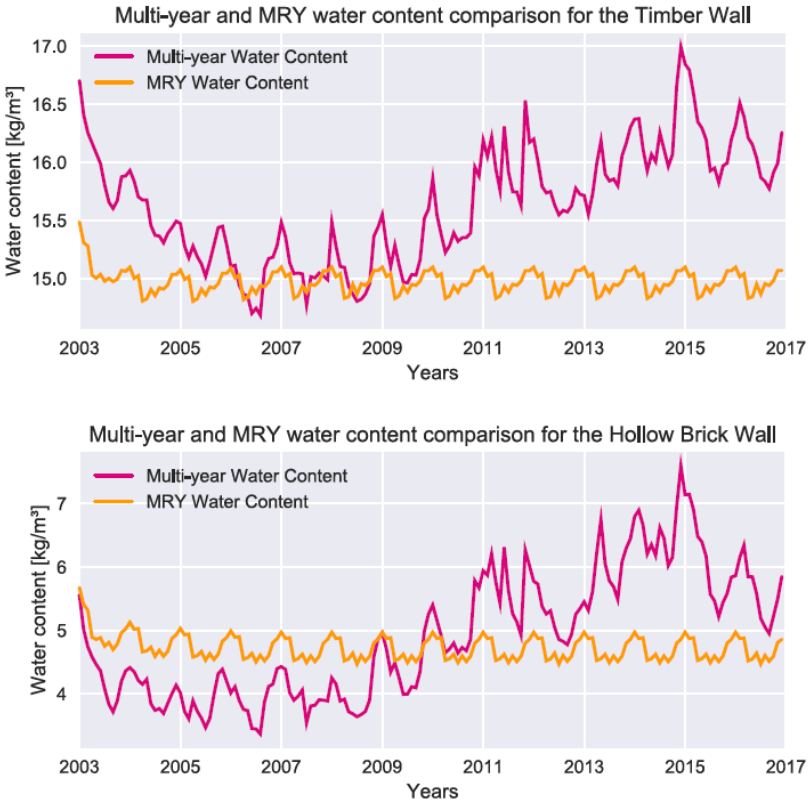

Figure 9.4: Annual mean water contents of the hollow brick wall for the measured weather files simulations for the East exposition (top plot) and the West exposition (bottom plot). The representative year is referred to as MRY (adapted from [8]).

mean moisture content and comparing it to the one evaluated with the historical data set. An example of the results is presented in Fig. 9.4. The moisture content of the wall obtained from the representative year (in the Fig. is referenced as "MRY Water Content") is the result of the repetition of the simulation of the same representative year, while the "Multi-year Water Content" is obtained with the measured weather data, thus every year is different from each other. the initial conditions of the simulations are obtained after a simulation of a year, the representative year for the "MRY Water Content" and the 2003 for the "Multi-year Water Content". In these simulations a large contribution of moisture content comes from the driving rain.

The reference years from number 1 to number 24 have been simulated considering the design orientation (for example the reference year 1, designed considering the rain deposition on vertical wall facing South has been used for the simulation of the wall build-up facing South), while the reference years from number 25 to 34 have been used for the simulations for the five expositions considered (since normal rain has a general effect on all the expositions).

9.2 Results

The walls passed the moisture accumulation assessment and the condensation risk assessment for every representative year considered and for the historical data set. For this reason the annual mean results (Fig. 9.5) have been compared in terms of relative standard deviation from the annual mean values obtained by the measured weather data. The Timber wall results show effective representative years, with lower values of the relative standard deviation, with respect to the Hollow brick wall results.

9.2.1 Rain influence

The aim of this analysis is to evaluate the influence of the rain on the months selection and the consequent effects on the results of the simulations. The influence of rain can be seen in 9.6, where the moisture content results are compared with the driving rain for two simulations. It has to be noted that also the duration of rain, not the intensity alone, has an influence on the simulation results. The exposition of the walls present some common trends. For the Timber wall, the ID 34 (based on $r_\perp$) better represents the South, East and North expositions, while the West exposition is better described by the ID 25 (based on φ) and the Horizontal by the ID 28 (based on I). The ID ISO and the ID 28 are the years better representing the walls in the five directions. The Hollow brick wall shows different exposition specific trends: the South facing exposition is better represented by the ID 34 (based on T and φ), the East and West by the ID ISO, the North by the ID 7 (based on T , φ, r_d) and the Horizontal by the ID 32 (based on T and φ). From Fig. 9.5 it is also possible to observe some overall results. The ID from 1 to 24, considering r_d are generally less representative for the most rain exposed directions (West and Horizontal). Exclusively r_d based years (21-24) are less representative than ID from 29 to 34, based also on $r_\perp$. For the Timber wall the ID from 25 to 28 and the ID ISO (not based on $r_\perp$ or r_d) are better performing than the $r_\perp$ based ones, while for the Hollow brick wall, their behaviour is similar.

9.3 Material influence

The relative standard deviations of the Timber wall are lower than the Hollow brick wall. This difference is due to the different hygrothermal properties of the materials. The Hollow brick wall external layer has higher liquid transport coefficient values than the Timber wall, which has also higher moisture storage function values, and that could lead in faster responses to the rainfall (larger water content variations), with larger differences from the historical data set results. The moisture representative years depending on rain deposition on vertical wall (obtained from wind speed, direction and normal rain) led to less representative years than the ones generated by the standard method. This result could be related to the features of the climate of Turin (Italy), whose rains are brief and quickly dried afterwards. On the other hand, one of the reasons could also be the fact that the external material layers do not respond instantly to the transient hourly rainfall excitations (slower than the heat excitations) and that the total water content of the wall is more influenced by the long term mean values of the environmental excitations, which is also been discussed in [9].

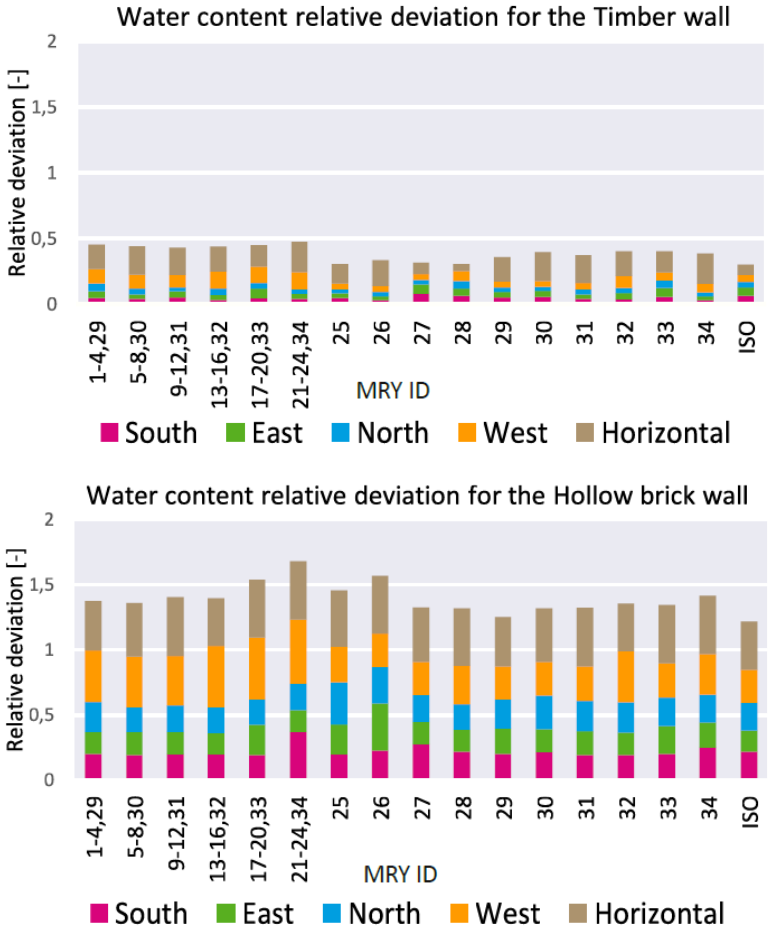

Figure 9.5: Relative standard deviations of the moisture contents between the simulation of the historical years and every reference year described in Table 9.1. The results for the timber wall are in the top plot, while the results for the hollow brick wall are in the bottom plot.The representative year is referred to as MRY (adapted from [8]).

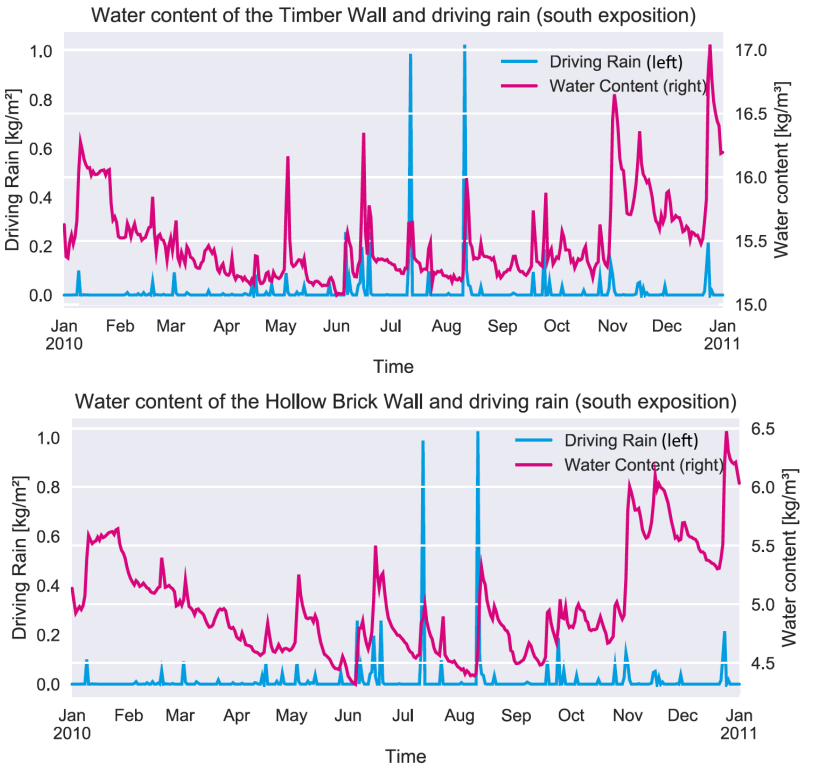

Figure 9.6: The water contents of the wall and the rain deposition on the southern wall for the year 2010 are shown in the plots. Two wall types (Timber wall and Hollow brick wall) are considered in the study. The walls are considered in South, East, North, West and Horizontal orientations. The simulations have been performed using the software WUFI Pro 6. The representative year is referred to as MRY (adapted from [8]).

9.4 Applications

The results suggest that, when the use of a single year is preferred, the proposed representative years obtained with the standard procedure EN ISO 15927-4:2005 better reproduces the results obtained with the simulation of the measured weather files. As expected, the response to the representative years is structure dependent and the results confirm that these weather years should not be used for risk assessment simulations alone, without other weather files designed to represent critical events.

Using these representative years for moisture related simulations instead of critical years can lead to a valid risk indicator for non-extreme weather and for the simulation of drying processes in which a critical reference year could lead to overestimations of the risk. This could be seen in Fig. 9.4. The moisture content of both walls calculated with the weather record show a peak at year 2015, which is not represented by the results of the representative year. On the other hand, the moisture accumulation condition is not met in both simulations, even if the moisture contents of the full weather record are higher than the ones of the representative year, the final moisture content is lower than the starting moisture content, showing that the wall is not accumulating moisture year after year.

Furthermore, if the risk assessment involves a threshold, extreme weather files (see Chapter 12) should be used. As an example, the wood decay risk analysis, that requires, as a rule of the thumb, to limit the moisture content under a threshold of 20% in mass, should be performed using an extreme reference year, selected to expose the wall to extreme moisture loads, in order to avoid to reach the wood decay conditions even in conditions with a low return period.

Further work should be carried out to establish if the approach of the representative years could be extended to other applications, like energy simulations, in which the efficiency of the components of the systems depends on moisture related environmental conditions, such as evaporative towers [124], evaporative cooling systems for industrial buildings [125], shopping malls [126] and other heat recovery systems [127].

10

Influence of rainfall duration

In Section 9.2.1 the influence of rain on the results of the simulations has been evaluated and it has been observed that the duration of the rain events influences the moisture content of the wall 9.6.

On the other hand, the Finkelstein-Schafer statistic application methodologies are based on daily means, which implies that only the total rainfall of the day is considered in the statistic and the rain duration is not considered.

If a rain event lasts 10 hours and has a hourly rainfall intensity of 1 $\frac{\text{kg}}{\text{m}^2}$, the daily mean rainfall intensity will be of 10 $\frac{\text{kg}}{\text{m}^2}$, which is the same mean rainfall intensity of an event with a duration of 1 hour and a rainfall intensity of 10 $\frac{\text{kg}}{\text{m}^2}$. Depending on the materials of the wall, the former rain event will cause a larger ingress of water in the structure, with respect to the second one.

In order to consider this effect, a new parameter, the rain duration t_r is considered among the primary variables for the representative weather files composition. This parameter will be created counting the hours of consecutive rain in the weather file and assigning the time duration of the rain event in hours, at the end of the said event. In this way the two rains described above would evaluated by their duration and not by their intensity better representing the influence on the building envelopes. This work is presented in [128].

10.1 Method

With a similar analysis procedure followed in Chapter 9, the influence of the duration of the rain events in the selection of the representative months is evaluated. In this case the values of the statistic are summed together using a weighting coefficient, similarly to [123].

10.1.1 MRY generation procedure

The following procedure is followed:

1. Calculation the daily means $\bar{p}$ of the primary variables p from the selected set, for the whole multi-year.

2. Calculation of the cumulative distribution function $\Phi(p, m(i), i)$ of the daily means $\bar{p}$ over the whole multi-year for each day i of a selected calendar month m, for each p. The variable i represents the ordered number of a day in the multi-year, from 1 to N (number of days in the multi-year), and it will be used as a timestamp. The function Φ is obtained from the ranking $K(\bar{p}, m, i)$ by numbering the values of the distributions of the considered p, separately for each m:

$$\Phi(p, m(i), i) = \frac{K(\bar{p}, m(i), i)}{N + 1} \tag{10.0}$$

3. Calculation of the cumulative distribution function of the daily means within each calendar month m of each year y, $F(p, y(i), m(i), i)$ from the rank order $J(\bar{p}, m(i), i)$, obtained by ordering the daily means $\bar{p}$ within the calendar month m and the year y:

$$F(p, m(i), i) = \frac{J(\bar{p}, y(i), m(i), i)}{n + 1} \tag{10.0}$$

   where n is the number of days of the m calendar month considered.

4. The Finkelstein-Schafer statistic F_S is calculated for each p and each calendar month m in the multi-year as:

$$F_S(p, y, m) = \sum_{i=1}^{n} |F(p, y(i), m(i), i) - \Phi(p, m(i), i)| \tag{10.0}$$

5. For each p, the ranking R is assigned to each calendar month m, obtained from the ordering of the $F_S(p, y, m)$ of each y separately for each calendar month m:

$$R(p, y, m) = \frac{L(F_S)}{n_y + 1} \tag{10.0}$$

   with n_y the number of years of the multi-year.

6. The modification of the procedure is applied at this point. The ranking R of each calendar month is calculated for all the primary parameters of the chosen set and then summed, using the weighting parameters a_p from Table 10.1 to obtain the total ranking R_{tot}:

$$R_{tot}(y, m) = \sum_{p \in I_{ID}} a_p \cdot R(p, y, m) \tag{10.0}$$

7. The representative year is composed of the hourly series of the weather variables of the selected months and the continuity between months is set with a linear interpolation, in order to provide a smooth transition between months from different years.

Table 10.1: Combinations of weighting factors a_p of the variables used for the representative year generation procedure. The MRY numbers are used to identify the combinations.

ID	T	p_v	E_g	v_w	$r_\perp$	t_r
1	1	1	1	1	1	0
2	1	1	1	0	1	0
3	1	1	0	0	1	0
4	1	0	0	0	1	0
5	0	0	1	0	1	0
6	0	1	0	0	1	0
7	1	1	1	1	0	1
8	1	1	1	0	0	1
9	1	1	0	0	0	1
10	1	0	0	0	0	1
11	0	0	1	0	0	1
12	0	1	0	0	0	1
13	1	1	1	1	1	1
14	1	1	1	0	1	1
15	1	1	0	0	1	1
16	1	0	0	0	1	1
17	0	0	1	0	1	1
18	0	1	0	0	1	1
19	1	1	1	1	0,2	0,8
20	1	1	1	0	0,2	0,8
21	1	1	0	0	0,2	0,8
22	1	0	0	0	0,2	0,8
23	0	0	1	0	0,2	0,8
24	0	1	0	0	0,2	0,8
25	1	1	1	1	0,8	0,2
26	1	1	1	0	0,8	0,2
27	1	1	0	0	0,8	0,2
28	1	0	0	0	0,8	0,2
29	0	0	1	0	0,8	0,2
30	0	1	0	0	0,8	0,2
31	1	1	1	1	0	0
32	1	1	1	0	0	0
33	1	1	0	0	0	0
34	1	0	0	0	0	0
35	0	0	1	0	0	0
36	0	1	0	0	0	0

In this analysis, for simplicity, only the rain fall on the horizontal plane is considered, and the other vertical wall expositions are not considered.

10.1.2 Representative year evaluation

The 36 representative weather files are compared first in therms of Wetting Index (normalised annual average rainfall intensity), Drying Index (normalised saturation deficit) and Moisture Index. The three indexes are defined in Section 9.1.2. The Wetting Index is presented in Fig. 10.1. The values are generally close to 0.4, the average of the weather record. It is observed that the years ID from 31 to 36 have the most extreme values, accordingly to the fact that the rainfall intensity or the rainfall duration has not been considered in the design process. The IDs that do not take in consideration the E_g and v_w, ID 3,9,15,21,27,33 produced years with lower Wetting Index values than the other IDs. The larger Wetting Indexes are obtained from the IDs designed considering T, φ, E_g and v_w togheter with a combination of r and t_r. The IDs that considered the t_r in the procedure with weighting factors of 0.8 or more (IDs from 7 o 12 and from 19 to 24) produced conservative values of MI.

The Drying index values in Fig. 10.2 are also generally close to the weather record average (0.3). Also for this index, the ID 3,9,15,21,27,33 years produced more dry years, with Drying Index values slighlty higher than the other IDs, differently in this case, the highest DI values are the ID 4,10,16,22,28 and 34 produced by the combinations that consider only T and with other rainfall variables.

As a result, the Moisture Index values (Fig.10.3) confirm that the ID 3,9,15,21,27,33 years are the most dry years and that considering the rain duration as a principal variable, with a coefficient higher than 0.8, lead to Moisture Index values closer to the weather record average 0.8. Not considering the rainfall intensity and duration (IDs from 31 to 36) causes higher or lower Moisture Indexes.

10.1.3 Risk analysis

The evaluation of the MRY has been performed comparing the probability of failure for three failure conditions, presented in Table 10.3, for six wall types typically used in the Friuli-Venezia Giulia region. The wall layers are listed in Table 10.2 and the layer compositions is illustrated in Fig. 10.4. The material properties are taken from the Delphin material database and for each material the conductivity, the moisture retention curve, the vapour permeability, and the liquid diffusivity are provided in function of the relative humidity.

10.1.4 Simulations

The simulations are performed using DELPHIN 6. The internal conditions are set to "normal moisture load", defined in the standard EN 15026:2007. The initial conditions of the walls are set to constant values: the temperature is set to 20 °C C and the relative humidity to 80%. The wall is set as horizontal, fully exposed to rain. This modelling choice is not a realistic situation, but it is considered to reduce the influence of the direction of the wall exposure. The risk of failure has been calculated using the damage criteria presented in Table 10.3. The risk evaluations have been performed for

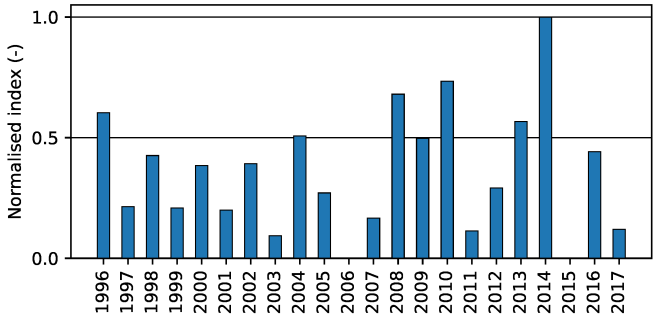

a) Index for the Udine weather record.

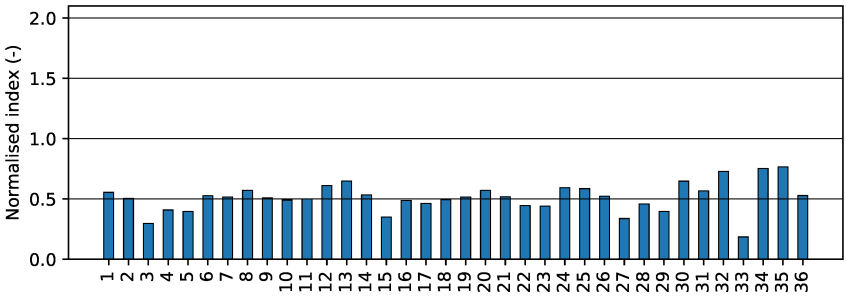

b) Index for the Udine moisture representative years.

Figure 10.1: Characterization of the designed moisture representative years with respect to the rainfall on a horizontal plane (Wetting Index). The average of the weather record is 0.4.

Table 10.2: Building envelopes considered in this analysis. The walls are described by the thickness d, the total thermal transmittance U, the total thermal resistance R, and the diffusion-equivalent air-layer thickness S_d.

ID	Description	d_{tot} (m)	U_{tot} (W/m^{2}K)	R_{tot} (m^{2}K/W)	$S_{d,tot}$ (m)
SW	Stone wall	0,38	0,70	1,44	5
SWi	Well insulated stone wall	0,53	0,13	7,76	50
HB	Hollow brick wall	0,49	0,39	2,59	7
HBi	Well insulated hollow brick wall	0,58	0,15	6,72	41
TWa	Timber wall with internal vapour barrier	0,53	0,13	7,45	56
TWb	Timber wall with external vapour barrier	0,53	0,13	7,45	56

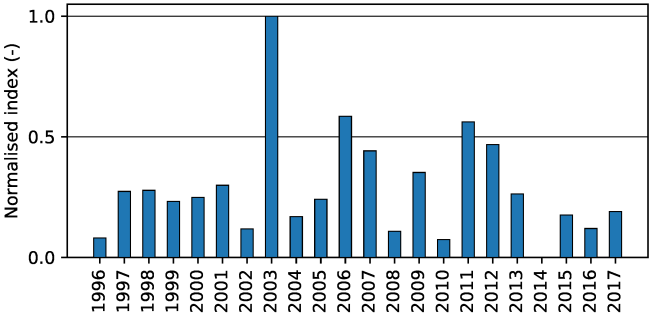

a) Index for the Udine weather record.

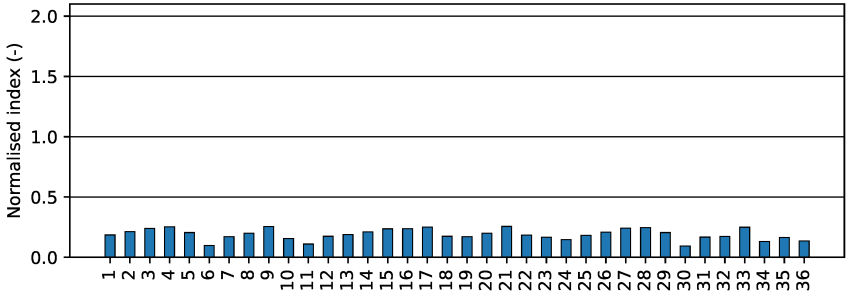

b) Index for the Udine moisture representative years.

Figure 10.2: Characterization of the designed moisture representative years with respect to the Drying Index on a horizontal plane. The average of the weather record is 0.3.

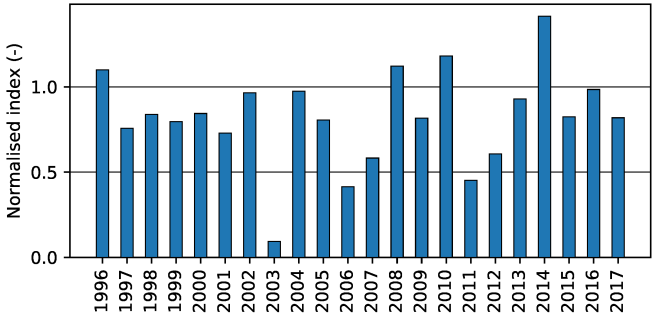

a) Index for the Udine weather record.

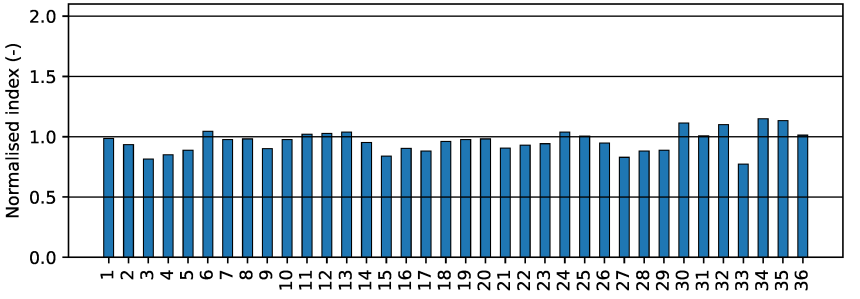

b) Index for the Udine moisture representative years.

Figure 10.3: Characterization of the designed moisture representative years with respect to the Moisture Index on a horizontal plane. The average of the weather record is 0.8.

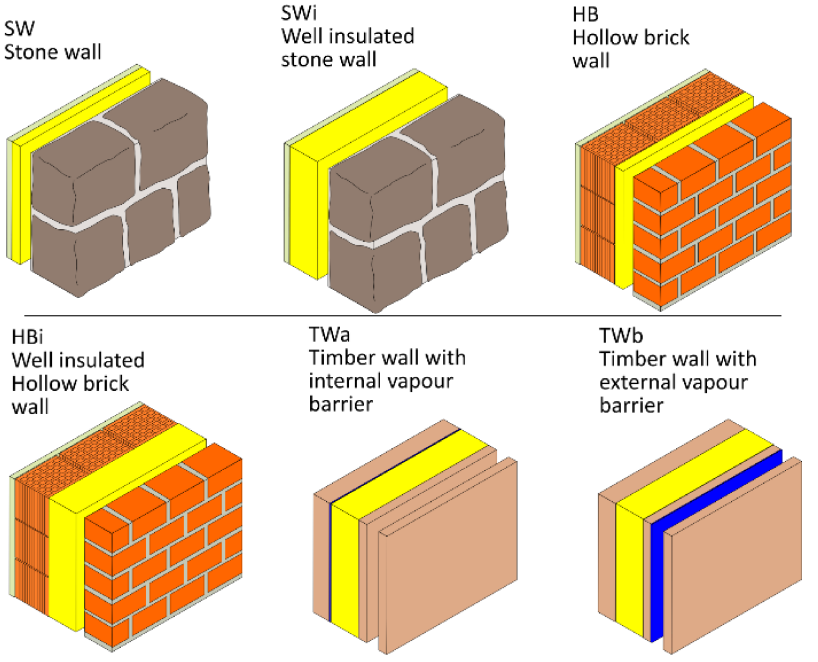

Figure 10.4: Wall types considered for the evaluation of the MRY. These walls are typical of the Friuli region. The internal surface is considered to be on the left.

Table 10.3: Description of the failure modes considered in the analysis. The involved parameters are the relative humidity φ and the temperature T.

Failure mode	Position	Condition
Mould growth	Internal surface	φ >80%
Moisture Accumulation	Internal layers	φ >95%
Freeze damage	External surface	φ >98% and T <0°C

the mould growth , the interstitial condensation and the freeze-thaw damage. The used failure criteria are simplified, for the sake of the representative years comparison. The risk has been calculated as the rate of days in which the risk condition is found.

10.1.5 Multi-year weather file

The multi-year weather file used as source has been measured by the weather station of Udine Sant Osvaldo. The data has been kindly supplied by ARPA FVG. The worse missing data rate is of the 1,5 % for the wind direction measurements. For the other variables the missing data rate is less than the 1 %. The missing data is corrected with a linearisation when shorter than 5 hours and with an averaging between the previous known day and the following known day for the larger data gaps. For gaps larger than seven days found in rain and wind data series only, the values are integrated with values of the previous years.

10.2 Results

The risk analysis is performed on the resulting distributions of relative humidity and temperature. For each wall, the calculated risk for each representative year is compared with the calculated risk of the multi-year. The superficial mould growth risk has been found to be 0% for every simulation performed in agreement between the multi-year results and the representative year results. For the accumulation risk assessment calculation, the external layers of the walls, exposed to rain and sun, thus frequently wet and easily dried, have not been considered.

10.2.1 Moisture accumulation risk

The resulting moisture accumulation risks for the six walls and for every representative year and the multi-year are used for the comparison of the representative years' set of variables. For the comparison, the difference between the risk of every representative year and the multi-year is calculated for every wall, and the mean value of the difference is plotted in Fig. 10.5. The moisture accumulation risk of the multi-year is found to be better represented by the results of the IDs 2,8,14,20,26 generated by the statistical combination of air temperature, vapour pressure, global irradiation and a combination of rain intensity and rain duration. Among the combinations of rain duration and intensity, the one with the lower mean risk difference is the one obtained with the

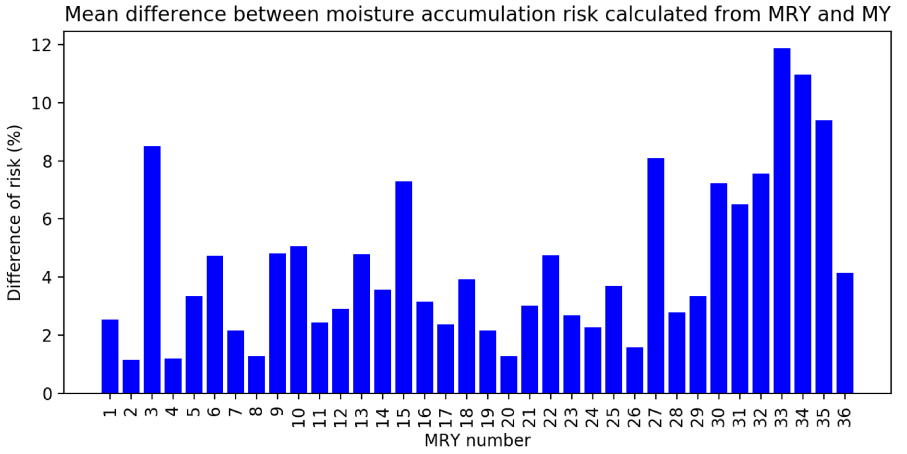

Figure 10.5: Mean differences between the moisture accumulation risk calculated using the representative year weather file and the risk calculated using the multi-year weather file for the six wall types considered presented in Table 10.4 and illustrated in Fig. 10.4.

coefficients a_{t_r}=0.8 for rain duration and $a_{r_\perp}$0.2 for rain intensity (IDs from 19 to 24). The most effective rain combination is the group with the coefficients 0.8 for rain duration and 0.2 for rain intensity (representative year from 19 to 24). Even if the most representative risk is obtained from the representative year number 2, the number 20 should be considered the most suitable to be used, as the intersection between the most representative groups of representative years, with a result similar to the one of the representative year number 2. The representative year number 20 is intended to be more representative of the rain duration than of the rain intensity, which is secondary for the moisture accumulation risk (a light, but longer rain could be more influential than a short but intense rain, that could bring the surface of the porous material to saturation quickly).

10.2.2 Freeze-thaw risk

The mean differences for the freezing risk are plotted in Figure 5.

The representative year that resulted in a better representation of the multi-year freezing damage risk are the representative year 1,7,13,19,25 and 31 based on the combination of air temperature, vapour pressure, irradiation, wind speed and a combination of rain intensity and rain duration. The combination of rain duration and rain intensity that resulted in the most representative year is the one of the years from 1 to 6, with rain intensity multiplied by a factor of $a_{r_\perp}$=1 and the rain duration by $a_{t_r} = 0$. The minimum mean risk difference is found for the representative year number 32, while the most representative groups of representative year are the ones obtained from the combinations of dry bulb air temperature T, vapour pressure p_v, global irradiation E_g, wind speed v_w and a combination of rain intensity $r_\perp$ and rain duration t_r (IDs 1,7,13,19,25,31), while the combination of rain intensity and rain duration with the lower mean risk difference

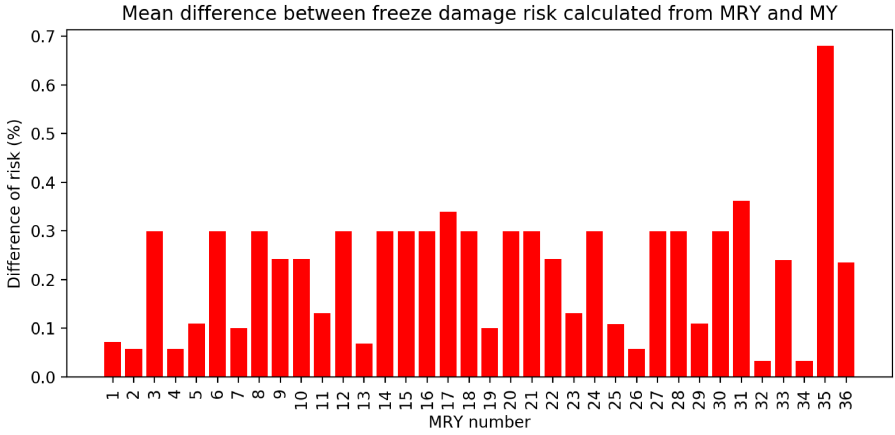

Figure 10.6: Mean differences between the freeze-thaw risk calculated using the multi-year weather file and the risk calculated using the representative year weather file for the six wall types considered presented in Table 10.4 and illustrated in Fig. 10.4.

is the one with the coefficient a_{t_r} =0 for the rain duration and $a_{r_\perp}$=1 for the rain intensity. The intersection of these two groups, the representative year number 1, could be use for this simulations. For the freeze risk, the moisture content of the wall is not the only relevant variable, also the temperature has to be considered. In addition to this, the risk is evaluated for the external surface only, and the penetration of the rain is not of interest. This is in agreement with the result obtained.

11

Influence of the multi-year length

To achieve a representative TRY, The standard [111] suggests using a multi-year of 10 years or longer. This requirement could be very restrictive, for example for recently installed weather stations. In this chapter the influence of the multi-year length on the moisture accumulation risk assessment performed using TRY and representative years is investigated for four cities of Northern Italy. This comparison is presented in [10]. Similar comparisons are presented in [129] and [130] where the impact of the weather record is evaluated for the building energy simulations and on the building optimisation procedures.

11.1 Method

Again, the representative weather files are obtained with a modification of the standard procedure presented in Chapter 9.1.1. For this comparison, the combination of primary parameters ID 14 from Table 10.1 is used: in addition to the primary parameters used in [111] for the generation of the TRY (dry-bulb air temperature T, vapour pressure p_v, global irradiation E_g) also rainfall intensity ($r_\perp$) and rainfall duration (t_r) are used. Moreover, the secondary selection is not performed. The rainfall duration has been calculated as the number of consecutive hours with rainfall. This choice has been made considering the fact that low intensity rainfalls with a long duration could be more influential on the moisture content of a wall than short high intensity rainfalls. The resulting representative years will be indicated in the plots, for brevity, as MRY (Moisture Representative Years).

11.1.1 Simulations

The multi-years measured by four weather stations of Northern Italy were considered, the cities and the weather station locations are listed in Table 11.1. The representative years and TRY were designed for every station, considering, when possible, 5 different multi-year lengths: 1996-2017, 1996-2006, 2002-2017, 2007-2017, 2012-2017. The

obtained weather files were compared and then evaluated by performing moisture accumulation risk analysis on six walls, illustrated in Fig. 10.4 and described in Table 10.2.

Table 11.1: Positions of the considered weather station and length of the Multi-year record.

Station	**Lat.** (°)	**Long.** (°)	**Alt.** (m a.s.l.)	**MY years**
Aosta	45.75	7.68	569	1996-2017
Bergamo	45.66	9.66	211	1996-2017
Torino	44.96	7.71	226	2002-2017
Udine	46.03	13.23	91	1996-2017

11.1.2 Multi-year weather record

To highlight the difference between the two additional variables, rainfall intensities and the rainfall duration, a short presentation of the rainfall intensities and the rainfall duration is illustrated in the plots of Fig. 11.1. Even though the two plots are different, the two show a similar behaviour with some exceptions. These differences are due to high intensity rainfalls with a duration of less than an hour, which could be less influential on the moisture content of building materials than long-lasting low intensity rains.

In Figure 11.2 the annual mean rainfall intensity in Udine is presented. The values are calculated as the total rainfall of the year divided by the number of hours of the year. The relatively large standard deviation shows that the $r_{\perp}$ has a large variability compared to that of the other variables.

For example, the air dry-bulb temperature plot in Figure 11.3 shows a relatively small standard deviation, indicating fewer extreme values and a more regular trend. Similar behaviours have been observed for the other stations.

This behaviour is explained in Figure 11.4 and in Figure 11.5, where the single year are plotted separately in order to appreciate the irregular distribution of the peaks among the months. They show the monthly mean values of the whole multi-year respectively of air dry-bulb temperature and rainfall intensity. The air dry-bulb temperature curves of every year closely match the multi-year mean, denoting an analogous behaviour, while the rainfall intensity has relatively larger variations from the multi-year mean.

11.1.3 Representative years evaluation

The obtained representative years are first evaluated comparing the Wetting Index, the Drying Index and the Moisture Index normalised over the full weather record. The Indexes are defined in Section 9.1.2.

For the case of Aosta the Wetting Index (Fig. 11.6) values are higher than the weather record average for all the MRY except for the one obtained with the full weather record (22 years), while the TMY have lower values. For the case of Bergamo the WI values are mostly lower than the record average, with the exception of the MRY 07-17

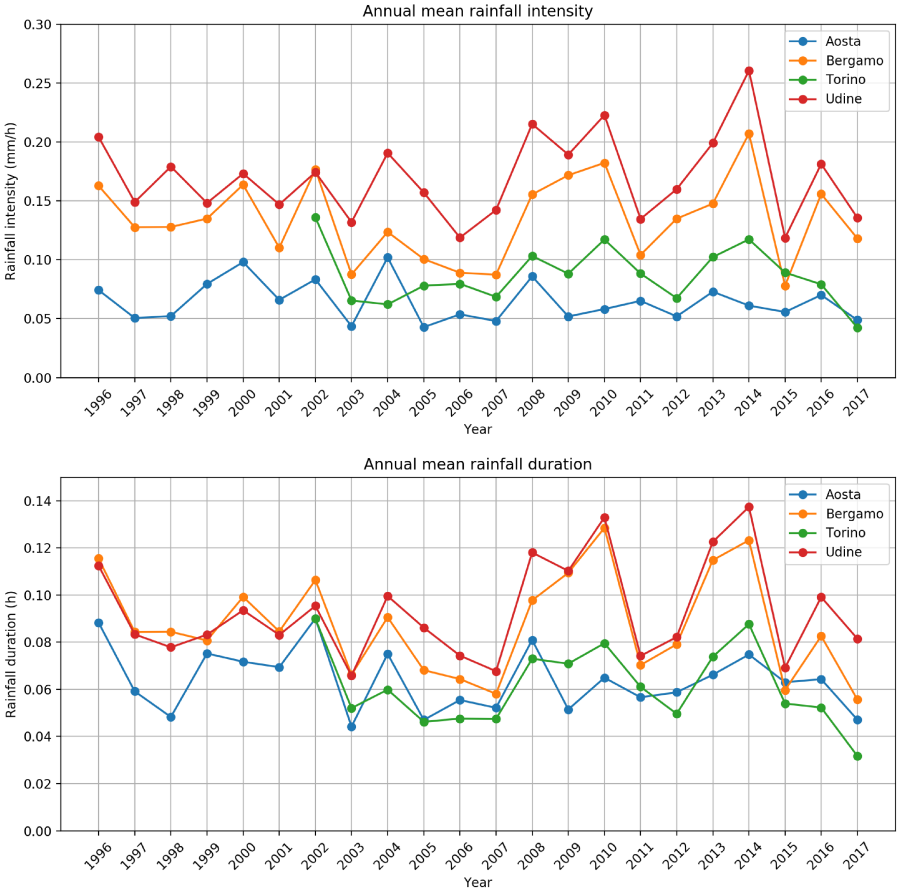

Figure 11.1: Annual mean rainfall intensity (upper plot) and annual mean rainfall duration (lower plot) of the multi-year weather records for the four stations considered (adapted from [10]).

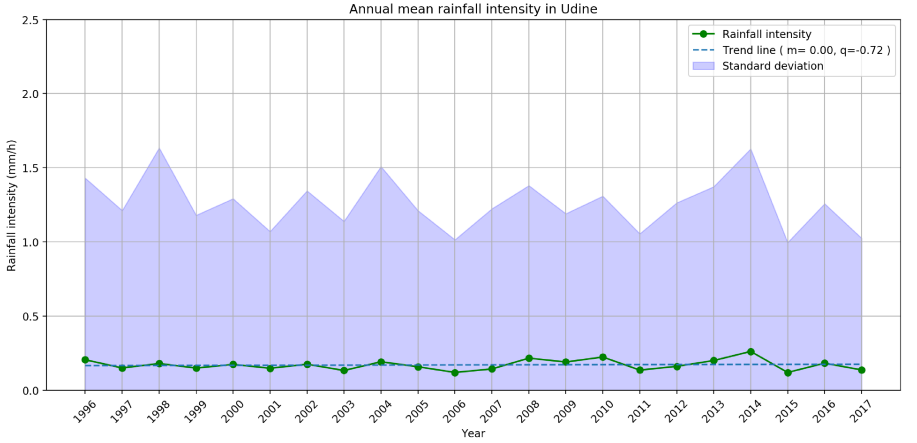

Figure 11.2: Annual mean rainfall intensity in Udine, linear trend and standard deviation calculated on the hourly values (adapted from [10]).

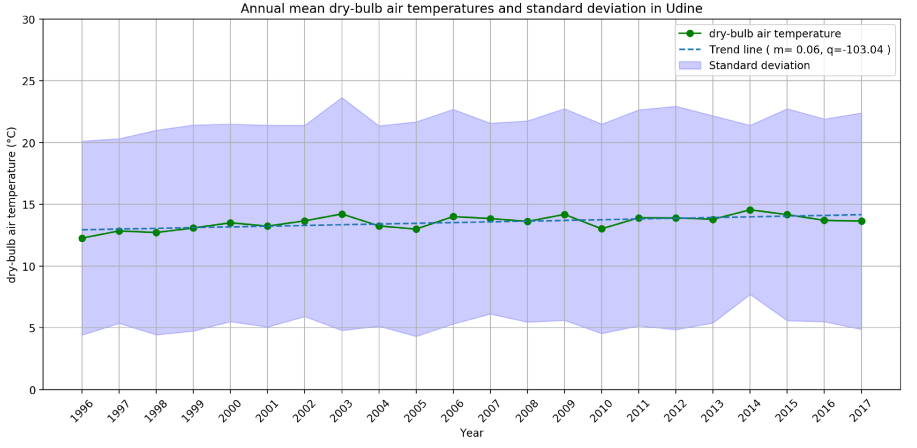

Figure 11.3: Annual mean dry-bulb air temperature in Udine, linear trend and standard deviation calculated on the hourly values (adapted from [10]).

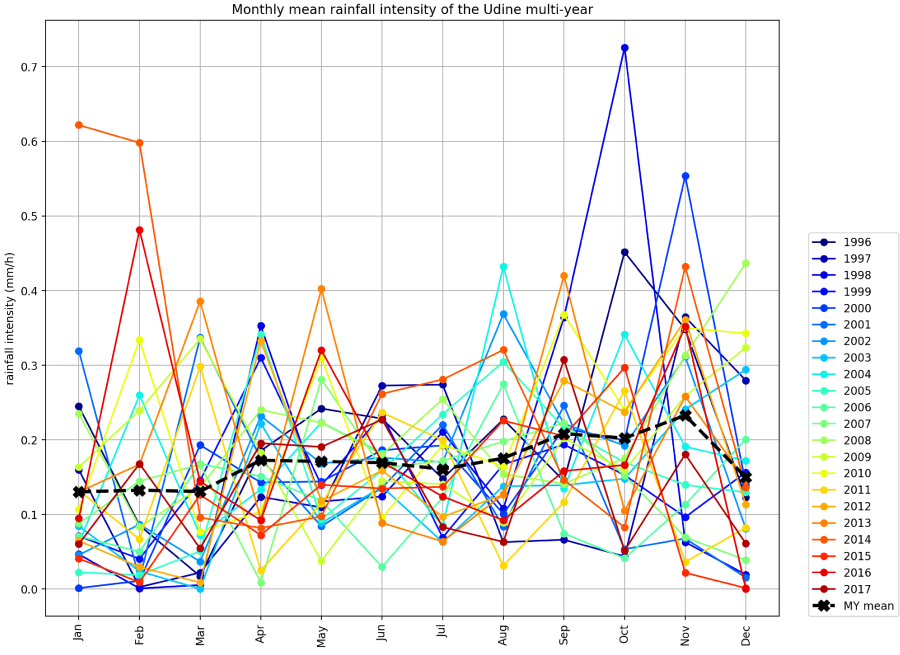

Figure 11.4: Monthly mean rainfall intensity in Udine for each year considered in the multi-year compared to the mean of every calendar month of the multi-year (MY mean) (adapted from [10]).

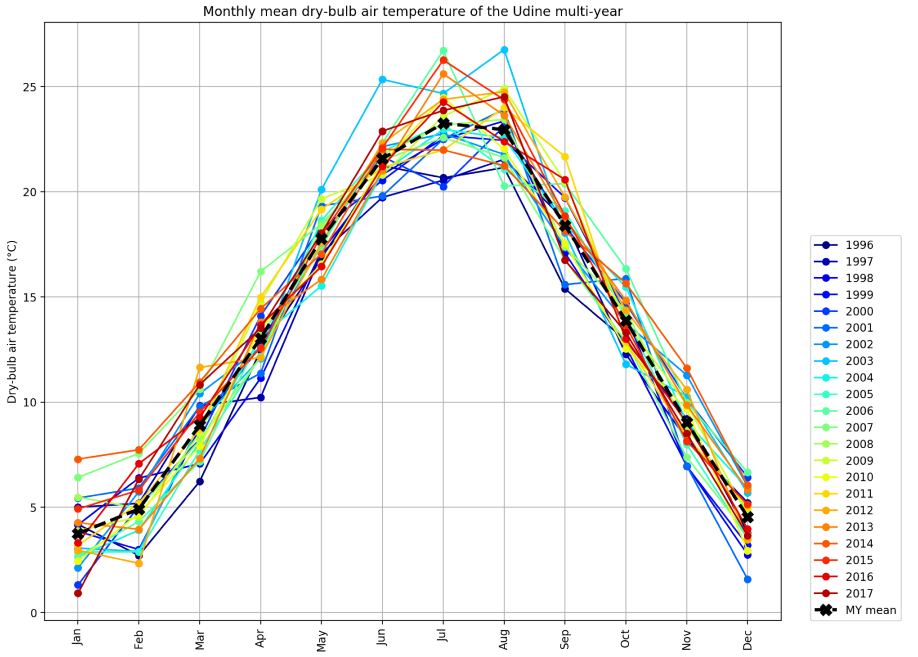

Figure 11.5: Monthly mean air dry-bulb temperature in Udine for each year considered in the multi-year compared to the mean of every calendar month of the multi-year (MY mean) (adapted from [10]).

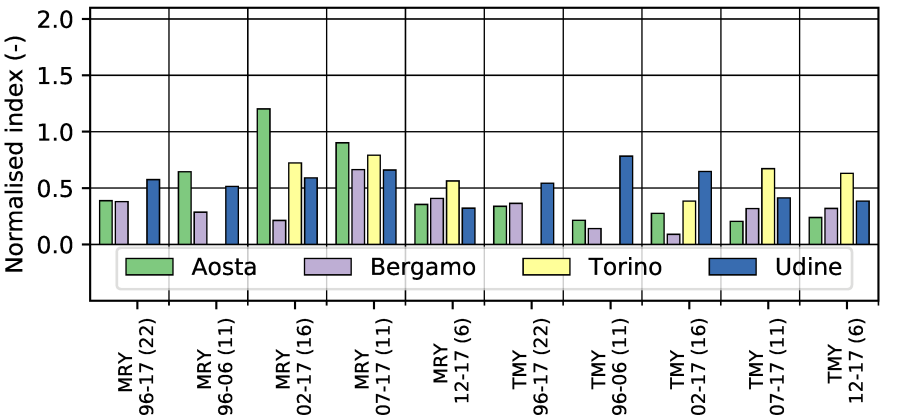

Figure 11.6: Characterization of the representative years with the Wetting Index. The weather record average values are Aosta: 0.38, Bergamo: 0.44, Torino: 0.47, Udine: 0.36 .

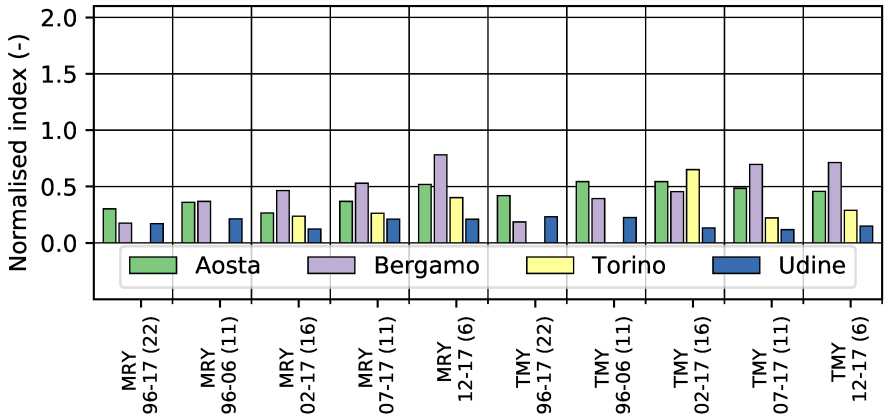

Figure 11.7: Characterization of the representative years with the Drying Index. The weather record average values are Aosta: 0.47, Bergamo: 0.48, Torino: 0.45, Udine: 0.28 .

(11 years). For Torino, all the representative years except the TMY 02-17 (16 years), produce WI values higher than the record average. The Results for Udine have all higher WI values than the average. Generally the most representative results are provided by the larger weather records, and not all the representative years obtained from shorter weather records provide larger WI index (not all the years are conservative for moisture contol related applications).

The Drying Index plot (Fig. 11.7) shows that for Bergamo the DI values are larger for shorter and more recent weather records, exceeding the weather record average. Similar results are found for Aosta, but with smaller values of DI. Torino MRY provide values of DI in agreement with the weather record average, while the TRY procedure has a DI higher than the average for the TMY 02-17 (16 years). The Udine representative years are in good agreement with the average DI. Also in this case larger weather records produced more representative DI.

Finally, the Moisture Index (Fig. 11.8) values confirm the previous trends of the Drying Index and the Wetting Index.

11.1.4 Risk assessment

The representative years are evaluated for the use in moisture accumulation risk assessment. The evaluation of the moisture content was performed using a simplified method, the Glaser method, using the script available at [89], and an advanced the HM model, using the software DELPHIN 6 [131]. The first method considers the air dry-bulb temperature and relative humidity, while the advanced model considers also the rainfall intensity, solar global irradiance, and, if required, the wind speed and direction for the calculation of driving rain. For the sake of simplicity, in this evaluation, the wind speed

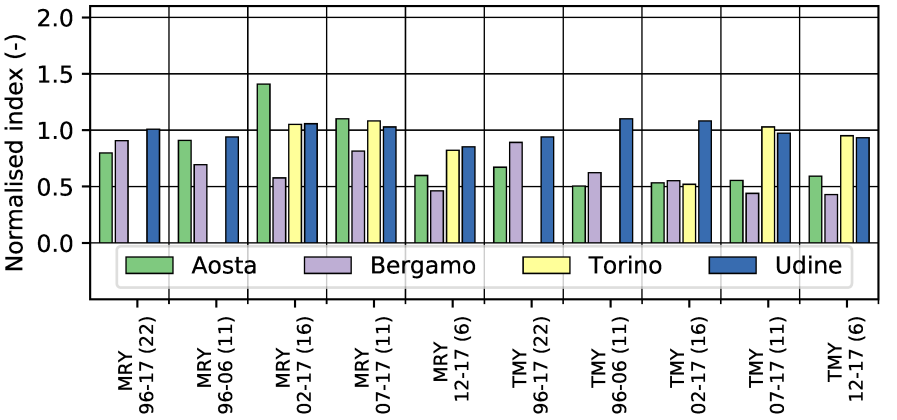

Figure 11.8: Characterization of the representative years with the Moisture Index. The weather record average values are Aosta: 0.68, Bergamo: 0.72, Torino: 0.73, Udine: 0.82 .

and direction have not been used, and the whole rainfall intensity has been considered as driving rain on the wall. With this hypothesis the representativeness of the reference years could be evaluated with higher moisture content variations.

The evaluation of the risk parameter was performed with a simplified method for both simulation procedures. The risk P_y^G for the Glaser method (G) over the period y was calculated evaluating the ratio between $n_{m|\varphi=1}$, number of months with liquid water between the layers (with the relative humidity equal to 1), and the total number of months N_m of y as in Eq. 11.1.4.

$$P_y^G = \frac{n_{m|\varphi=1}}{N_m} \tag{11.0}$$

The evaluation for the multi-year was performed considering all the monthly mean variables for all the months of the multi-year, while, the assessment for the reference years was performed for a period of five years. The assessment of the risk P_y^D for the advanced simulation method has been performed using the same number of years. Five years is the time required in the the HM simulations for the total moisture content of the wall at the first time-step of the year to be equivalent to the moisture content of the first time-step of the following year. The risk P_y^D was calculated as the ratio between $n_{h|\varphi=0.95}$, number of hours with values of relative humidity higher than 0.95 on an internal layer of the wall, and N_h, the total number of hours considered in the simulation (Eq. 11.1.4).

$$P_y^D = \frac{n_{h|\varphi=0.95}}{N_h} \tag{11.0}$$

The external layer has not been considered for this evaluation. The indoor and out-

door surface boundary conditions for the the HM simulation simulations are set using the weather files in accordance with [132], the internal boundary conditions are calculated using the "normal occupancy" conditions described in the standard. The Glaser method boundary conditions are set in accordance with the [17] and the internal conditions are obtained from the external climate with the "normal occupancy" condition. The material properties are taken from the DELPHIN material database. In both approaches the internal surface thermal resistance is set to 0.25 $m^2 \cdot K/W$ and the external thermal resistance to 0.04 $m^2 \cdot K/W$. In the the HM simulation simulations the surface vapour exchange equivalent air layer thickness is set to 0.003 m on the outside and to 0.008 m on the inside. For both simulation procedures, a risk of 0 indicates that the water condensation has never occurred, while a risk equal to 1, denotes the presence of liquid water in a layer of the wall in every time-step of the simulation period. The risk assessment was performed for six walls, typical of the Northern Italy regions [133], redesigned to have liquid water condensation and accumulation between the material layers. The walls are described in Figure 10.4. The wall properties are summarized in Table 10.2.

The values used for the comparison and presented in the plots are differences ΔP^I (defined in Eq. 11.1.4) between the risk P^I_{RY} calculated with the use of a representative year (specified on the x axis) and the risk P^I_{MY}, obtained using the multi-year from the year as boundary conditions. In order to be representative, the generated years, should provide interstitial condensation risk values close to the ones obtained with the multi-year. Larger ΔP^I values indicate less representative years. The superscript I indicates the calculation method used: G for the Glaser method and D for the the HM simulation simulation.

$$\Delta P^I = P^I_{RY} - P^I_{MY} \tag{11.0}$$

Negative values of ΔP^I indicate greater values of P^I_{MY}, meaning the the representative year is not conservative (not desirable for risk analyses).

11.2 Results

The representative years (MRY) and TRY generated from the five different multi-year tend to have rainfall intensities closer to the multi-year mean values. The months with the extreme values are excluded by the ranking procedure in both reference year generation methods. The same behaviour is found considering the rainfall intensity annual mean values in Figure 11.10 and for the rainfall duration. In Figure 11.11 the rainfall intensity monthly mean value is presented for the five multi-year considered, showing that a common evolution is not found. This behaviour of the variable could prevent the statistical framework used in this work from identifying a main trend to be represented by the reference years. The results of the evaluation are presented in Figures from 11.12 to 11.19.

The multi-year for the stations of Aosta, Bergamo and Udine is from the year 1996 to 2017, while the one for Torino is form the 2002 to 2017. Positive values of ΔP^I indicate higher P^I_{RY} values, meaning that the reference year simulation is conservative.

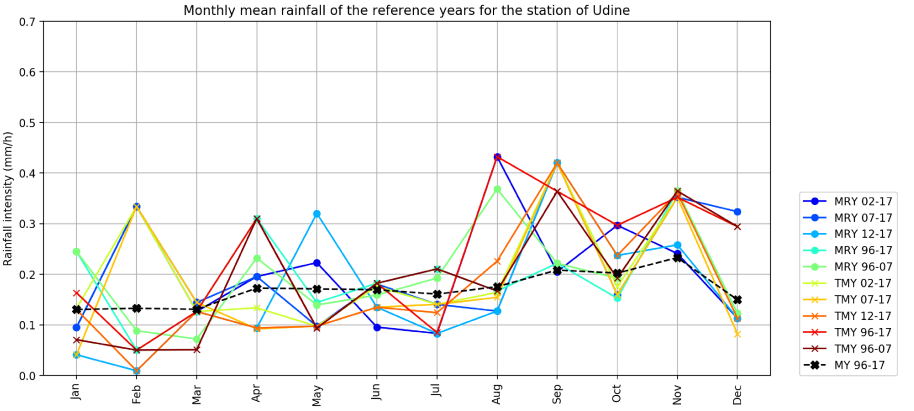

Figure 11.9: Monthly mean rainfall intensity in Udine for each representative years (indicated in the plot as MRY) compared to the overall mean rain intensity of the multi-year and its standard deviation (adapted from [10]).

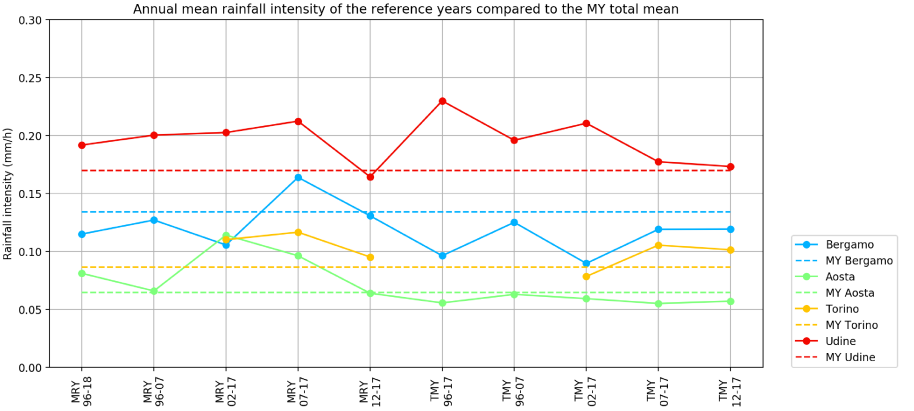

Figure 11.10: Annual mean rainfall intensity for each representative years (indicated in the plot as MRY) presented compared to the overall mean rain intensity of the multi-year of the four stations considered (adapted from [10]).

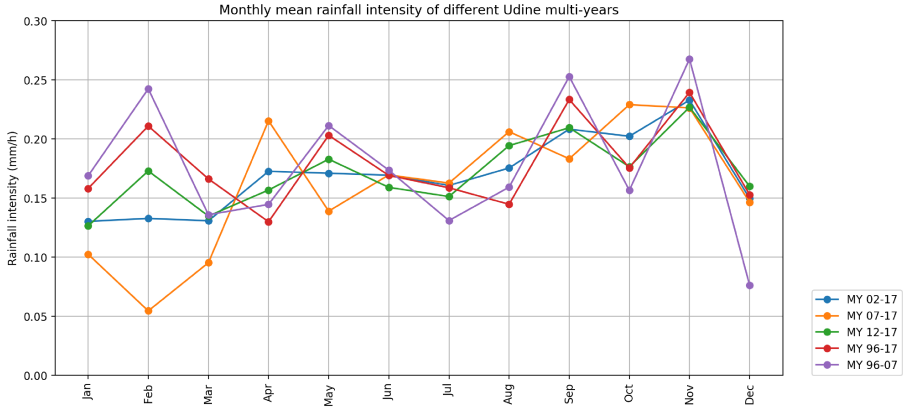

Figure 11.11: Monthly mean rainfall intensity for the five multi-year considered for the station of Udine (adapted from [10]).

11.2.1 Simulations

The the HM simulation simulations performed using the reference years are generally in accordance with the multi-year simulations. The results are shown in 11.12, 11.13, 11.14 and 11.15. The exceptions are visible in the plot for the station of Aosta in Figure 11.12, where the representative years obtained with the records 1996-2017, 2002-2018, 2007-2017 of the station of Aosta produce over-conservative results for the HB, HBi, SWi walls (the wall identifiers are listed in Figure 10.4).

The reference years obtained from the station of Bergamo are coherent with the multi-year simulations except for the not acceptable underestimations given by the representative years from the records 1996-2007, 2002-2007 and 2012-2017 and the TRY from 2002-2017 and 2012-2017. For the station of Torino the results of the reference years follow the multi-year risks with the exception of the representative years 2012-2017 that underestimates the risk. The representative years 2002-2017 and 2007-2017 and the TRY 2007-2017 overestimate the risk in a relevant manner for the SWi wall.

The results of the reference years for the station of Udine are mostly conservative compared to the multi-year. The most representative results are given by the representative years 1996-2017 and by the TRY 1996-2007.

As a general trend, the representative years (MRY) and TRY obtained from the full MY produced the most representative results, while the representative years (MRY) and TRY from the shorter MY intervals resulted less representative. In some cases, the reference years obtained from periods shorter than 10 years could lead to underestimations of the risks.

The Glaser method results, presented in Figures 11.16, 11.17, 11.18 and 11.19, denote a general good agreement between the reference years and the multi-year, for every station. The results for the station of Bergamo in Fig.11.17 slightly underestimate the risk of moisture accumulation for each reference year, with peaks in the reference years of the period 2012-2017.

The differences of risk are always less than 0.25, while for the walls with thicker

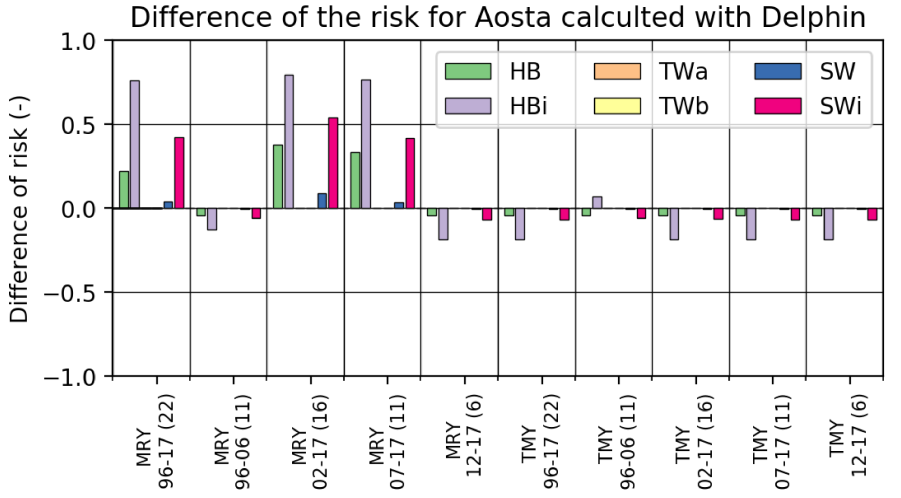

Figure 11.12: Evaluation of the reference years in terms of moisture accumulation risk calculated with the HM simulation for the Aosta station (the representative years are referred as MRY) (adapted from [10]).

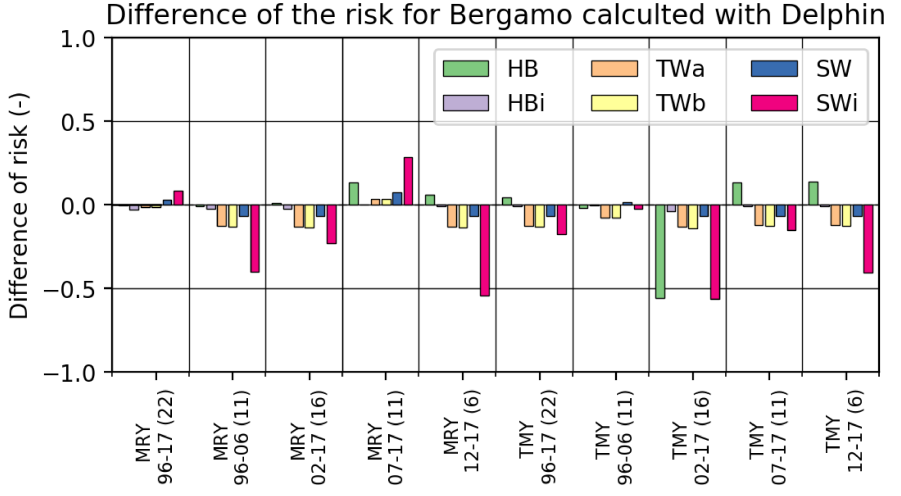

Figure 11.13: Evaluation of the reference years in terms of moisture accumulation risk calculated with the HM simulation for the Bergamo station (the representative years are referred as MRY) (adapted from [10]).

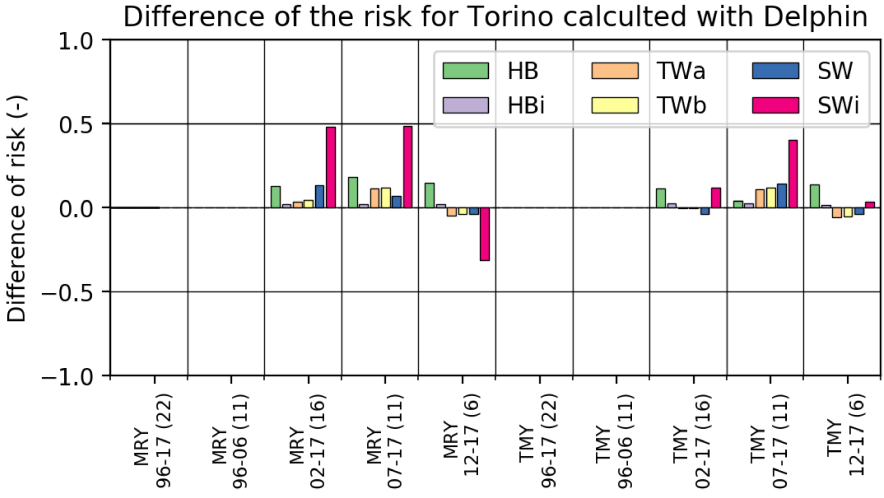

Figure 11.14: Evaluation of the reference years in terms of moisture accumulation risk calculated with the HM simulation for the Torino stations (the representative years are referred as MRY) (adapted from [10]).

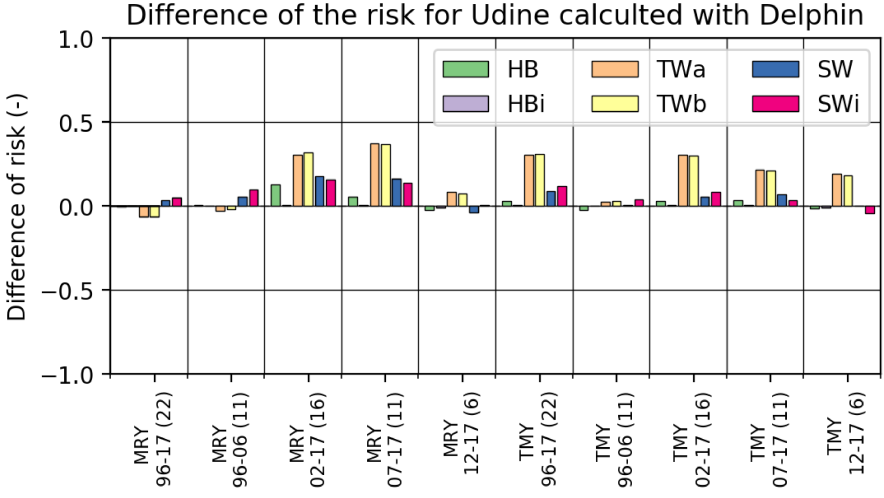

Figure 11.15: Evaluation of the reference years in terms of moisture accumulation risk calculated with the HM simulation for the Udine station (the representative years are referred as MRY) (adapted from [10]).

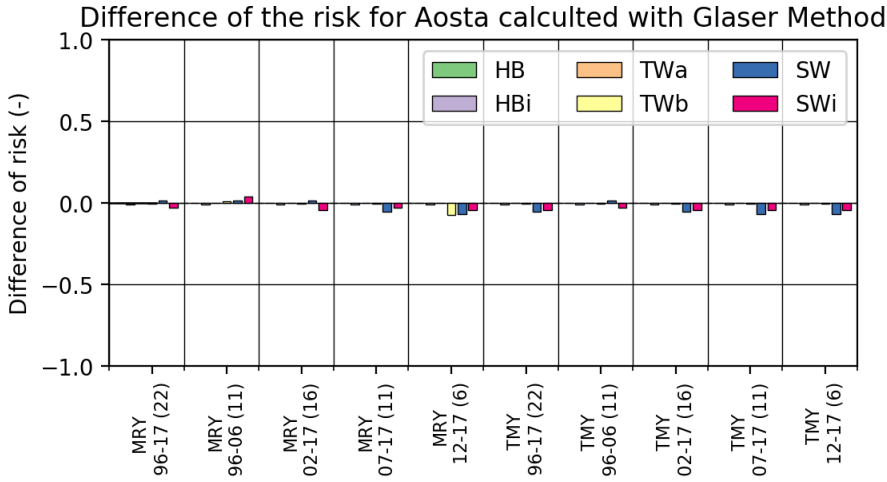

Figure 11.16: Evaluation of the reference years in terms of moisture accumulation risk calculated with the Glaser method for the Aosta station (the representative years are referred as MRY) (adapted from [10]).

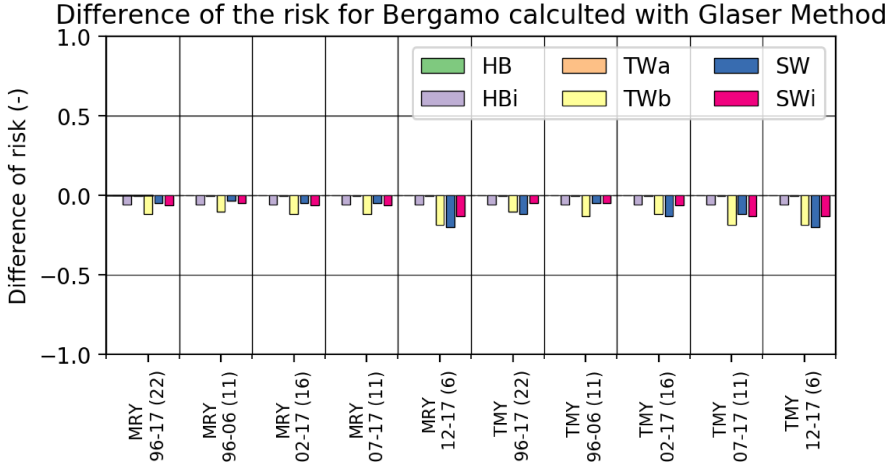

Figure 11.17: Evaluation of the reference years in terms of moisture accumulation risk calculated with the Glaser method for the Bergamo station (the representative years are referred as MRY) (adapted from [10]).

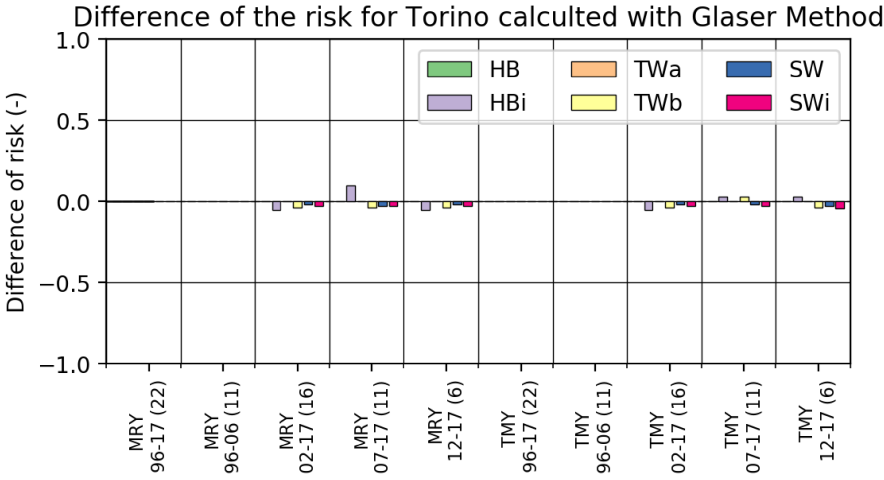

Figure 11.18: Evaluation of the reference years in terms of moisture accumulation risk calculated with the Glaser method for the Torino station (the representative years are referred as MRY) (adapted from [10]).

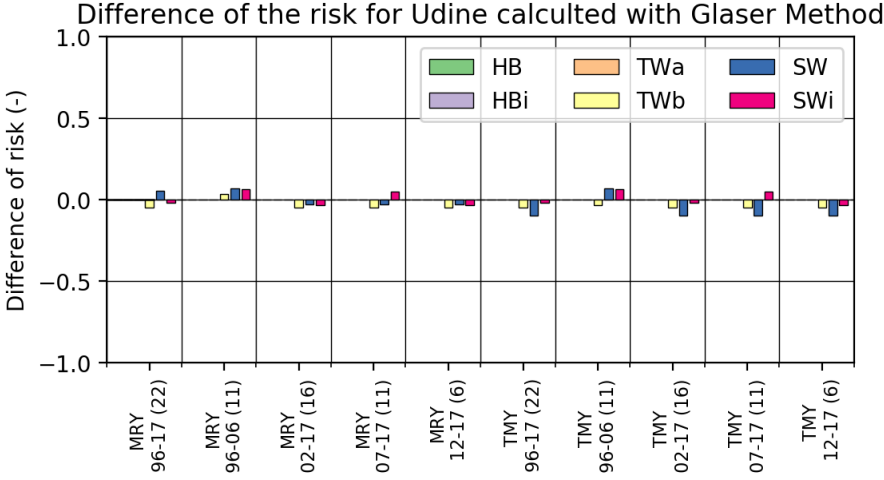

Figure 11.19: Evaluation of the reference years in terms of moisture accumulation risk calculated with the Glaser method for the Udine stations (the representative years are referred as MRY) (adapted from [10]).

layers of insulation, the risk differences calculated with the HM simulation, are from 0.5 to 0.75, showing that the choice of the weather file is more relevant for the transient coupled heat and moisture transfer simulations.

12

Extreme reference years

The representative years generated in the previous chapters are designed to represent the average year for a given location. However, the produced years, thanks to the application of the Finkelstein-Schafer statistic, are selected to not contain extreme weather events. These extreme weather events are the ones that can possibly bring the buildings to failure, therefore they should be used to design the building envelopes.

In this chapter, two Extreme Moisture Reference Year design procedures (ERY_{m1} and ERY_{m2}), already presented in [11] are reported. The Extreme Moisture Reference Years are designed, contrary to the representative years, to contain the most extreme weather events, in order to provide a conservative weather file for the moisture risk analyses.

The selection of the critical weather events is obtained simply reversing the rankings obtained using the Finkelstein-Schafer and applying a secondary selection. In this way, the presented reference year design produced are not structure-dependent and also suitable for the risk assessments that involve extreme weather variable values.

The reference for the selection of the extreme weather series can be found in [134], in particular, it is used for the development of Extreme Reference Years ERY to be used in building energy simulations.

12.1 Method

Three locations from the Northern Italy are considered:

- Gemona del Friuli (Udine, Friuli-Venezia Giulia), provided by ARPA FVG (OSMER) - series from 2000 to 2018;
- Legnaro (Padova, Veneto), provided by ARPA Veneto - series from 2008 to 2018;
- Trento (Trentino – Alto Adige / Südtirol), provided by the Autonomous Province of Trento (IASMA Fondazione Edmund Mach) - series from 1986 to 2014.

and for each of these multi-years, three reference years are generated:

- $\mathrm{TRY_{EN}}$, Typical Reference Year according to the EN ISO 15927-4:2005, with dry-bulb air temperature (T), irradiation (E_g) and relative humidity (φ) as primary variables and wind speed (v_w)as secondary variable;
- $\mathrm{ERY_{m1}}$, Extreme Moisture Reference Year with dry-bulb air temperature (T) and air humidity ratio (x) as primary variables;
- $\mathrm{ERY_{m2}}$, Extreme Moisture Reference Year with air humidity ratio (x) as primary variable.

12.1.1 Extreme moisture reference years generation

For the generation of the $\mathrm{ERY_{m1}}$ and $\mathrm{ERY_{m2}}$ from the MY, the following procedure is used:

1. Calculation the daily means $\bar{p}$ of the variables p in the set of primary variables I_{ID} for the whole MY. Where ID is the considered reference year.
2. Calculation of the cumulative distribution function $\Phi(p, m(i), i)$ of the daily means $\bar{p}$ over the whole MY for each day i of a selected calendar month m, for each p. The variable i represents the ordered number of a day in the MY, from 1 to N (number of days in the MY), and it will be used as a time-stamp. The function Φ is obtained from the ranking $K(\bar{p}, m, i)$ by numbering the values of the distributions of the considered p, separately for each m:

$$\Phi(p, m(i), i) = \frac{K(\bar{p}, m(i), i)}{N + 1} \tag{12.0}$$

3. Calculation of the cumulative distribution function of the daily means within each calendar month m of each year y, $F(p, y(i), m(i), i)$ from the rank order $J(\bar{p}, m(i), i)$, obtained by ordering the daily means $\bar{p}$ within the calendar month m and the year y:

$$F(p, m(i), i) = \frac{J(\bar{p}, y(i), m(i), i)}{n + 1} \tag{12.0}$$

   where n is the number of days of the m calendar month considered.

4. The Finkelstein-Schafer statistic F_S is calculated for each p and each calendar month m in the MY as:

$$F_S(p, y, m) = \sum_{i=1}^{n} |F(p, y(i), m(i), i) - \Phi(p, m(i), i)| \tag{12.0}$$

5. For each p, the ranking R is assigned to each calendar month m, obtained from the ordering of the $F_S(p, y, m)$ of each y separately for each calendar month m:

$$R(p, y, m) = \frac{L(F_S)}{n_y + 1} \tag{12.0}$$

with n_y the number of years of the MY.

6. The ranking R of each calendar month is calculated for all the primary parameters and then summed, to obtain the total ranking R_{tot}:

$$R_{tot}(y,m) = \sum_{p \in I_{ID}} R(p,y,m) \tag{12.0}$$

7. Each calendar month m of the reference year is chosen among the months m of the MY with a further secondary selection. Ranking the months with the R_{tot} the variable series more distant from the mean values are selected, but it is not specified if they are greater or smaller values with respect to the mean values. To resolve this ambiguity, a further selection is performed:

   - For each month ranking, the months with the highest R_{tot} are selected;
   - The deviation from the mean value of the primary variables is calculated for every month;
   - The month m that complies with the desired criteria is chosen (low temperatures or high specific humidity values).

8. The reference year is composed of the hourly series of the weather variables of the selected months and the continuity between months is set with a linear interpolation, in order to provide a smooth transition between months from different years.

12.1.2 Extreme moisture reference year evaluation

The resulting $\mathrm{TRY_{EN}}$ and $\mathrm{ERY_m}$ weather files have been used as input for heat and moisture transfer simulations with the software DELPHIN in a moisture-related risk analysis on a set of three typical Italian walls and two single-material walls used as a reference (listed in Table 12.1). The simulations have been performed without considering the rain for four wall orientations (North, East, South and West) and with rain only for Gemona del Friuli.

Two different indoor boundary conditions have been considered in the simulation:

- typical residential dwelling (normal moisture load according to WTA 6.2 guidelines, with the relative humidity values included between the 20% and the 60%);
- larger indoor humidity generations (high moisture load according to WTA 6.2 guidelines, with the relative humidity values included between the 40% and the 70%);

Two comparisons have been held with the calculated results: the comparison of the annual moisture contents in the walls and the occurrences of interstitial moisture accumulation.

Table 12.1: Properties of the walls used in the simulations.

Wall	d_{tot} (cm)	U_{tot} (W/m2K)	$S_{d,tot}$ (m)
Timber wall (TW)	53	0.13	56
Hollow brick wall (HB)	51	0.36	8
Stone wall (SW)	34	0.19	4
Concrete layer (CONC)	20	10.50	15
Timber layer (TIMB)	20	1.75	4

12.2 Results

A relevant difference has been found between the mean values of the temperatures and the relative humidities of the generated reference years.

12.2.1 Weather file comparison

The obtained years $\mathrm{ERY_{m1}}$ and $\mathrm{ERY_{m2}}$ for the three considered cities are compared in terms of monthly average dry-bulb temperature values and monthly average air humidity ratio. The comparisons show a general agreement with the month selection criteria:

- $\mathrm{ERY_{m1}}$ extreme values dry-bulb air temperature (lower values) and relative humidity (higher values);
- $\mathrm{ERY_{m2}}$ extreme relative humidity values (higher values);
- $\mathrm{TRY_{EN}}$ representative values of temperature and relative humidity.

Observing the plots 12.3, 12.4 and 12.5, it is possible to compare the general behaviour of the reference files. The position of the curves and their extension in the plane can be used to compare the years considering both the effects of temperature and relative humidity. In Fig.12.3 the monthly mean dry-bulb air temperatures and the relative humidity values for the three reference years of Gemona del Friuli are presented. The temperatures of the $\mathrm{TRY_{EN}}$ lower than the $\mathrm{ERY_{m1}}$, while the $\mathrm{ERY_{m2}}$ are in between the other two, because the temperatures are not constrained by the selection method. Similarly the relative humidity monthly average values of the three reference year for the same location show that the $\mathrm{ERY_{m2}}$ has higher values of relative humidity than the $\mathrm{TRY_{EN}}$, while the $\mathrm{ERY_{m1}}$ values are in between, given that its selection procedure is also involving the air temperature values. Similar behaviours have been found for the location of Legnaro, while for the location of Trento the $\mathrm{TRY_{EN}}$ presented some extreme values during the year. This is due to the fact that some of the selected months of the reference year resulted to have some extreme weather events. This is confirmed in Fig. 12.4, where the plot of the $\mathrm{TRY_{EN}}$ has three months with air temperature values shifted to the right (high temperature values). This feature has been presented and discussed in [134].

The effect of the selection on an annual base is presented in Fig. 12.1 , in terms of means of the humidity ratio values. In each case the humidity ratio is lower for the

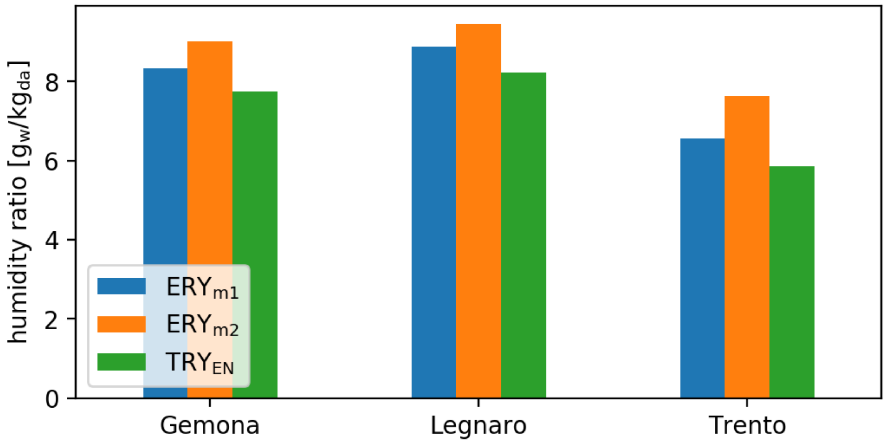

Figure 12.1: Annual mean humidity ratio values of the reference years for the three considered locations (adapted from [11]).

TRY_{EN} and the ERY_{m1} is lower than the ERY_{m2}. On the other hand in Fig. 12.2 shows that the the ERY_{m1} has a lower annual average saturation deficit, and thus a lower drying capacity. The TRY_{EN} and the ERY_{m2} saturation deficit values are similar, except for Trento, where the TRY_{EN} value is larger.

12.2.2 Simulation results

The simulations of the concrete and timber single layer walls showed for all the three locations higher moisture content values for the ERY_{m1}, and the lowest for the TRY_{EN} weather files for most of the days. As an example, the moisture contents of the concrete single layer are shown in Fig.12.6 for the case of Gemona del Friuli. The other considered walls showed more complex behaviours (Fig.12.6), although the annual average moisture contents (Fig.12.7) show also that the TRY_{EN} simulations have lower annual mean moisture contents. Considering the wall build ups, the interstitial moisture accumulation risk is used as a parameter of comparison. For the sake of comparison, the interstitial moisture accumulation risk is calculated as the number of days in which the relative humidity is higher than the 80% in the wall material, with the exception of the material layer exposed to the outside. Although Fig.12.8 shows that the response of the walls to the external conditions are highly structure dependent, the ERY_{m1} and the ERY_{m1} provide higher risks than the TRY_{EN} with the exception for the Stone wall located in Gemona del Friuli. Similar results are obtained for the other orientations. The simulations have been performed also considering higher internal moisture loads. As shown in Fig.12.10, the moisture contents are higher than the simulations with normal internal moisture loads and the relation between the results of the three reference years are the same. For the climate of Gemona del Friuli, thanks to the availability of the required weather data, it has been possible to run simulations considering also the driving rain. Rainfall intensity is not used in the weather file design procedures of all the three

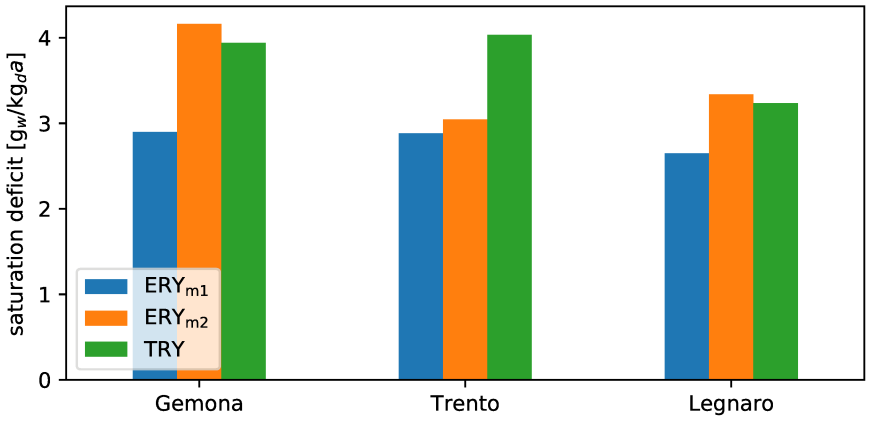

Figure 12.2: Annual mean saturation deficit values of the reference years for the three considered locations.

reference years used in this comparison. In this case the higher moisture contents are obtained using the ERY_{m2} (Fig.12.11, 12.12, 12.13 and 12.14). A possible explanation for this effect could be that the months with extreme relative humidity values are also the months with the higher rainfall intensity values and with the lower drying potential. It has to be noted that the different orientations have different moisture contents, yet the ERY_{m2} are always the reference years with the higher moisture contents.

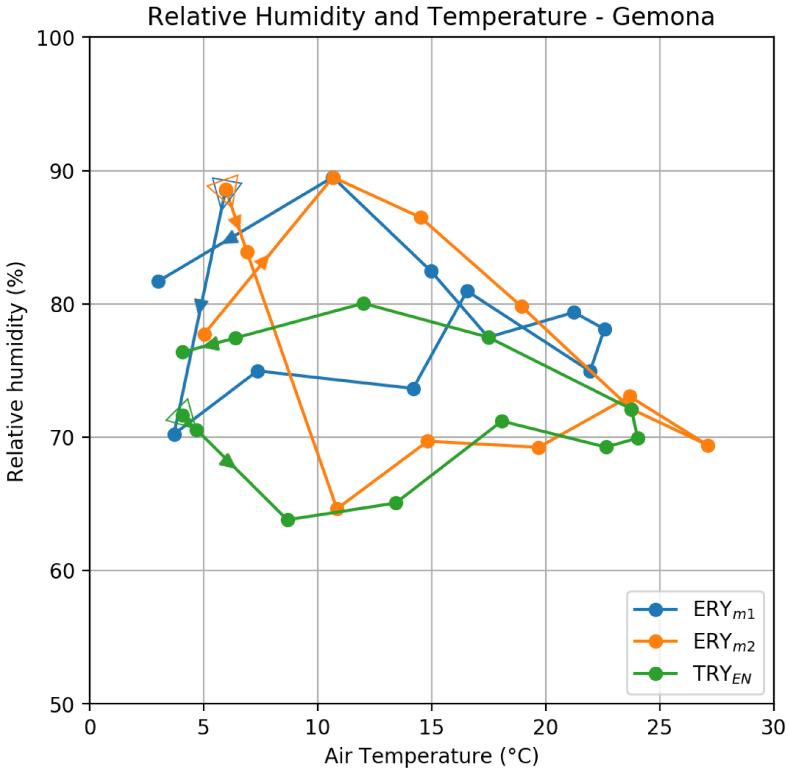

Figure 12.3: Monthly mean dry-bulb air temperature and relative humidity for the reference years of Gemona del Friuli. The values of January are marked with a triangle (adapted from [11]).

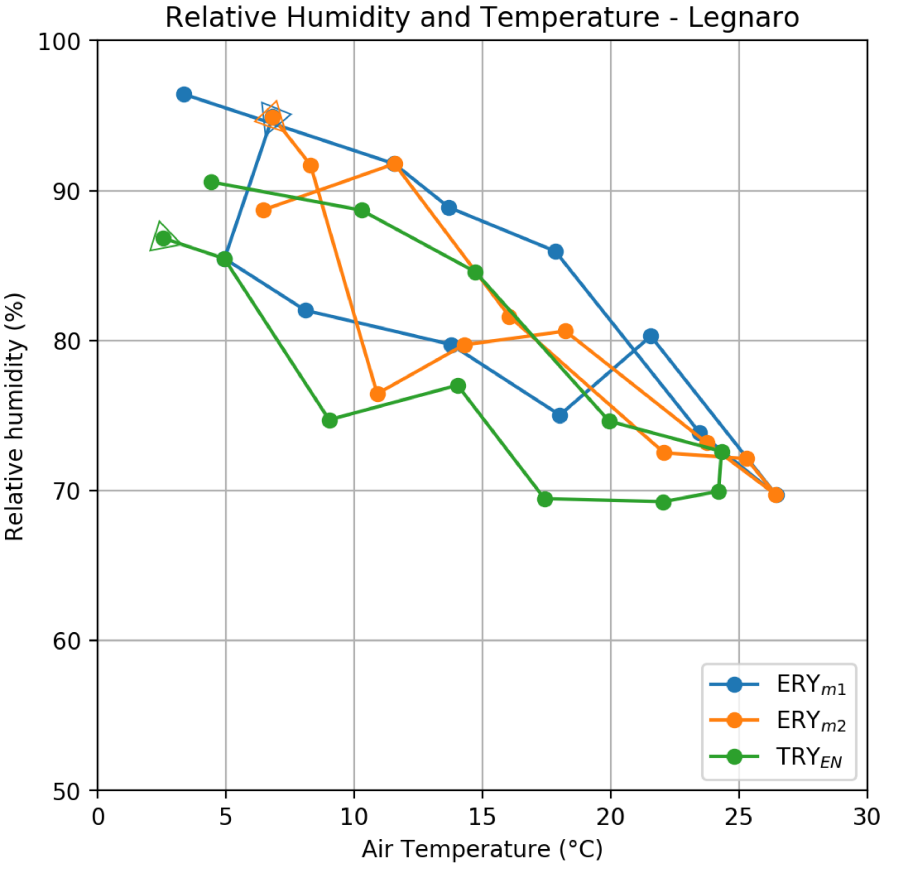

Figure 12.4: Monthly mean dry-bulb air temperature and relative humidity for the reference years of Legnaro. The values of January are marked with a triangle (adapted from [11]).

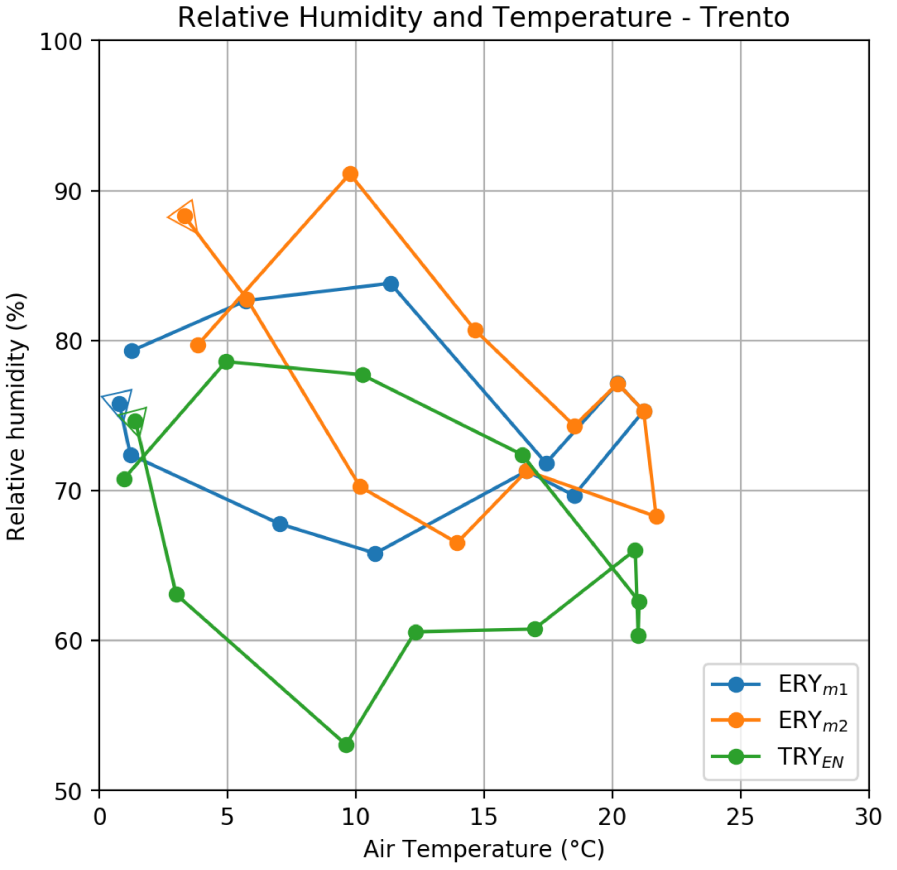

Figure 12.5: Monthly mean dry-bulb air temperature and relative humidity for the reference years of Trento. The values of January are marked with a triangle (adapted from [11]).

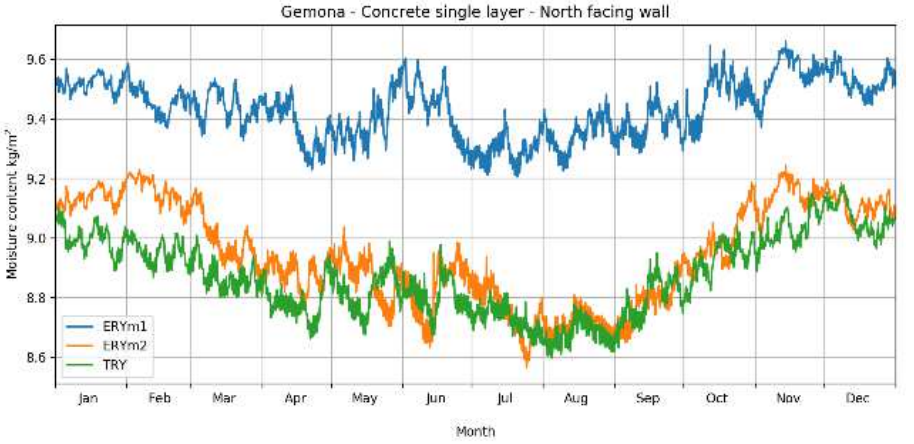

Figure 12.6: Moisture content of the concrete single layer facing North, for Gemona del Friuli (adapted from [11]).

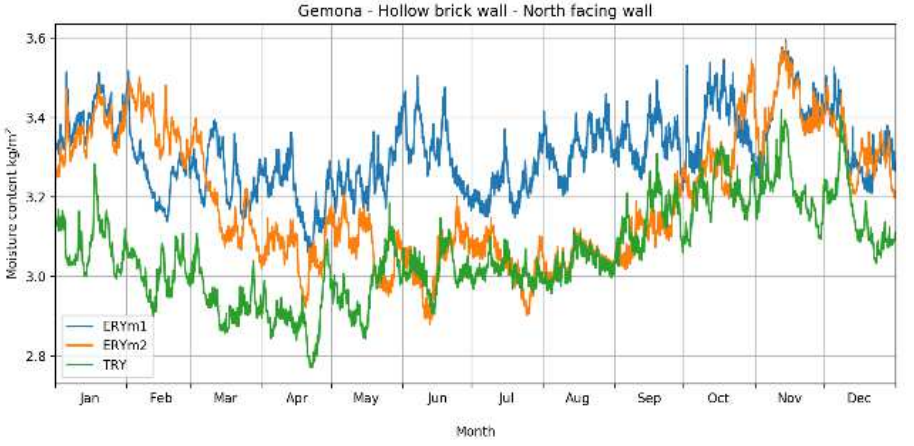

Figure 12.7: Moisture content of the hollow brick wall facing North, for Gemona del Friuli (adapted from [11]).

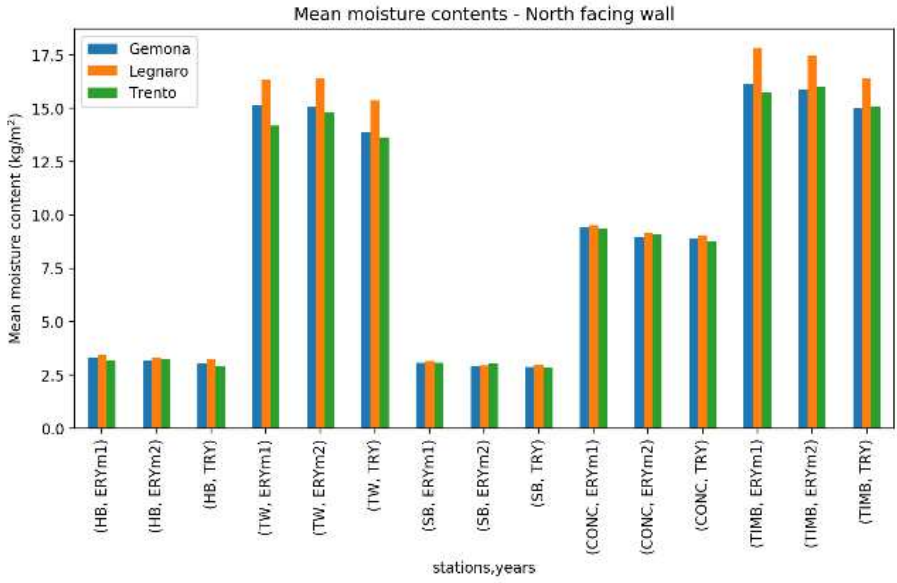

Figure 12.8: Annual mean total moisture contents of the five walls considered for the North orientation (adapted from [11]).

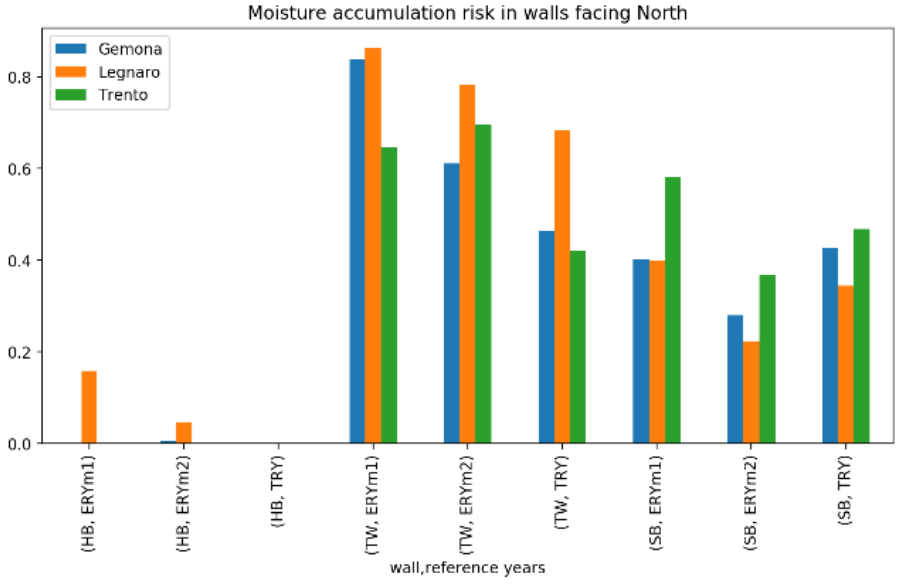

Figure 12.9: Moisture accumulation risk (days with relative humidity values over the 80%) for the considered walls (adapted from [11]).

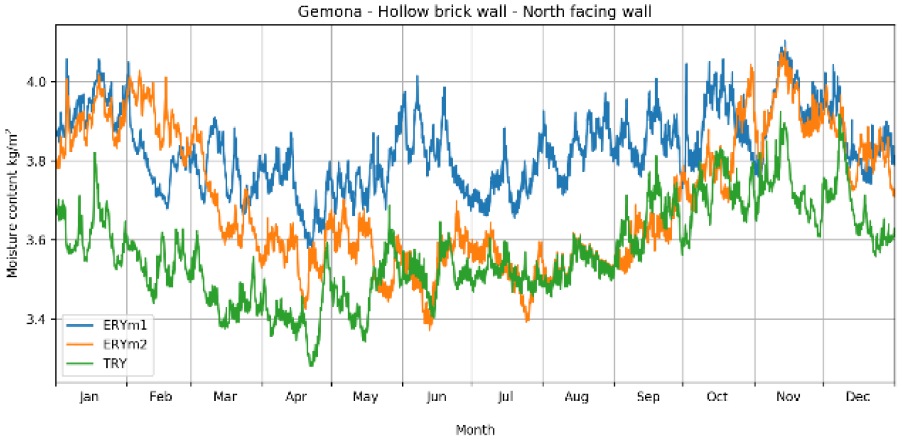

Figure 12.10: Moisture accumulation risk (Moisture content of the hollow brick wall facing North, for Gemona del Friuli with high internal loads (adapted from [11]).

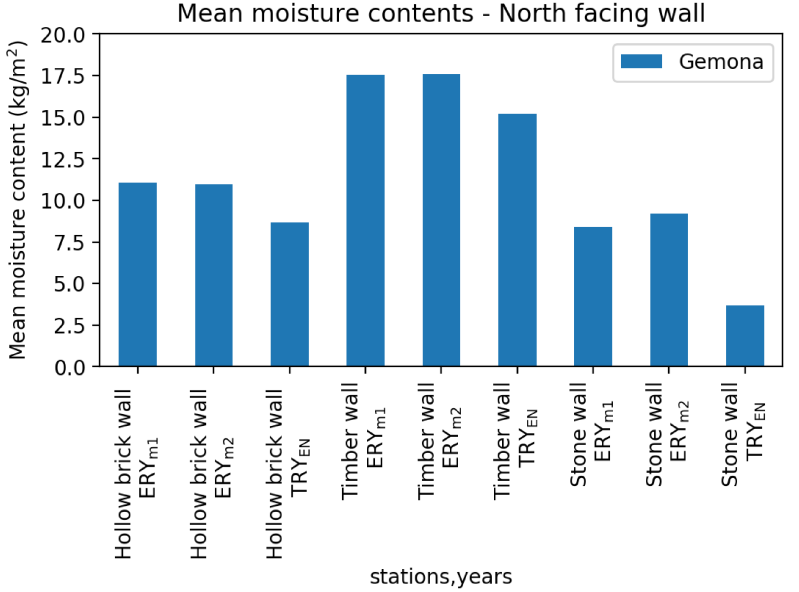

Figure 12.11: Annual mean moisture contents of the three considered walls facing North, for Gemona del Friuli, considering driving rain (adapted from [11]).

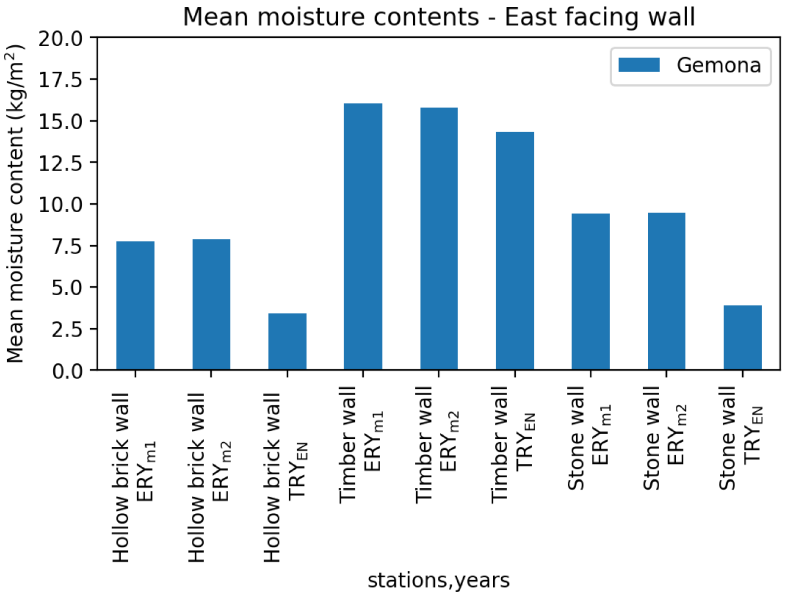

Figure 12.12: Annual mean moisture contents of the three considered walls facing East, for Gemona del Friuli, considering driving rain (adapted from [11]).

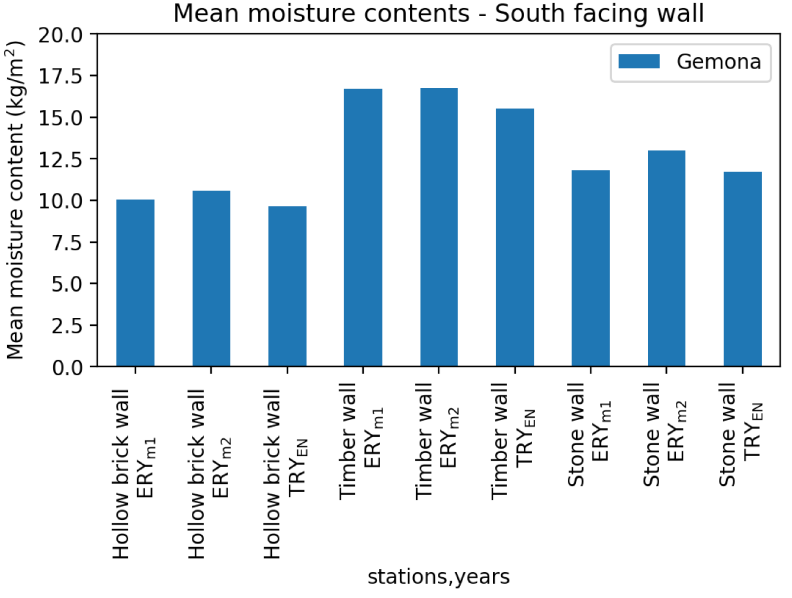

Figure 12.13: Annual mean moisture contents of the three considered walls facing South, for Gemona del Friuli, considering driving rain (adapted from [11]).

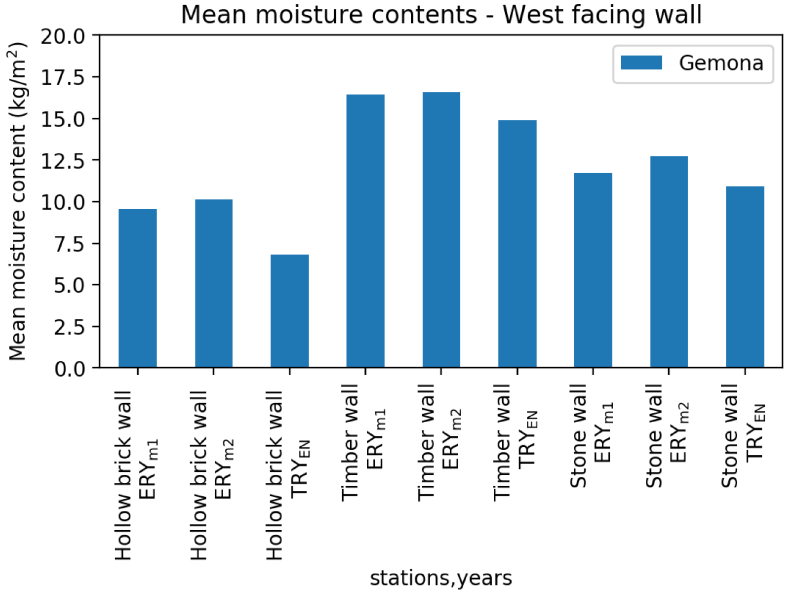

Figure 12.14: Annual mean moisture contents of the three considered walls facing West, for Gemona del Friuli, considering driving rain (adapted from [11]).

V

Conclusions

Conclusions

The problem of the modelling of the coupled heat and moisture transfer in buildings, depends strictly by the hygrothermal behaviour of the materials. In this thesis, it has been analysed with advanced simulation methods from the point of view of its applications.

First, a knowledge gap has been identified (Chapter 1): the rising damp has been pointed out as the most common moisture related damage found in public buildings and it has been clarified that the practitioners and the contractors are not able to assess quantitatively if a restoration project could be used effectively to solve the problem. The reduced availability of material parameter values for the materials used locally and the absence of a database of weather files to be used as boundary conditions, have been identified as the main obstacle to the utilisation of the heat and moisture transfer models for these assessments.

Then, the theoretic principles of the heat and moisture transfer modelling in building materials have been shortly presented (Chapters 2 and 3) with the most commonly used damage models (Chapter 4). For the interstitial moisture accumulation risk analysis, a comparison between the widely used Glaser method and an advanced simulation procedure for the moisture accumulation risk assessment, is presented (Chapter 5). The results show that the Glaser method could be used a conservative simplified analysis for the typical wall types of Central and Southern Europe, but with caution, given that some exceptions are found.

In order to identify two simplified procedures for the material property estimation, two experimental activities have been presented (Chapter 6), one concerning the identification of the parameters describing the vapour transfer in a wood based insulation (Section 6.1) and one focusing on the liquid water transport in solid bricks (Section 6.2). In both cases the new material properties are derived from other similar materials and then compared with the experimental results by means of heat and moisture transfer transient simulations. The obtained results are close to the experimental measurements, showing that heat flux and temperature measurements could be used to analyse moisture migration in the materials and to perform validation of the numerical simulations.

In the evaluation of the water vapour transport of the wood based insulation the phenomenon of the hysteresis of the moisture retention of the material has been observed. In Chapter 7 a method for modelling the hysteresis is presented and its influence on the simulation of heat and moisture transfer in buildings is presented. The simulations have been performed for a cross-laminated timber wall and it has

been found that the differences calculated could be relevant for risk assessment calculations and considering hysteresis reduces the peaks of moisture content found in critical points of the wall layers. It has been proven that the hysteresis should be included in simulations and that it is crucial for the risk evaluation methods based on threshold values of moisture content.

The problem of the boundary conditions is then addressed. The focus is given on the representativeness of the available weather files and on the proposal of new methodologies for the generation of reference years (extreme weather conditions) and representative years (average weather conditions) to be used in the heat and moisture transfer simulations. First, the generation of the representative years for the moisture related simulations is presented and discussed (Chapter 8). Then, further modifications are proposed, in order to identify the most relevant weather parameters for the selection of the weather files (Chapters 11 and 10). It has been shown that other weather file generation procedures could provide weather files more representative for the heat and moisture transfer simulations. Depending on the application of the weather file, the relevance of the weather variables is different, and this could be considered in the generation of the representative wether files.

Finally, the reference year generation method - to be used in the risk analyses - is presented in Chapter 12. The resulting weather files are compared to the representative weather files and it has been shown that the obtained risk values are higher, confirming that the proposed extreme weather files should be preferred to the typical reference years weather files when performing moisture accumulation risk assessments.

In conclusion, few small steps have been made towards the accessibility and the usability of the heat and moisture transfer simulations. Even if the software tools are user friendly, other obstacles are in the way, preventing from a widespread use of these advanced models.

Future work

Starting from the results reported in this thesis, further studies should be carried on, focusing on the influence of the modelling tools and of the different models on the results of the risk assessment analyses. It is also not clear yet which is the impact of hysteresis on the risk analysis and how the moisture transfer through the building envelope affects the whole building energy simulations.

After the evaluation of the proposed procedures for the generation of reference and representative weather files, the research effort could be moved on the assessment of the risk levels for the most common building typologies of a climate region, obtaining an overall evaluation of the presence of moisture damages.

Bibliography

[1] *Bible, Leviticus*, chapter 14:33-53.

[2] G. Massari and I. Massari. *Risanamento igienico dei locali umidi.* HOEPLI EDITORE, 1981.

[3] R. Myllykangas-Luosujarvi, M. Seuri, T. Husman, R. Korhonen, K. Pakkala, and K. Aho. A cluster of inflammatory rheumatic diseases in a moisture-damaged office. *Clinical and experimental rheumatology*, 20(6):833–836, 2002.

[4] R. A. Luosujärvi, T. M. Husman, M. Seuri, M. A. Pietikäinen, P. Pollari, J. Pelkonen, H. T. Hujakka, O. A. Kaipiainen-Seppänen, and K. Aho. Joint symptoms and diseases associated with moisture damage in a health center. *Clinical Rheumatology*, 22(6):381–385, Dec 2003.

[5] S. N. Baxi, J. M. Portnoy, D. Larenas-Linnemann, W. Phipatanakul, C. Barnes, S. Baxi, C. Grimes, W. E. Horner, K. Kennedy, D. Larenas-Linnemann, E. Levetin, J. D. Miller, W. Phipatanakul, J. M. Portnoy, J. Scott, and P. B. Williams. Exposure and Health Effects of Fungi on Humans. *The Journal of Allergy and Clinical Immunology: In Practice*, 4(3):396–404, may 2016.

[6] V. Valtonen. Clinical Diagnosis of the Dampness and Mold Hypersensitivity Syndrome: Review of the Literature and Suggested Diagnostic Criteria. *Frontiers in Immunology*, 8:951, aug 2017.

[7] J. Wang, M. Pindus, C. Janson, T. Sigsgaard, J.-L. Kim, M. Holm, J. Sommar, H. Orru, T. Gislason, A. Johannessen, R. J. Bertelsen, and D. Norbäck. Dampness, mould, onset and remission of adult respiratory symptoms, asthma and rhinitis. *The European respiratory journal*, 53(5):1801921, may 2019.

[8] M. Libralato, G. Murano, O. Saro, A. De Angelis, and V. Corrado. Hygrothermal modelling of building enclosures: reference year design for moisture accumulation and condensation risk assessment. In *7th International Building Physics Conference, IBPC2018 at Syracuse, NY, USA*, 2018.

[9] M. Libralato, O. Saro, A. D. Angelis, and S. Spinazzè. Comparison between Glaser Method and Heat, Air and Moisture Transient Model for Moisture Migration in Building Envelopes. In *Applied Mechanics and Materials*, volume 887, pages 385–392, 2019.

[10] M. Libralato, G. Murano, O. Saro, A. De Angelis, and V. Corrado. Generation of moisture reference years for interstitial condensation risk assessment: Influence of the meteorological record length. In *Building Simulation 2019, Rome*, 2019.

[11] M. Libralato, G. Pernigotto, A. Prada, A. D. Angelis, O. Saro, and A. Gasparella. Design and evaluation of extreme moisture reference years for moisture-related risk assessments. In *BSA 2019 - 4th IBPSA-Italy conference June, 19th-21st 2019, Bolzano*, 2019.

[12] M. Danovska, M. Libralato, G. Pernigotto, A. D. Angelis, O. Saro, P. Baggio, and A. Gasparella. Numerical and experimental study on the impact of humidity on the thermal behavior of insulated timber walls. In *BSA 2019 - 4th IBPSA-Italy conference June, 19-21 2019, Bolzano*, 2019.

[13] A. De Angelis, M. Libralato, and O. Saro. Numerical simulations of coupled conduction-free convection in low conductive vertical finned surfaces. *Modelling, Measurement and Control C*, 79(3):98–102, 2018.

[14] M. Libralato, A. De Angelis, and O. Saro. Evaluation of the ground-coupled quasi-stationary heat transfer in buildings by means of an accurate and computationally efficient numerical approach and comparison with the iso 13370 procedure. *Journal of Building Performance Simulation*, pages 1–9, 2019.

[15] G. Comini. *Fondamenti di termodinamica applicata*, chapter 8, pages 233,275. SGE, 2000.

[16] G. Comini and G. Cortella. *Fondamenti di trasmissione del calore*. SGEditoriali, 2013.

[17] International Organisation for Standardisation. Hygrothermal performance of building components and building elements – internal surface temperature to avoid critical surface humidity and interstitial condensation – calculation methods (ISO 13788:2012), 2012.

[18] J. Grunewald. *Diffusiver und konvektiver Stoff-und Energietransport in kapillar-porösen Baustoffen*. PhD thesis, University of Technology Dresden, 1997.

[19] A. Nicolai. *Modeling and numerical simulation of salt transport and phase transitions in unsaturated porous building materials*. PhD thesis, Syracuse University, 2008.

[20] G. Scheffler. *Validation of hygrothermal material modelling under consideration of the hysteresis of moisture storage*. PhD thesis, Dresden University of Technology, 2008.

[21] A. J. Maneffa, R. Stenner, A. S. Matharu, J. H. Clark, N. Matubayasi, and S. Shimizu. Water activity in liquid food systems: A molecular scale interpretation. *Food Chemistry*, 237:1133 – 1138, 2017.

[22] L. Horka, O. Sikula, and J. Weyr. Numerical simulation of subsoil freezing risk under the freezer room. In *Science and Engineering 2015*, volume 797 of *Applied Mechanics and Materials*, pages 225–230. Trans Tech Publications Ltd, 1 2016.

[23] M. Krajčík and O. Šikula. The possibilities and limitations of using radiant wall cooling in new and retrofitted existing buildings. *Applied Thermal Engineering*, 164:114490, 2020.

[24] M. Šimko, M. Krajčík, O. Šikula, P. Šimko, and D. Kalús. Insulation panels for active control of heat transfer in walls operated as space heating or as a thermal barrier: Numerical simulations and experiments. *Energy and Buildings*, 158:135 – 146, 2018.

[25] O. Šikula. *Software CalA User Manual*, 2011.

[26] S. Rouchier. Hamopy: Heat, air and moisture transfer in python, 2015.

[27] E. Vereecken, S. Roels, and H. Janssen. Hygric property determination based on dynamic measurement techniques and metaheuristic strategies. *Energy Procedia*, 132:279 – 284, 2017. 11th Nordic Symposium on Building Physics, NSB2017, 11-14 June 2017, Trondheim, Norway.

[28] S. Rouchier, T. Busser, M. Pailha, A. Piot, and M. Woloszyn. Hygric characterization of wood fiber insulation under uncertainty with dynamic measurements and markov chain monte-carlo algorithm. *Building and Environment*, 114:129 – 139, 2017.

[29] J. M. Delgado, E. Barreira, N. M. Ramos, and V. P. de Freitas. *Hygrothermal numerical simulation tools applied to building physics*. Springer Science & Business Media, 2012.

[30] H. Janssen. Simulation efficiency and accuracy of different moisture transfer potentials. *Journal of Building Performance Simulation*, 7(5):379–389, 2014.

[31] C. Rode. *Combined heat and moisture transfer in building constructions*. PhD thesis, Technical University of Denmark, 1990.

[32] C. R. Pedersen. Prediction of moisture transfer in building constructions. *Building and Environment*, 27(3):387 – 397, 1992.

[33] C. Rode and L. Juhl. On the use of the logarithmicof the capillary pressure for numerical simulation of moisture flow. In *Proceedings of the second Central European Symposium on Building Physics*, pages 409–413, 2013.

[34] H. M. Künzel and K. Kiessl. Calculation of heat and moisture transfer in exposed building components. *International Journal of Heat and Mass Transfer*, 40(1):159–167, 1996.

[35] K. Sedlbauer. Prediction of mould fungus formation on the surface of and inside building components. *Fraunhofer Institute for Building Physics*, 2001.

[36] E. B. Møller, B. Andersen, C. Rode, and R. Peuhkuri. Conditions for mould growth on typical interior surfaces. *Energy Procedia*, 132:171 – 176, 2017. 11th Nordic Symposium on Building Physics, NSB2017, 11-14 June 2017, Trondheim, Norway.

[37] S. K. Lie, T. K. Thiis, G. I. Vestøl, O. Høibø, and L. R. Gobakken. Can existing mould growth models be used to predict mould growth on wooden claddings exposed to transient wetting? *Building and Environment*, 152:192 – 203, 2019.

[38] K. Gradeci, N. Labonnote, B. Time, and J. Köhler. Mould growth criteria and design avoidance approaches in wood-based materials – a systematic review. *Construction and Building Materials*, 150:77 – 88, 2017.

[39] E. Vereecken and S. Roels. Review of mould prediction models and their influence on mould risk evaluation. *Building and Environment*, 51:296 – 310, 2012.

[40] E. Vereecken, K. Vanoirbeek, and S. Roels. A preliminary evaluation of mould prediction models based on laboratory experiments. *Energy Procedia*, 78:1407 – 1412, 2015. 6th International Building Physics Conference, IBPC 2015.

[41] E. Vereecken, K. Vanoirbeek, and S. Roels. Towards a more thoughtful use of mould prediction models: A critical view on experimental mould growth research. *Journal of Building Physics*, 39(2):102–123, sep 2015.

[42] H. Viitanen, M. Krus, T. Ojanen, V. Eitner, and D. Zirkelbach. Mold risk classification based on comparative evaluation of two established growth models. *Energy Procedia*, 78:1425 – 1430, 2015. 6th International Building Physics Conference, IBPC 2015.

[43] H. Viitanen and A. C. Ritschkoff. *Mould growth in pine and spruce sapwood in relation to air humidity and temperature*. Swedish University of Agricultural Sciences, Department of Forest Products, 1991.

[44] H. Viitanen and T. Ojanen. Improved model to predict mold growth in building materials. In *Proceedings of the Thermal Performance of the Exterior Envelopes of Whold Building X, Florida, USA*. Oak Ridge National Laboratory, 2007.

[45] H. Viitanen, J. Vinha, K. Salminen, T. Ojanen, R. Peuhkuri, L. Paajanen, and K. Lähdesmäki. Moisture and bio-deterioration risk of building materials and structures. *Journal of Building Physics*, 33(3):201–224, 2010.

[46] J. Hiscox, M. Savoury, S. Toledo, J. Kingscott-Edmunds, A. Bettridge, N. A. Waili, and L. Boddy. Threesomes destabilise certain relationships: multispecies interactions between wood decay fungi in natural resources. *FEMS microbiology ecology*, 93(3), 2017.

[47] L. Meyer and C. Brischke. Fungal decay at different moisture levels of selected European-grown wood species. *International Biodeterioration & Biodegradation*, 103:23–29, sep 2015.

[48] F. P. L. (US). *Wood handbook: Wood as an engineering material*, volume 72, pages 14,3. The Service, 1987.

[49] C. Brischke, A. Soetbeer, and L. Meyer-Veltrup. The minimum moisture threshold for wood decay by basidiomycetes revisited. A review and modified pile experiments with Norway spruce and European beech decayed by Coniophora puteana and Trametes versicolor. *Holzforschung*, 71(11):893–903, jan 2017.

[50] C. Brischke and S. Thelandersson. Modelling the outdoor performance of wood products – A review on existing approaches. *Construction and Building Materials*, 66:384–397, sep 2014.

[51] T. C. Scheffer. A climate index for estimating potential for decay in wood structures above ground. *Forest products journal*, 21(10), 1971.

[52] T. Odgaard, S. P. Bjarløv, and C. Rode. Interior insulation – experimental investigation of hygrothermal conditions and damage evaluation of solid masonry façades in a listed building. *Building and Environment*, 129:1 – 14, 2018.

[53] S. Ameri and N. Rüther. Hygrothermal Risk Analysis of Recently Constructed Timber Buildings Exposed to Outdoor Climate Changes by the End of the Century in Germany. *IOP Conference Series: Earth and Environmental Science*, 290(1):012005, jun 2019.

[54] N. F. Jensen, S. P. Bjarløv, C. Rode, and T. R. Odgaard. Hygrothermal assessment of internally insulated solid masonry walls fitted with exterior hydrophobization and deliberate thermal bridge. *ce/papers*, 2(4):79–87, sep 2018.

[55] H. Viitanen. Factors affecting the development of biodeterioration in wooden constructions. *Materials and Structures*, 27(8):483–493, oct 1994.

[56] H. Saito, K. Fukuda, and T. Sawachi. Integration model of hygrothermal analysis with decay process for durability assessment of building envelopes. *Building Simulation*, 5(4):315–324, Dec 2012.

[57] H. A. Viitanen. Modelling the time factor in the development of mould fungi - The effect of critical humidity and temperature conditions on pine and spruce sapwood. *Holzforschung*, 51(1):6–14, 1997.

[58] H. Viitanen, T. Toratti, L. Makkonen, R. Peuhkuri, T. Ojanen, L. Ruokolainen, and J. Räisänen. Towards modelling of decay risk of wooden materials. *European Journal of Wood and Wood Products*, 68(3):303–313, aug 2010.

[59] C. Brischke and A. O. Rapp. Dose–response relationships between wood moisture content, wood temperature and fungal decay determined for 23 European field test sites. *Wood Science and Technology*, 42(6):507–518, aug 2008.

[60] C. Brischke and L. Meyer-Veltrup. Modelling timber decay caused by brown rot fungi. *Materials and Structures*, 49(8):3281–3291, oct 2015.

[61] T. Isaksson, C. Brischke, and S. Thelandersson. Development of decay performance models for outdoor timber structures. *Materials and Structures*, 46(7):1209–1225, jul 2013.

[62] O. B. Isgor and A. Razaqpur. Finite element modeling of coupled heat transfer, moisture transport and carbonation processes in concrete structures. *Cement and Concrete Composites*, 26(1):57 – 73, 2004.

[63] L. Coppola. *Concretum*, pages 161,167. Collana Università/strumenti: Tecnologie. McGraw-Hill, 2007.

[64] A. Lindvall. Duracrete–probabilistic performance based durability design of concrete structures. In *2nd Int. PhD. Symposium in civil engineering*, 1998.

[65] J. Ahlström. Corrosion of steel in concrete at various moisture and chloride levels, 2014. Licentiate Thesis.

[66] L. Bertolini, M. Carsana, B. Daniotti, and E. Marra. Environmental factors affecting corrosion of steel inserts in ancient masonry. In *Durability of Building Materials and Components*, pages 229–252. Springer, 2013.

[67] E. Marra, D. Zirkelbach, and H. M. Künzel. Prediction of steel corrosion in porous building materials by means of a new hygrothermal model. *Energy Procedia*, 78:1299 – 1304, 2015. 6th International Building Physics Conference, IBPC 2015.

[68] S. Rouchier. *Hygrothermal performance assessment of damaged building materials.* Theses, Université Claude Bernard - Lyon I, October 2012.

[69] S. Rouchier, G. Foray, M. Woloszyn, and J.-J. Roux. Influence of diffuse damage on the water vapour permeability of fibre-reinforced mortar. *Transport in Porous Media*, 93(3):543–559, Jul 2012.

[70] S. L. Zelinka, D. Derome, and S. V. Glass. Combining hygrothermal and corrosion models to predict corrosion of metal fasteners embedded in wood. *Building and Environment*, 46(10):2060–2068, 2011.

[71] F. Pinzano. Valutazione della migrazione dell'umidità nei componenti edilizi in calcestruzzo armato per la previsione della corrosione. Master's thesis, Università degli Studi di Udine, 2016.

[72] K. Sedlbauer. Frost damage of masonry walls - a hygrothermal analysis by computer simulations. *Journal of Thermal Envelope and Building Science*, 23(JAN.):277–281, 2000.

[73] M. van Aarle, H. Schellen, and J. van Schijndel. Hygro thermal simulation to predict the risk of frost damage in masonry; effects of climate change. *Energy Procedia*, 78:2536–2541, 2015.

[74] P. Mensinga. *Determining the Critical Degree of Saturation of Brick Using Frost Dilatometry.* PhD thesis, University of Waterloo, 2009.

[75] J. Straube, C. Schumacher, and P. Mensinga. Assessing the freeze-thaw resistance of clay brick for interior insulation retrofit projects. In *Proceedings of the Conference on Performances of Envelopes of Whole Buildings XI, Clearwater Beach, Florida*, pages 5–9, 2010.

[76] Vandemeulebroucke, Isabeau, Caluwaerts, Steven, and Van Den Bossche, Nathan. Freeze-thaw risk in solid masonry: are moisture reference years able to represent real climate conditions? *MATEC Web Conf.*, 282:02034, 2019.

[77] M. Gutland, S. Bucking, and M. S. Quintero. Assessing durability of historic masonry walls with calibrated energy models and hygrothermal modeling. *International Journal of Architectural Heritage*, 0(0):1–17, 2019.

[78] C. Feng, S. Roels, and H. Janssen. Towards a more representative assessment of frost damage to porous building materials. *Building and Environment*, 164:106343, 2019.

[79] X. Zhou, D. Derome, and J. Carmeliet. Hygrothermal modeling and evaluation of freeze-thaw damage risk of masonry walls retrofitted with internal insulation. *Building and Environment*, 125:285 – 298, 2017.

[80] P. Baggio, C. Bonacina, and B. A. Schrefler. Some considerations on modeling heat and mass transfer in porous media. *Transport in Porous Media*, 28(3):233–251, 1997.

[81] D. A. De Vries. Simultaneous transfer of heat and moisture in porous media. *Eos, Transactions American Geophysical Union*, 39(5):909–916, 1958.

[82] G. Comini and R. W. Lewis. A numerical solution of two-dimensional problems involving heat and mass transfer. *International Journal of Heat and Mass Transfer*, 19(12):1387 – 1392, 1976.

[83] A. W. M. van Schijndel. Multiphysics modeling of building physical constructions. In *Building Simulation*, volume 4, pages 49–60. Springer, 2011.

[84] O. Adan, H. Brocken, J. Carmeliet, H. Hens, S. Roels, and C.-E. Hagentoft. Determination of liquid water transfer properties of porous building materials and development of numerical assessment methods: Introduction to the ec hamstad project. *Journal of Thermal Envelope and Building Science*, 27(4):253–260, 2004.

[85] H. M. Künzel. Simultaneous heat and moisture transport in building components. *One-and two-dimensional calculation using simple parameters. IRB-Verlag Stuttgart*, 1995.

[86] D. Zirkelbach, S.-R. Mehra, K.-P. Sedlbauer, H.-M. Künzel, and B. Stockl. A hygrothermal green roof model to simulate moisture and energy performance of building components. *Energy and Buildings*, 145:79–91, 2017.

[87] G. R. Finken, S. P. Bjarløv, and R. H. Peuhkuri. Effect of façade impregnation on feasibility of capillary active thermal internal insulation for a historic dormitory – a hygrothermal simulation study. *Construction and Building Materials*, 113:202 – 214, 2016.

[88] J. W. Eaton, D. Bateman, S. Hauberg, and R. Wehbring. *GNU Octave version 5.1.0 manual: a high-level interactive language for numerical computations*, 2019.

[89] M. Libralato. EN ISO 13788:2013 Glaser methods implemented in Octave. Website: https://github.com/michele-libralato/glaser_method_octave, June 2018. Accessed: 2018-06-21.

[90] H. M. Künzel. Moisture risk assessment of roof constructions by computer simulation in comparison to the standard glaser-method. In *International Building Physics Conference, Eindhoven*, pages 225–232, 2000.

[91] J. Van Der Kooi. *Moisture transport in cellular concrete roofs*. Uitgeverij Waltman, 1971.

[92] L. Mazzarella. Dati climatici g. de giorgio. *Proceedings of Giornata di Studio Giovanni De Giorgio, Politecnico di Milano, Milano*, 18, 1997.

[93] ASHRAE. International Weather for Energy Calculations (IWEC Weather Files) Users Manualand CD-ROM. Technical report, ASHRAE, Atlanta, 2001.

[94] M. Danovska, G. Pernigotto, M. Baratieri, P. Baggio, and A. Gasparella. Influence of moisture content, temperature and absorbed solar radiation on the thermal performance of a spruce xlam wall in the italian climates. In *37th UIT Heat Transfer Conference 2019At: Padova, Italy*, 06 2019.

[95] M. Petris. Uso della termografia per la determinazione della risalita capillare dell'umidità in componenti edilizi. Master's thesis, Università degli studi di Udine, 2019.

[96] Y. Mualem. A conceptual model of hysteresis. *Water Resources Research*, 10(3):514–520, 1974.

[97] J. Kool and J. C. Parker. Development and evaluation of closed-form expressions for hysteretic soil hydraulic properties. *Water Resources Research*, 23(1):105–114, 1987.

[98] P. N. Peralta. Modeling wood moisture sorption hysteresis using the independent-domain theory. *Wood and Fiber Science*, 1995.

[99] J. Carmeliet, M. H. D. de Wit, and H. Janssen. Hysteresis and moisture buffering of wood. In *Proceedings of the 7th Symposium on Building Physics in the Nordic Countries : Reykjavik*, pages 55–62, 2005.

[100] C. Rode and C. O. Clorius. Modeling of moisture transport in wood with hysteresis and temperature-dependent sorption characteristics. In *Performance of Exterior Envelopes of Whole Buildings IX: International Conference, 2004, Clearwater, Florida*, 2004.

[101] G. Costantine, C. Maalouf, T. Moussa, E. Kinab, and G. Polidori. Impact of including hemp concrete hysteresis on the modelling of its hygrothermal behavior at wall and room scales. In *Building Simulation 2019, Rome*, 2019.

[102] D. Lelièvre, T. Colinart, and P. Glouannec. Modeling the Moisture Buffering Behavior of a Coated Biobased Building Material by Including Hysteresis. *Energy Procedia*, 78:255–260, nov 2015.

[103] T. Colinart, M. Bendouma, and P. Glouannec. Indicateurs de pathologies liées à l'humidité: analyse des modèles et influence de l'hystérésis des isothermes de sorption. In *IBPSA France 2016*, may 2016.

[104] G. Lupato, M. Manzan, and S. Cirilli. Comparison of direct radiation split algorithms for energy simulation of buildings. In *3rd IBPSA Italy conference Bozen-Bolzano, 8th – 10th February 2017*, 2018.

[105] G. Lupato. *The Climate data effect in building energy simulation.* PhD thesis, Università degli Studi di Trieste, 2018.

[106] S. Petersen, T. Broholt, L. Christensen, and P. Brix Purup. Thermal performance simulation of complex fenestration systems in the early design stage. In *Proceedings of BSO 2018*, pages 573–580. International Building Performance Simulation Association, 9 2018.

[107] I. Vrachimi and D. Costóla. Predicting wind-driven rain catch ratios in building simulation using machine learning techniques. In *Building Simulation 2019, Rome*, 2019.

[108] B. Blocken and J. Carmeliet. Spatial and temporal distribution of driving rain on a low-rise building. *Wind and Structures*, 5(5):441–462, 2002.

[109] H. Janssen, B. Blocken, S. Roels, and J. Carmeliet. Wind-driven rain as a boundary condition for ham simulations: analysis of simplified modelling approaches. *Building and Environment*, 42(4):1555–1567, 2007.

[110] A. Kubilay, D. Derome, B. Blocken, and J. Carmeliet. Numerical simulations of wind-driven rain on an array of low-rise cubic buildings and validation by field measurements. *Building and Environment*, 81:283 – 295, 2014.

[111] International Organisation for Standardisation. Hygrothermal performance of buildings -calculation and presentation of climatic data- part 4: Hourly data for assessing the annual energy use for heating and cooling (ISO 15927-4:2005), 2005.

[112] J. M. Finkelstein and R. E. Schafer. Improved goodness-of-fit tests. *Biometrika*, 58(3):641, 1971.

[113] H. Hens. *Applied building physics: ambient conditions, building performance and material properties*, chapter 1, pages 31,35. John Wiley & Sons, 2016.

[114] S. Cornick, R. Djebbar, and W. A. Dalgliesh. Selecting moisture reference years using a moisture index approach. *Building and Environment*, 38(12):1367–1379, 2003.

[115] T. Kalamees and J. Vinha. Estonian Climate Analysis for Selecting Moisture Reference Years for Hygrothermal Calculations. *Journal of Building Physics*, 2004.

[116] M. Salonvaara, K. Sedlbauer, A. Holm, and M. Pazera. Effect of Selected Weather Year for Hygrothermal Analyses. In *Proceedings of the Thermal Performance of the Exterior Envelopes of Whole Buildings XI International Conference*, 2010.

[117] X. Zhou, D. Derome, and J. Carmeliet. Robust moisture reference year methodology for hygrothermal simulations. *Building and Environment*, 110:23 – 35, 2016.

[118] T. Schöner and D. Zirkelbach. Development of hygrothermal reference years for germany. In *Central European Symposium on Buildings Physics (CESBP)*, 2016.

[119] G. Riva, G. Murano, V. Corrado, P. Baggio, and G. Antonacci. Definizione degli anni tipo climatici delle province di alcune regioni italiane (in Italian). *ENEA, Ministero dello Sviluppo Economico*, page 347, 2010.

[120] G. Riva, G. Murano, V. Corrado, P. Baggio, and G. Antonacci. Aggiornamento parametri climatici nazionali e zonizzazione del clima nazionale ai fini della certificazione estiva. Technical report, ENEA, 2012.

[121] G. Murano, V. Corrado, and D. Dirutigliano. The new Italian Climatic Data and their Effect in the Calculation of the Energy Performance of Buildings. *Energy Procedia*, 101:153–160, nov 2016.

[122] G. Pernigotto, A. Prada, A. Gasparella, and J. L. M. Hensen. Analysis and improvement of the representativeness of en iso 15927-4 reference years for building energy simulation. *Journal of Building Performance Simulation*, 7(6):391–410, 2014.

[123] G. Murano, D. Dirutigliano, and V. Corrado. Improved procedure for the construction of a Typical Meteorological Year for assessing the energy need of a residential building. *Journal of Building Performance Simulation*, pages 1–14, aug 2018.

[124] A. De Angelis, O. Saro, G. Lorenzini, S. D'Elia, and M. Medici. Simplified models for assessing heat and mass transfer in evaporative towers. *Synthesis Lectures on Engineering*, 8(2):1–124, 2013.

[125] A. De Angelis, O. Saro, and M. Truant. Evaporative cooling systems to improve internal comfort in industrial buildings. *Energy Procedia*, 126:313–320, 2017.

[126] A. De Angelis, D. Chinese, and O. Saro. Free-cooling potential in shopping mall buildings with plants equipped by dry-coolers boosted with evaporative pads. *INTERNATIONAL JOURNAL OF HEAT AND TECHNOLOGY*, 35(4):853–862, 2017.

[127] D. Chinese, M. Santin, and O. Saro. Water-energy and ghg nexus assessment of alternative heat recovery options in industry: A case study on electric steelmaking in europe. *Energy*, 141:2670–2687, 2017.

[128] M. Libralato, A. D. Angelis, and O. Saro. Durability of building materials: Evaluation of alternative moisture reference years generation procedure for the climate of udine. *Friulian Journal of Science*, In press.

[129] G. Lupato and M. Manzan. Italian trys: New weather data impact on building energy simulations. *Energy and Buildings*, 185:287 – 303, 2019.

[130] L. Giorgio, M. Manzan, and A. Pezzi. The effect of climatic data on building performance optimization. In *4th Building Simulation and Optimization Conference, Cambridge, UK: 11-12 September 2018*, 2018.

[131] L. Sontag, A. Nicolai, and S. Vogelsang. Validierung der Solverimplementierung des hygrothermischen Simulationsprogramms Delphin, nov 2013.

[132] European Committee for Standardisation. Hygrothermal performance of building components and building elements - assessment of moisture transfer by numerical simulation (EN 15026:2007), 2007.

[133] I. Ballarini, S. P. Corgnati, and V. Corrado. Use of reference buildings to assess the energy saving potentials of the residential building stock: The experience of tabula project. *Energy Policy*, 68:273–284, 2014.

[134] G. Pernigotto, A. Prada, and A. Gasparella. Development of extreme reference years for building energy simulation scenarios. In *Applied Mechanics and Materials*, volume 887, pages 129–139. Trans Tech Publ, 2019.